DESIGN OF A HIGH SPEED DECOY UAV

A THESIS SUBMITTED TO
THE GRADUATE SCHOOL OF NATURAL AND APPLIED SCIENCES
OF
MIDDLE EAST TECHNICAL UNIVERSITY

BY

UMUT BAYKARA

IN PARTIAL FULFILLMENT OF THE REQUIREMENTS
FOR
THE DEGREE OF MASTER OF SCIENCE
IN
AEROSPACE ENGINEERING

JUNE 2016

Approval of the thesis:

DESIGN OF A HIGH SPEED DECOY UAV

submitted by **UMUT BAYKARA** in partial fulfillment of the requirements for the degree of **Master of Science in Aerospace Engineering Department, Middle East Technical University** by**,**

Prof. Dr.Gülbin Dural Ünver _____

Dean, Graduate School of **Natural and Applied Sciences**

Prof. Dr.Ozan Tekinalp _____

Head of Department, **Aerospace Engineering**

Prof. Dr.Nafiz Alemdaroğlu _____

Supervisor, **Aerospace Engineering Dept., METU**

Examining Committee Members:

Prof. Dr.Serkan Özgen _____

Aerospace Engineering Dept., METU

Prof. Dr.Nafiz Alemdaroğlu _____

Aerospace Engineering Dept., METU

Prof. Dr.Altan Kayran _____

Aerospace Engineering Dept., METU

Assoc. Prof.Dr. Mustafa Kaya _____

Flight Training Dept., UTAA

Assoc. Prof. Dr. Dilek Funda Kurtuluş _____

Aerospace Engineering Dept., METU

Date: _____

I hereby declare that all information in this document has been obtained and presented accordance with academic rules and ethical conduct. I also declare that, as required by these rules and conduct, I have fully cited and referenced all material and results that are not original to this work.

Name, Last name: Umut BAYKARA

Signature :

ABSTRACT

DESIGN OF A HIGH SPEED DECOY UAV

BAYKARA, Umut

M.S., Department of Aerospace Engineering

Supervisor: Prof. Dr. Nafiz Alemdaroğlu

June 2016, 175 pages

This study consists of design, CFD aerodynamic analysis and optimized selection of a high speed decoy UAV. The mission requirements for the high speed decoy are based upon the previous experiences in literature. The requirements are specified as: Maximum altitude of 15000 ft, maximum speed of 450 kts and an endurance of at least 1 hour.

The decoy UAV is launched from a pneumatic catapult and lands via a parachute system. It is a highly agile aircraft having a very high maneuverability capability. The aircraft has a 6g sustained and 9g instantaneous load factor. Required payload capacity is set to be as 22 lbs, consisting of a smoke dispenser, a passive radar cross section augmenter (luneberg lens), a chaff and IR dispenser and a miss distance indicator.

Since, the aim of this study is to design an optimized high speed decoy that surpasses its predecesors, a new generation CFD tool is used to achieve the high speed decoy configuration which gives the best aerodynamic performance. Baseline design and other configurations were created according to their vertical wing and tail geometry designs. All models were created in CAD environment and analyzed for different

flow regimes and envelopes. Finally, configuration is selected considering various design and performance criteria.

Keywords: Decoy, UAV, Design, CFD, Optimization

ÖZ

YÜKSEK HIZLI HEDEF İHA TASARIMI

BAYKARA, Umut

Yüksek Lisans, Havacılık ve Uzay Mühendisliği Bölümü

Tez Yöneticisi: Prof. Dr. Nafiz Alemdaroğlu

Haziran 2016, 175 sayfa

Bu tez yüksek hızlı hedef İHA tasarımını, CFD aerodinamik analizini ve en iyi aerodinamik performansı veren yüksek hızlı İHA nın seçilmesini içermektedir. Temel gereksinimler geçmiş tasarımlardan elde edilen tecrübelere dayanmaktadır.Gereksinimler şunları içermektedir. 15000 ft yüksekliğe çıkabilme, 450 knot hıza çıkabilme, en az 1 saat dayanım süresine sahip olma.

Hedef İHA pnömatik mancınık tarafından fırlatılıp, paraşüt sistemi ile inecektir.İleri derecede çevik olacak bu uçak, yüksek manevra kabiliyetine sahip olacaktır. Devamlı 6g ve anlık 9g yük faktörü kabiliyetine sahip olması amaçlanmıştır. Gerekli görülen yük kapasitesi 10 kg olarak ayarlanmıştır ve duman atıcısı, pasif radar iz arttırıcı ve karşı tedbir atım sistemi içerir.

Bu çalışmanın amacı akranları ile rekabet edebilecek düzeyde optimize edilmiş bir yüksek hızlı İHA tasarlamak olduğu için, yeni jenerasyon hesaplamalı akışkanlar dinamiği yazılımı kullanılacak ve en uygun aerodinamik performansı gösteren yüksek hızlı hedef İHA konfigurasyonu seçilecektir. Ana tasarım ve diğer konfigürasyonlar farklı kanat ve kuyruk geometrik şekillerinde oluşturulmuştur. Bütün geometriler, bilgisayar destekli tasarım yazılımında oluşturulmuş ve farklı akış

rejimlerinde analiz edilmiştir. Son olarak, farklı dizayn ve performans kriterlerine göre konfigürasyon seçimi yapılmıştır.

Anahtar kelimeler: Hedef, İHA, Dizayn, HAD, Optimizasyon

Dedicated to my parents

ACKNOWLEDGEMENTS

I would like to thank to my supervisor Prof. Dr. Nafiz Alemdaroğlu for his guidance, encouragement and patience during my thesis study. He has been very kind, helpful and understanding to me during this long period.

I would like to thank to the Bias Engineering employees namely Gökay Sedef, Görkem Turan, Süleyman Turnaoğlu and Furkan Gültekin for giving endless technical support during CFD analysis period. I am also thankful for Bias Engineering for letting me use their powerful analysis computer during CFD analysis.

I would like to thank to Berk Akar, Haluk Akçay and Seda Baykara for their technical support during CFD analysis period.

I would like to thank to my family and my grandmother Sevim Baykara for their encouragement, understanding, moral and financial support during my thesis study.

TABLE OF CONTENTS

LIST OF TABLES

LIST OF FIGURES

LIST OF SYMBOLS

Symbol	Description	Unit
a	Speed of Sound	KTS
AR_{Wing}	Wing Aspect Ratio	-
AR_{HT}	Horizontal Tail Aspect Ratio	-
AR_{VT}	Vertical Tail Aspect Ratio	-
b_{Wing}	Wing Span	ft
b_{VT}	Vertical Tail Span	ft
c_{HT}	Horizontal Tail Volume Coefficient	-
c_{VT}	Vertical Tail Volume Coefficient	-
C_{Cruise}	Cruise Specific Fuel Consumption	1/h
C_{Combat}	Combat Specific Fuel Consumption	1/h
C_{Loiter}	Loiter Specific Fuel Consumption	1/h
$C_{r\,Wing}$	Wing Root Chord	ft
C_{rHT}	Horizontal Tail Root Chord	ft
C_{rHT}	Vertical Tail Root Chord	ft
C_t	Wing Tip Chord	ft
$C_{t\,HT}$	Horizontal Tail Tip Chord	ft
$C_{t\,VT}$	Vertical Tail TipChord	ft
$\bar{C}_{Wing}$	Wing Mean Aerodynamic Chord	ft
$\bar{C}_{HT}$	Horizontal Tail Mean Aerodynamic Chord	ft
$\bar{C}_{VT}$	Vertical Tail Mean Aerodynamic Chord	ft

$C_{l\,0}$	Airfoil Lift Coefficient at zero angle of attack	-
$C_{l\,i}$	İdeal Lift Coefficient or Design Lift Coefficient	-
C_{l_α}	Lift Curve Slope	deg $^{-1}$
$C_{l_{\alpha\,Wing}}$	Lift Curve Slope of the Wing	deg $^{-1}$
$C_{l_{\alpha\,HT}}$	Lift Curve Slope of the Horizontal Tail	deg $^{-1}$
$C_{l_{Max}}$	Maximum Lift Coefficient of the Airfoil	-
$C_{L_{Max}}$	Maximum Lift Coefficient of the Wing	-
C_{m_0}	Airfoil Moment Coefficient at 0 Angle of attack	-
C_{D_0}	Parasitic Drag Coefficient	-
C_f	Friction Coefficient	-
d_{fus}	Fuselage Diameter	-
D	Drag Force	lbf
e	Oswald efficiency Factor	-
E	Endurance	sec
f	Slenderness Ratio	-
FF	Component Form Factor	-
$l_{fuselage}$	Fuselage Length	ft
l_{HT}	Horizontal Tail Span	ft
L_{HT}	Horizontal Tail Moment Arm	ft
L_{VT}	Vertical Tail Moment Arm	ft
M	Mach Number	-
n	Load Factor	-
n_{max}	Maximum Load Factor	-

n_{lim}	Limit Load Factor	-
$n_{neg\ lim}$	Negative Limit Load Factor	-
n_{ult}	Ultimate Load Factor	-
$n_{neg\ ult}$	Negative Ultimate Load Factor	-
R	Turn Radius	ft
R_{min}	Minimum Turn Radius	ft
Re_{cruise}	Reynolds Number at cruise	-
Re_{combat}	Reynolds Number at combat	-
Re_{loiter}	Reynolds Number at loiter	-
S	Leading Edge Suction Factor	-
S_{Wing}	Wing Reference Area	ft^2
S_{HT}	Horizontal Tail Reference Area	ft^2
S_{VT}	Vertical Tail Reference Area	ft^2
S_{exp}	Exposed Area	ft^2
S_{wet}	Wetted Surface Area	ft^2
T	Thrust Force	lbf
$T_{A\ max}$	Maximum Available Thrust	lbf
V_{cruise}	Cruise velocity	ft/s
V_{combat}	Combat velocity/Corner velocity	ft/s
V_{corner}	Corner velocity/Combat velocity	ft/s
V_{loiter}	loiter velocity	ft/s
V_{max}	Maximum velocity	ft/s
V_{stall}	Stall velocity	ft/s
q_{cruise}	Dynamic Pressure during cruise	lb/ft^2

q_{combat}	Dynamic Pressure during combat	lb/ft^2
q_{loiter}	Dynamic Pressure during loiter	lb/ft^2
q_{stall}	Dynamic Pressure at stall	lb/ft^2
W	Weight	lbs
W_0	Maximum Take off Weight	lbs
W_e	Empty Weight	lbs
W_f	Fuel Weight	lbs
$W_{payload}$	Payload Weight	lbs

LIST OF GREEK SYMBOLS

Λ_{LE}	Leading Edge Sweep Angle	deg
$\Lambda_{c/4}$	Quarter Chord Sweep Angle	deg
$\Lambda_{\max t}$	Maximum Thickness Sweep Angle	deg
$\Lambda_{LE\ HT}$	Horizontal Tail Leading Edge Sweep Angle	deg
$\Lambda_{\max t\ HT}$	Maximum Thickness Sweep Angle	deg
$\Lambda_{LE\ VT}$	Vertical Tail Leading Edge Sweep Angle	deg
$\Lambda_{\max t\ VT}$	Maximum Thickness Sweep Angle	deg
λ	Taper Ratio of the Wing	-
λ_{HT}	Taper Ratio of the Horizontal Tail	-
λ_{HT}	Taper Ratio of the VerticalTail	-
μ	Dynamic viscosity	kg/m.s
ν	Kinematic viscosity	m^2/s
ρ	Air Density	kg/m^3
ω	Turn Rate	rad/s
ω_{max}	Maximum Turn Rate	rad/s

LIST OF ABBREVIATIONS

UAV	Unmanned Aerial Vehicle
UCAV	Unmanned Combat Aerial Vehicle
ETM	Enhanced Turbulence Model
CAD	Computer aided design
CFD	Computational fluid dynamics
2SWF	Two Scale Wall Function

CHAPTER 1

INTRODUCTION

1.1 Unmanned Aerial Vehicles(UAV) and their functions

UAV(Unmanned Aerial Vehicle) can be defined as an aircraft without a pilot. The U.S. Department of Defense (DOD) unmanned aircraft is defined as

"A powered vehicle that does not carry a human operator, can be operated autonomously or remotely, can be expendable or recoverable, and can carry a lethal or nonlethal payload."[1]

UAV's can be classified according to their size, Range/Altitude and functions.

UAV functions can be mainly given as:

a)Reconnaissance:

-Provides battlefield or environmental intelligence.

b)Combat:

–Provides attack capability for high-risk missions.

c)Logistics:

–Designed for cargo and logistics operations.

d)Target and decoy:

-Provide ground and aerial gunnery a target that simulates an enemy aircraft or missile.

e)Research and development

1.2 Decoy UAV definition

Decoy UAV's are used to simulate an enemy aircraft or missile in order to test new weapon systems and to educate pilots to air to air combat scenarios. According to ref[1], decoy UAV's (Aerial targets) are categorized in three forms:

a)Low speed surface gunnery targets:

They were used at world war-II to train Anti Air gunners. Lots of numbers of low speed targets were created.

b) High speed targets

Since faster new aircrafts and missiles were created, faster targets were produced. Fighter jet aircraft pilots started to use high speed decoy in order to test new missile systems and to practice dogfighting manuevers.

c) Manned aircraft conversions

As aircrafts became older and older, they have been converted to aerial targets. Since manned conversions are old aircrafts, they are able to represent perfectly an enemy aircraft. Until now, U.S. have converted F-86, F-100, F-4 and F-16 old fighters to aerial targets.

1.3 Decoy UAV Special Systems

To operate a decoy UAV, special systems are required. In this section, some of these systems are listed below.

a) Luneberg Lens:

"The Luneberg lens is a passive radar augmentation device used to increase the radar reflectivity of a target without the use of additional energy. The lens reflector is a sphere in shape, usually composed of concentric dielectric shells. By the proper selection of dielectric constants for each shell, radar energy incident on one of the faces of the lens is focused at a point on the rear surface of the lens. The rear conductive surface reflects radar energy back to the source."[19]

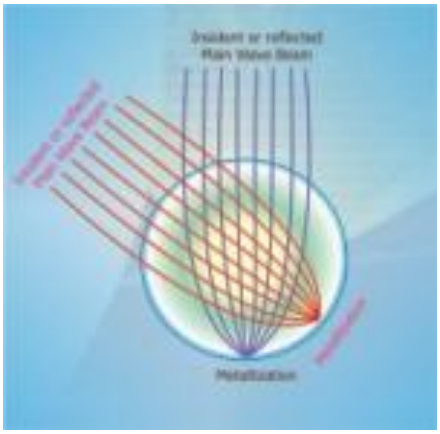

Figure 1.1 Luneberg Lens [19]

b) Miss Distance Indicator:

"This system measures the miss distance between a projectile such as a missile or a burst of gun rounds and a target vehicle such as a remotely piloted drone. The distance is determined by post processing analysis of the images of the encounter from the two trackers, and using triangulation to determine the relative trajectories of the projectile and target vehicle. The miss distance is defined as the minimum separation between the two bodies."[20]

Figure 1.2 Acoustic Miss Distance Indicator used by Meggit Defence Systems [21]

c) Chaff and Flare (Countermeasures) Dispenser:

In combat, countermeasure system is used to fool incoming missiles. Chaff is dispensed to fool incoming radar missiles whereas, flare is used to fool incoming heat seeking missiles. High speed decoy is supposed to equip chaff and flare dispenser in order to simulate combat.

1.4 Literature Survey

A literature survey has been made to get hint from previous high speed decoy designs, competitor study was made and average values of some variables were calculated.

Competitor study consists of high speed decoy aircrafts such as Şimşek[18], Meggit BansheeTwinjet[10], yperion[24], Nemisis[25] and Firejet[9]. Results for high speed decoy aircrafts are given as,

Table 1.1 Competitor Study Aircraft Values for high speed aerial targets

	Şimşek	Nemisis	Yperion	Firejet	Meggit Banshee Twinjet
Max. take-off weight	75 kg	33 kg	45 kg	145 kg	95 kg
Payload weight	10 kg	7 kg	10 kg	45 kg	N/A
Take off	Launcher	Launcher	Launcher	Launcher	Launcher
Landing	Parachute	Parachute	Parachute	Parachute	Parachute
Engine power	40 kg	25 kg	31 kg	73.5 kg	110 kg
Length [m]	2.3 m	2.3 m	2.45 m	3.3 m	2.95 m
Wing span [m]	1.5 m	1.6 m	1.7 m	1.9 m	2.49 m
Max. flight speed	180 m/s	200 m/s	308 m/s	231.5 m/s	200 m/s
Service ceiling	15000 ft	18000 ft	N/A	30000 ft	26000 ft
Range	100 km	120 km	100 km	N/A	100 km
Endurance	0.5 hr	>1 hr	<1 hr	1.25 hr	>0.75 hr

Table 1.2 Competitor study mean values for high speed aerial targets

Engine type	Turbojet
Take off gross weight	78.6 (kg)
Wing Span	1.84 (m)
Length	2.66 (m)
Maximum Velocity	220 (m/s)
Endurance	0.9 (h)
Service Ceiling	15 ft-40166.66 ft
Range	105 km
Take off and Landing	Launch&Parachute

These values gives idea of some characteristics of the high speed target UAV's. Since the aim is to design an high speed decoy UAV in order to satisfy given requirements, it is crucially important to check previously designed decoy aircrafts in Turkey.

Ender Özyetiş from METU Aerospace Engineering Department has designed and manufactured a high speed decoy for his study in 2013[3].

Table 1.3 Decoy UAV Specifications designed by Ender Özyetiş [3]

Decoy UAV Designed By :	Ender Özyetiş
Type:	high subsonic speed
Launch and Landing	Launcher&parachute
Endurance(min):	30
MTOW(kg):	25.8
Maximum speed(m/s):	172
Range(km):	N/A
Max Ceiling(m)	1700
Maneuverability	9g instantaneous 6g sustained

The CAD Drawing of the UAV created by Ender Özyetiş is given as,

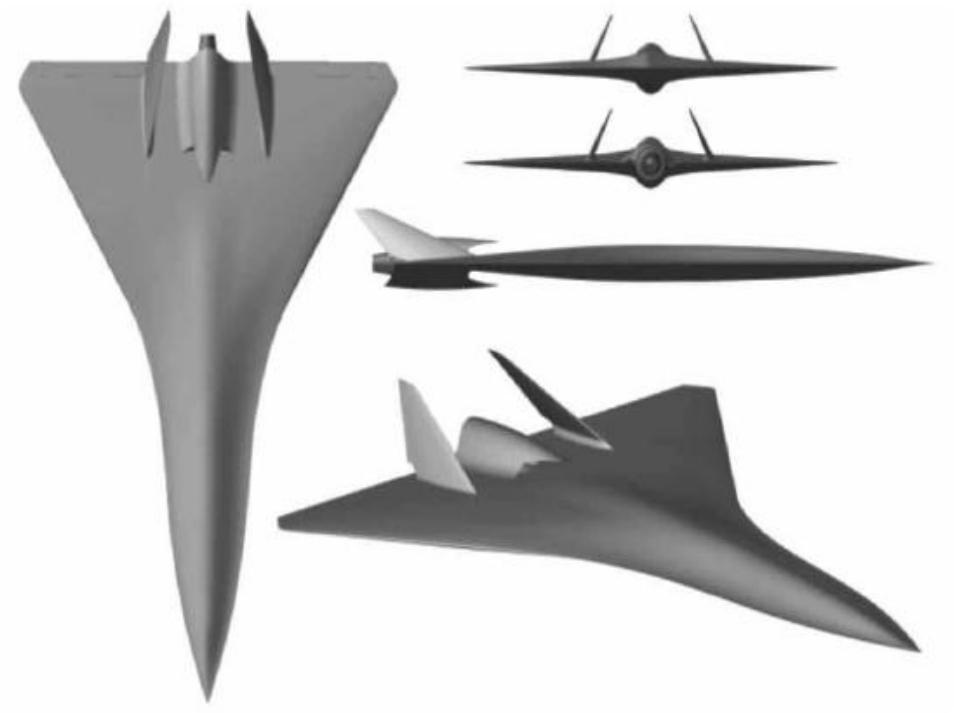

Figure 1.3 High Speed Decoy UAV CAD Model Designed by Ender Özyetiş [3]

TAI(Turkish Aerospace Industries) in Turkey, has designed and created three different decoy UAV to test weapon systems for Turkish Air Force.While, Keklik and Turna were designed to operate at low subsonic speeds, Şimşek was designed to operate at high subsonic speeds.

The specifications of these designed decoy UAV are given in the following table.

Table1.3 Decoy UAV specifications designed by TAI [18]

Decoy UAV Name:	Keklik	Turna	Şimşek
Type:	Low subsonic speed	Low subsonic speed	High subsonic speed
Launch and Landing	Launcher&parachute	Launcher&parachute	Launcher&parachute
Endurance(min):	30	90	30
MTOW(kg):	10	70	75
Maximum speed(m/s):	41	93	180
Range(km):	N/A	More than 50	100
Max Ceiling(ft)	12000	More than 12000	15000

Out of these three designed UAV's, expecially Şimşek attracted special attention since it was designed to operate at high subsonic speeds.

Figure 1.4 Şimşek High Speed Decoy UAV Designed by TAI [18]

To sum up, these previous high speed decoy experiences in literature gave inspiration to design a decoy UAV, which will be able to operate at higher maximum speeds, and spent more time in operation.

CHAPTER 2

DECOY UAV DESIGN

2.1 Introduction to Aircraft Design

Aircraft design is a process which includes the combination of the areas of aerodynamics, structures, controls and propulsion. Design process cannot start without identifying the requirements of the aircraft. Because, some parameters such as engine size and wing area can only be calculated according to the requirements. These requirements may alter during the design process[5]. Requirements given for this study is given in table 2.1.

Table 2.1 Requirements for high speed decoy

Payload	22 lbs(10kg)
Maximum velocity	450 knots
Endurance	1 hr
Maximum altitude	15000 ft ASL
Manueverability	9g instantaneous 6g sustained
Take off and Landing	Launch&parachute
Range	100 km

Aircraft design has three phases. Conceptual design, preliminary design and detail design. Design phases are given in the figure 2.1[5].

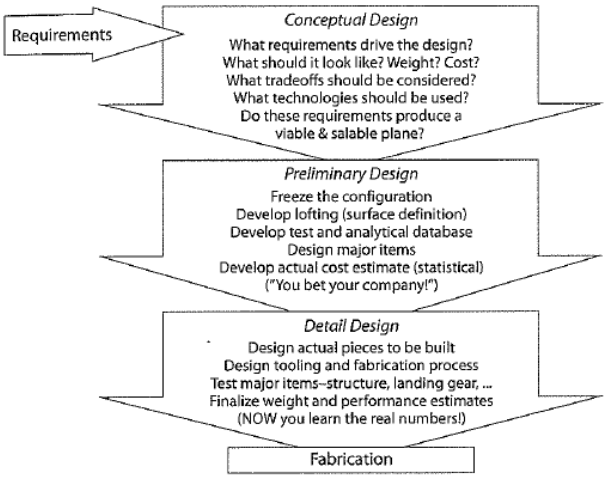

Figure 2.1 Three Phases of Aircraft Design [5]

In this study, Aim is to conceptually design and optimize an high speed decoy, design methodology pivot points are given in the figure2.2 Ref[4].

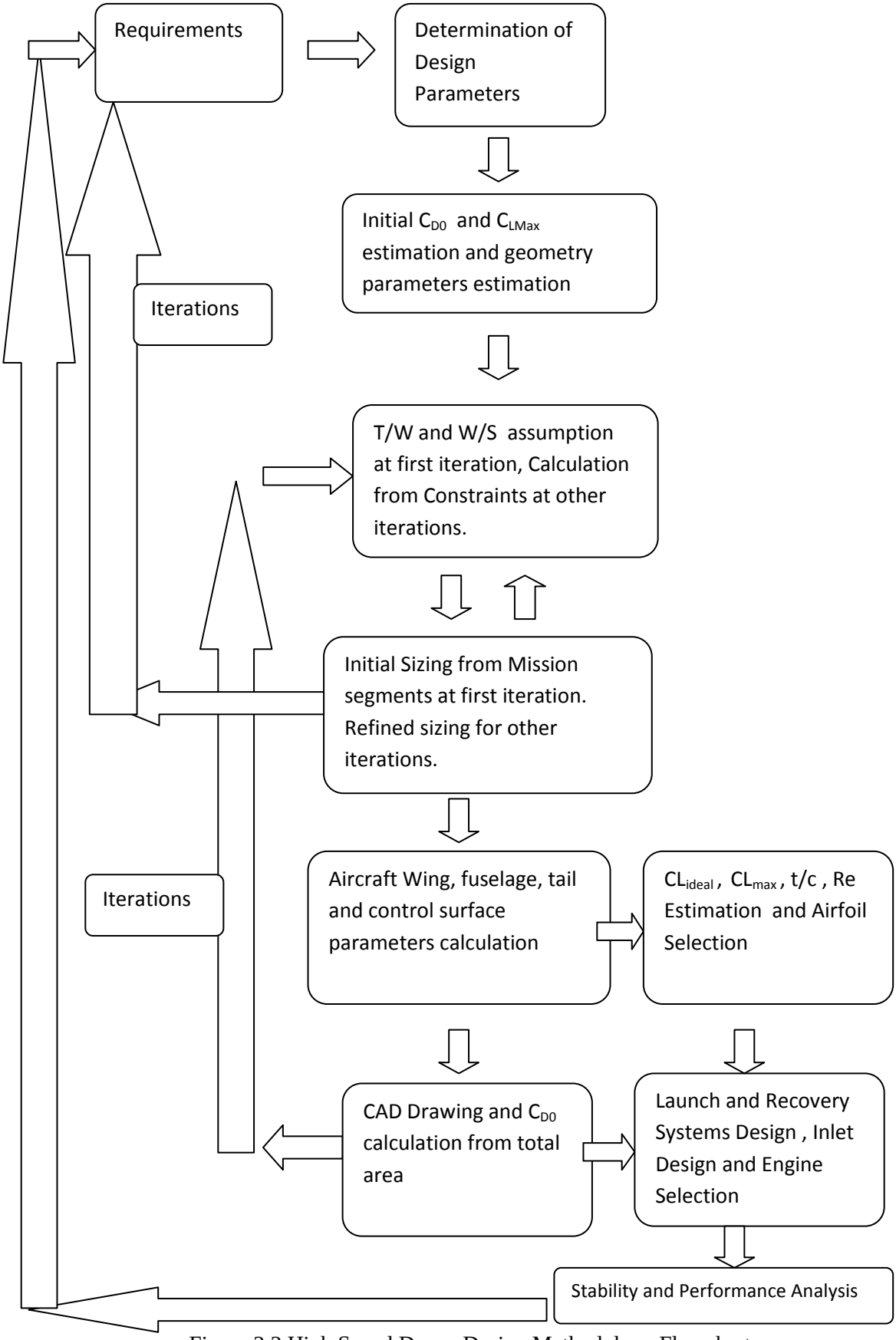

Figure 2.2 High Speed Decoy Design Methodology Flowchart

Thesis procedure is shown in the next figure.

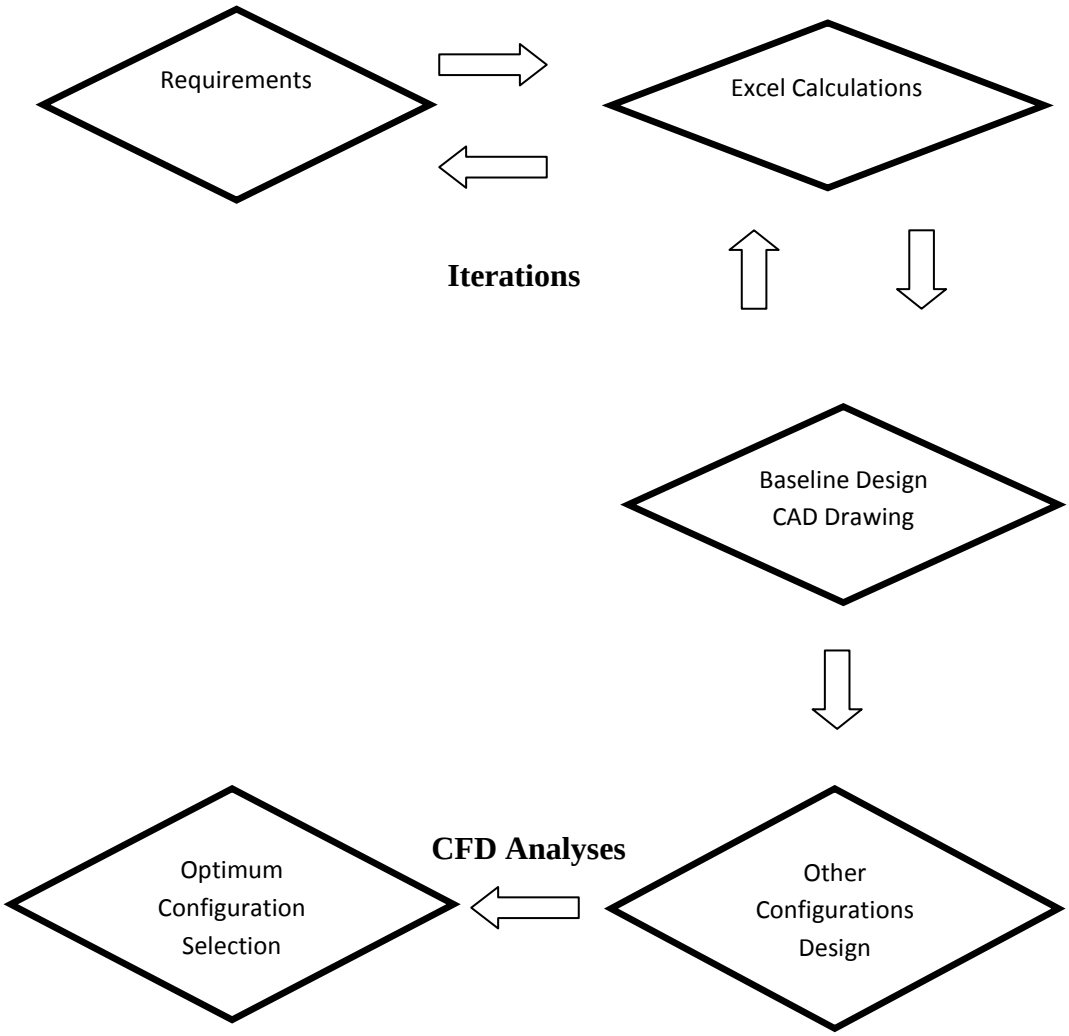

Figure 2.3 Thesis Procedure Flowchart

2.2 Initial Sizing

Sizing is the starting step of the iterative design process. This step is used to estimate the take off gross weight(W_0). W_0 is the total weight of the aircraft before starting to its mission. For this step Raymer weight calculation formula is used[5].

$$W_0 = W_{crew} + W_{payload} + W_{fuel} + W_{empty} \tag{2.1}$$

Where, empty weight is given as,

$$W_e = W_{avionics} + W_{propulsion} + W_{structural} + W_{control} + W_{other} \tag{2.2}$$

W_f and W_e are changed when W_0 changes. these quantities can be non-dimensionalized and finally W_0 can be solved. Note that W_{crew} is 0 for UAV. Following equation is formed [5].

$$W_0 = \frac{W_{payload}}{1-\left(\frac{W_f}{W_0}\right)-\left(\frac{W_e}{W_0}\right)} \tag{2.3}$$

In this equation, there are two unknowns, empty weight fraction and fuel fraction. Empty weight fraction can be estimated from historical trends[5]. Fuel fraction can be calculated by mission segments weight fraction.

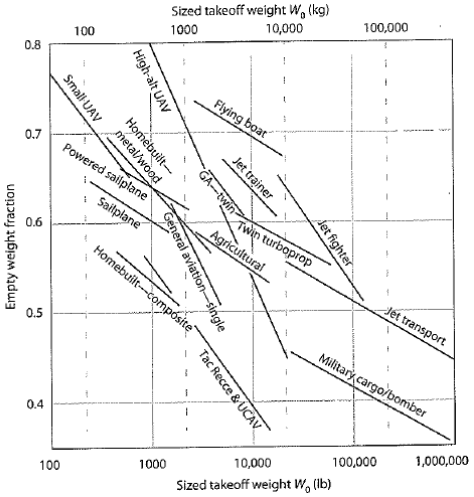

Figure 2.4 Empty weight fraction trends [5]

In fact, Aerial Target UAV is a type of UCAV. An high speed decoy is a subscale UAV which reflects a jet fighter characteristics. They can be considered as a UCAV. Therefore, for empty weight fraction can be assumed as 0.48 from Figure 2.5[5].

Fuel fraction(W_f/W_0) estimation formula is given below[5] assuming that 6% of the fuel is trapped and can not be pumped out of tanks. Ref[8] yields that, the total fuel weight of the aircraft should be 20% more than obtained by range equation.

$$\frac{W_f}{W_0} = 1.06\left(1 - \frac{W_x}{W_0}\right) \quad (2.4)$$

In order to estimate the fuel fraction(W_f/W_0) the mission profile is needed.

Mission profile given for a decoy UAV is given below,

a) 0 - 1: Takeoff at sea level

b) 1 - 2: Climb to 15,000 ft

c) 2 - 3: Cruise to 100km from base at 15,000 ft

d) 3 - 4: Loiter 50 minutes at 15,000 ft

e) 4 - 5: Combat for 10 minutes at 15,000

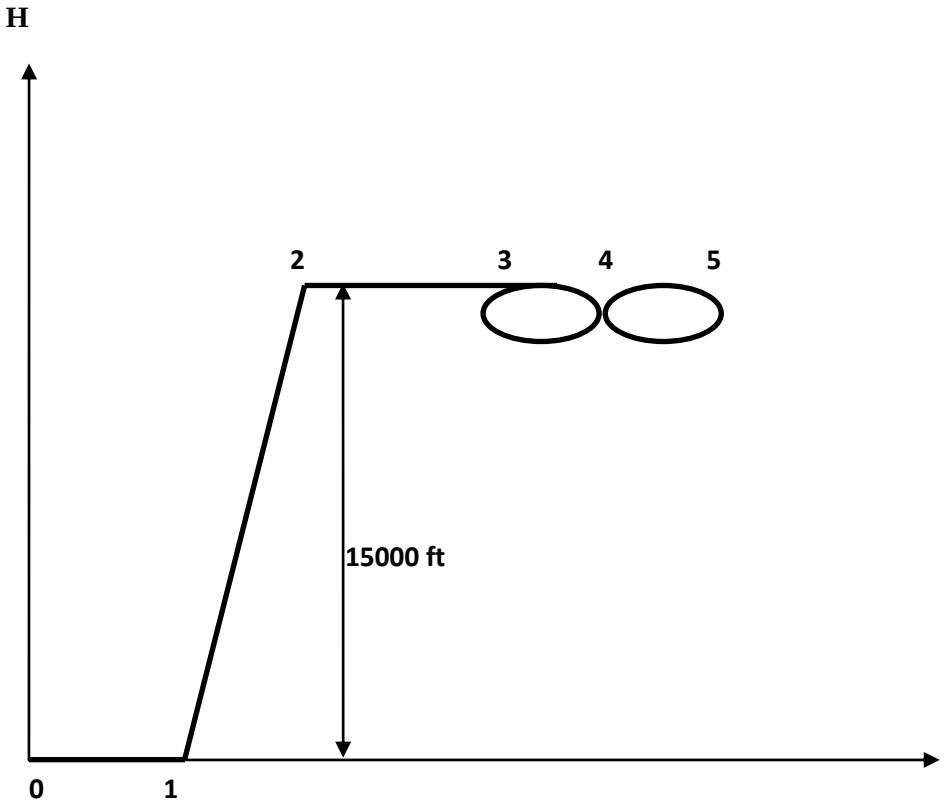

Figure 2.5 High Speed Decoy Mission profile

2.2.1 Mission segments

a) Launch: This is the mission segment in which aircraft takes off from ground. The decoy UAV is going to use a pneumatic catapult. For this mission segment weight fraction is estimated from [8].

$$\frac{W_1}{W_0} = 0.97 \tag{2.5}$$

b) Climb: This is the phase in which aircraft reaches to the cruising condition. The aircraft is assumed to have a launch speed of 45 m/s which comes from Banshee aerial target stall speed[10]. Since climb speed is close to 0.1 Mach, climb weight fraction is given as[5].

$$\frac{W_2}{W_1} = 1.0065 - 0.0325 M_{cruise} \tag{2.6}$$

Cruise speed was initially selected as 350 KTS, M=0.56, W_2/W_1 value becomes 0.9883

c) Cruise: Cruise is the mission segment where aircraft cruises until arrival to combat point.

$$\frac{W_3}{W_2} = e^{-\left(\frac{RC_{cruise}}{V(\frac{L}{D})cruise}\right)} \tag{2.7}$$

Where, R is the cruise range, V is cruise speed and C is the specific fuel consumption at cruise condition, given in the Table A1 in appendices section.

L/D at cruise can be calculated by the following formula[5],

$$(\frac{L}{D})_{cruise} = 0{,}866 * (\frac{L}{D})_{max} \tag{2.8}$$

d) Loiter: Loiter mission weight fraction is given as;

$$\frac{W_7}{W_6} = e^{-(\frac{EC_{loiter}}{(\frac{L}{D})max})} \quad (2.9)$$

Where E is endurance time(sec), L/D_{max} is approximated initially as 13 and the loiter time is selected as 50 mins.

e) Combat

Combat mission segment is defined as;

$$\frac{W_3}{W_2} = 1 - C_{combat}\left(\frac{T}{W}\right)_{combat} * (d) \quad (2.10)$$

Where, d is combat time(sec), and T/W ratio should be given for combat conditions. Initial take off T/W was calculated as from maximum Mach Number(M_{max}) and

$$\left(\frac{T}{W}\right)_{combat} = \left(\frac{T}{W}\right)_{take\ off}\left(\frac{1}{\frac{W_{combat}}{W_0}}\right)\left(\frac{T_{15000ft}}{T_{SL}}\right) \quad (2.11)$$

Initial T/W for take off is calculated as 0.533 from Mmax and T/W for combat is calculated as 0.425 from appendix A2 [5]. T/W of SL is 784N and T/W at altitude is taken as 500N from engine data table. The combat time is given as 10 mins.

Total mission weight fraction is given as;

Table 2.2 Mission Segment weight Fraction for Initial Sizing

W1/W0	W2/W1	W3/W2	W4/W3	W5/W4
0.97	0.9883	0.94687	0.86154	0.84155

$$\frac{W_5}{W_0} = \frac{W_1}{W_0} * \frac{W_2}{W_1} * \frac{W_3}{W_2} * \frac{W_4}{W_3} * \frac{W_5}{W_4} = 0.6729$$

Fuel Fraction is given as,

$$W_f = 1.06 * (1 - \frac{W_5}{W_0})$$

$$W_0 = \frac{22\ lb + 0\ lb}{1 - 0.34673 - 0.48} = 126.97 lb = 57.6\ kg$$

2.3 Wing loading(W/S) and thrust to weight ratio(T/W)

Wing loading and thrust to weight ratio effects the aircraft performance directly. Wing loading indicates how much weight is held by each unit area of the wing whereas Thrust to weight ratio indicates how heavy the aircraft is with respect to engine thrust [8].

2.3.1 Thrust to weight ratio(T/W)

An aircraft with a high T/W can accelerate and climb more rapidly, reach higher maximum speed and perform higher turn rates. A maneuverable high speed decoy should have an high T/W value. First estimation can be made statistically from table 2.12 below.

Table 2.3 T/W0 vs Maximum Mach Number [5]

$T/W_0 = aM_{max}^{C}$	a	C
Jet trainer	0.488	0.728
Jet fighter (dogfighter)	0.648	0.594
Jet fighter (other)	0.514	0.141

According to previous table, for a given 450 kts maximum speed requirement, the initial T/W ratio is calculated as 0.533 the calculation is given in Appendix A2.

After first estimation, this value is calculated from different requirement constraints. Finally, design value is chosen.

2.3.1.1 Cruise speed constraint

According to the method of thrust matching, at cruise condition, thrust should be equal to drag Therefore, T/W should be equal to inverse of L/D.

$$\left(\frac{T}{W}\right)_{cruise} = \frac{1}{\left(\frac{L}{D}\right)_{cruise}} \tag{2.12}$$

2.3.1.2 Maximum speed constraint

T/W at sea level calculation from maximum speed constraint formula is given as[8];

$$\left(\frac{T}{W}\right) = \rho_0 {V_{max}}^2 C_{D_0} \frac{1}{2(\frac{W}{S})} + \frac{2K}{\rho\sigma {V_{max}}^2} (\frac{W}{S}) \tag{2.13}$$

Where σ is given as ratio of altitude air density to sea level density (ρ/ρ_0)

2.3.1.3 Sustained Turn Rate constraint

For a given wing loading, the required T/W ratio is calculated according to the required sustained turn load factor (n_{max}).

$$\left(\frac{T}{W}\right) = \frac{qC_{D0}}{(\frac{W}{S})} + \left(\frac{W}{S}\right)\frac{n^2}{q\pi Ae} \tag{2.14}$$

2.3.2 Wing loading(W/S)

After first wing loading assumption, actual wing loading is calculated considering requirement constraints. Finally, lowest wing loading value is selected for design.

2.3.2.1 Stall speed constraint

Same formula which is used for C_{Lmax} calculation is used for stall speed constraint[8]. Previously, wing loading was assumed and C_{Lmax} value was calculated. For given C_{Lmax} and stall speed requirement, wing loading is calculated.

$$(\frac{W}{S}) = \frac{1}{2}\rho V_s^2 C_{L_{max}} \tag{2.15}$$

2.3.2.2 Catapult take off constraint

Designed aerial target is launched from catapult. Therefore, rather than take off distance, catapult take off wing loading should be calculated.

The catapult take off wing loading is given as[5];

$$(\frac{W}{S})_{takeoff} = \frac{1}{2}\rho(V_{end} + V_{thrust})^2(\frac{C_{L_{max}}}{1.21}) \tag{2.16}$$

2.3.2.3 Maximum jet range and jet loiter constraints

Max jet range formula is given as [5];

$$\frac{W}{S} = q\sqrt{\frac{\pi(AR)eC_{D_0}}{3}} \tag{2.17}$$

Max jet loiter formula is given as [5];

$$\frac{W}{S} = q\sqrt{\pi(AR)eC_{D_0}} \tag{2.18}$$

In this case the oswald efficiency factor must be calculated, for swept aircraft it is calculated from the formula given below[5].

$$e = 4.61(1 - 0.045(AR)^{0.68})(\cos \Lambda_{LE})^{0.15} - 3.1(\Lambda_{LE} > 30deg) \tag{2.19}$$

2.3.2.4 Instantaneous turn constraint

The wing loading for instantaneous turn constraint is given as [5];

$$(\frac{W}{S})_{combat} = \frac{qC_{L_{max}}}{n} \quad (2.20)$$

n is load factor which is going to be discussed later.

2.4 Refined Sizing

In refined sizing, empty weight fraction is calculated because the T/W and W/S are known. The parasitic drag is also updated in every iterations.

In fact, all iterations cannot be shown. Therefore, only last iteration step is shown below, since this is last iteration, the parasitic drag value is from the aerodynamics chapter 2.6 .

Since the T/W, W/S, AR and Mmax is known, the empty weight fraction can be calculated. Empty weight fraction is calculated from following formula[4];

$$\frac{W_e}{W_0} = a + bW_0{}^{c_1} AR^{c_2} * \left(\frac{T}{W_0}\right)^{c_3} \left(\frac{W_0}{S}\right)^{c_4} * M_{max}{}^{c_5}$$

(2.21)

Jet fighter and Jet trainer coefficients were discussed for maneuverable decoy UAV empty weight fraction and the coefficients are given in the following table.[5];

Table 2.4 Empty Weight Fraction vs W_0, AR, T/W_0, W/S and M_{max} coefficients[5]

	a	b	c_1	c_2	c_3	c_4	c_5
Jet Trainer	0	4.28	-0.1	0.1	0.2	-0.24	0.11
Jet Fighter	-0.02	2.16	-0.1	0.2	0.04	-0.1	0.08

The coefficients given above give unaccaptable empty weight fraction values for small UAV W_0 values. Therefore, empty weight fraction for a Decoy UAV cannot be calculated from the Raymer's formula.

Empty weight fraction assumption 0.48 is very close to the previous aerial target design empty weight fractions. Therefore, it was kept unchanged.

The avionics had been neglected at initial sizing part. In refined sizing, avionics were assumed as crew weight which is approximately 2 kg which becomes an extra 4.4lbs.

Table 2.5 Avionic Components[25]

Radio Modem	GPS Receiver	Pitot Tube with Heating	Data Processing Unit of Pitot Tube	Ultrasonic Altimeter
Onboard Antenna	Central Processing Unit	Interface Controller Unit	Onboard Power Controller	GPSR/ GLONASS

2.4.1 Mission segments

Mission segments weight fraction is calculated in appendix A3.

a) **Launch:** Since, the decoy UAV is going to use a pneumatic catapult. For this mission segment weight fractio estimation is increased from 0.97 to 0.99 because the pneumatic catapult system allows to save more energy than conventional take off.

$$\frac{W_1}{W_0} = 0.99 \tag{2.5}$$

b) **Climb:** Climb phase mission weight fraction is same with initial sizing.

$$\frac{W_2}{W_1} = 1.0065 - 0.0325 M_{cruise} \tag{2.6}$$

The cruise velocity altered to M=0.31, W_2/W_1 value becomes 0.996

c) Cruise: Cruise segment mission weight fraction is updated by changing the cruise velocity, parasitic drag.

$$\frac{W_3}{W_2} = e^{-\left(\frac{RC_{cruise}}{V(\frac{L}{D}cruise)}\right)} \tag{2.7}$$

Where, R is the cruise range and C is the specific fuel consumption

Best cruise speed for jet aircraft is found from maximizing $\frac{CL^{(1/2)}}{CD}$ and to maximize the jet range the cruise velocity becomes[4];

$$V_{cruise} = \sqrt{\frac{2(\frac{W}{S})_{cruise}}{\rho}\sqrt{\frac{3}{C_{D_0}\pi(AR)e}}} \tag{2.22}$$

L/D at cruise can be calculated by the following formula[5],

$$(\frac{L}{D})_{cruise} = \frac{1}{\frac{qC_{D_0}}{(\frac{W}{S})_{cruise}} + (\frac{W}{S})_{cruise}\frac{1}{q\pi(AR)e}} \tag{2.23}$$

L/D cruise is updated to 9.86 from calculations in Appendix A6

f) Loiter: Loiter mission weight fraction is given as;

$$\frac{W_4}{W_3} = e^{-\left(\frac{EC_{loiter}}{(\frac{L}{D}loiter)}\right)} \tag{2.10}$$

Where E is endurance time(sec), best loiter speed is calculated from;

$$V_{loiter} = \sqrt{\frac{2(\frac{W}{S})_{loiter}}{\rho}\sqrt{\frac{1}{C_{D_0}\pi(AR)e}}} \tag{2.24}$$

From best loiter speed, q at loiter condition is found and (L/D) at loiter condition is calculated from;

$$(\frac{L}{D})_{loiter} = \frac{1}{\frac{qC_{D_0}}{(\frac{W}{S})_{loiter}} + \frac{(\frac{W}{S})_{loiter}}{q\pi(AR)e}} \tag{2.25}$$

Now, loiter weight fraction can be calculated.

g) Combat:

Combat mission segment is altered by sustained turn rate constraint, T/W at combat condition is updated to 0.506 from the calculations at Appendix A2;

$$\frac{W_5}{W_4} = 1 - C_{combat}\left(\frac{T}{W}\right)_{combat} * (d) \quad (2.12)$$

Where, d is combat time(sec), and T/W ratio should be given for combat conditions.

2.4.2 Weight Calculation

It is reminded here that total take off gross weight is calculated by ;

$$W_0 = \frac{W_{payload}+W_{crew}}{1-\left(\frac{W_f}{W_0}\right)-\left(\frac{W_e}{W_0}\right)} \quad (2.3)$$

Total mission weight fraction is given as;

$$\frac{W_5}{W_0} = \frac{W_1}{W_0} * \frac{W_2}{W_1} * \frac{W_3}{W_2} * \frac{W_4}{W_3} * \frac{W_5}{W_4}$$

Total mission weight fraction is given as;

Table 2.6 Mission Segment weight fractions for Refined Sizing

W1/W0	W2/W1	W3/W2	W4/W3	W5/W4
0.99	0.9965	0.9354	0.8576	0.8112

$$W_0 = \frac{22\ lb + 4.4lb}{1 - 0.38 - 0.48} = 187.97\ lb = 85.26kg$$

2.5 Model Geometry and Airfoil selection

2.5.1 Wing Geometry

In this section, some wing design parameters were chosen and calculated. After considering the catapult, manuever and cruise constraints in the Appendix A2, the wing loading at take off condition is calculated as 23.209 lb/ft^2.

Advantages and disadvantages of high-wing, mid-wing and low-wing wing configuration types were considered. Mid wing configuration was selected considering properties given in Ref[8]. Mid-wing stands in between low-wing and high-wing and yields the properties of both of them. Moreover, it yields the lowest drag coming from wing-body interference minimization.

Wing incidence angle is set 0 degrees for this decoy design since, the wing incidence angle is generally set 0 degrees for Mid-wing jet fighter aircrafts.

Aspect ratio of the wing of high speed decoy is selected 5 and taper ratio value is selected as 0.36 from Firejet and BQM-167A successful aerial target designs. Moreover, according to figure 2.7[4] the induced drag factor makes a minimum for these AR and taper ratio. The taper ratio, wing area, wing sweep angle, aspect ratio values were approximately calculated via handwriting from Ref[9] and Ref[10].

Aspect ratio for wing is given as;

$$AR_{wing} = \frac{b^2}{S_{wing}} \tag{2.26}$$

From AR wing span(b) is found.

Wing loading is calculated from the formula and for this design, this value should have already been calculated from mission requirements . Finally, the wing area is found from the following formula.

$$\left(\frac{W}{S}\right)_{takeoff} = \frac{W_0}{S_w} \tag{2.27}$$

Wing area is given as;

$$S = \frac{(C_r + C_t) * b}{2} \tag{2.28}$$

Taper Ratio increases the lateral stability, reduces the wing weight and gives a better lift distribution. Taper ratio formula is given as;

$$\lambda = \frac{C_t}{C_r} \tag{2.29}$$

For the given taper ratio, mean aerodynamic chord(MAC) is calculated[11];

$$\overline{C} = \frac{2}{3} c_r \frac{1+\lambda+\lambda^2}{1+\lambda} \tag{2.30}$$

The position of the MAC in spanwise direction is given as;

$$\bar{y} = \left(\frac{b}{6}\right) \frac{1+2\lambda}{1+\lambda} \tag{2.31}$$

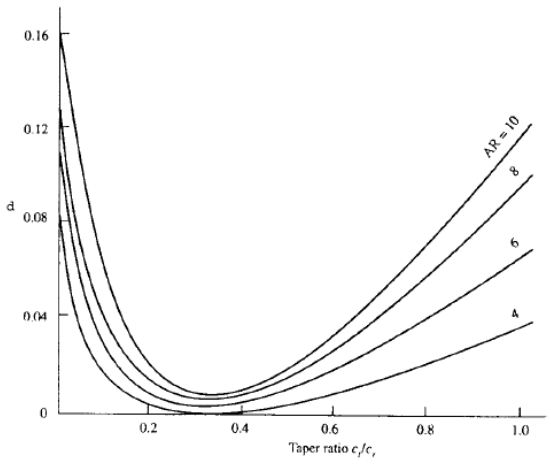

Figure 2.6 Induced drag factor as a function of taper ratio for wings of different AR. [4]

If the aircraft maximum speed is less than 0.3 Mach, wing sweep is not recommended. On the other hand, wing sweep angle is used for high speed aircrafts. Wing sweep brings lots of advantages, it helps to protect from shock formation by increasing the critical mach number (M_{crit}) and curves the streamline flow as shown in figure 2.8 [8].

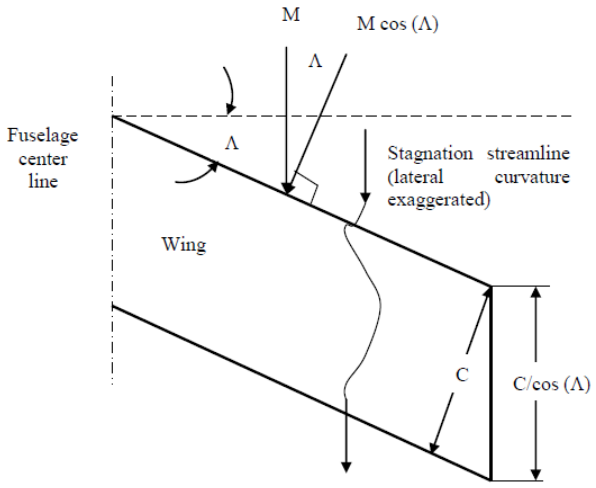

Figure 2.7 Effective of sweep angle of the normal M [8]

The leading edge sweep angle value increases as the aircraft maximum speed increases which is given in Table2.5[8], After considering the values in the table and high speed decoy maximum speed requirement, leading edge sweep angle is chosen as 30 degrees.

Table 2.7 LE sweep angle values for several low and high speed aircrafts [8]

No.	Aircraft	Type	First flight	Max speed (Mach, knot)	Λ_{LE} (deg)
1	Cessna 172	Single-piston engine GA	1955	121 knot	0
2	Tucano	Turboprop trainer	1983	247 knot	4
3	AIRTECH	Turboprop transport	1981	228 knot	3° 51′ 36″
4	ATR 42	Turboprop transport	1984	265 knot	3° 6′
5	Jetstream 31	Turboprop business	1967	Mach 0.4	5° 34′
6	Beech Starship	Turboprop business	1991	Mach 0.78	20
7	DC-9 series 10	Jet passenger	1965	Mach 0.84	24
8	Falcon 900B	Business jet	1986	Mach 0.87	24° 30′
9	Gulfstream V	Business jet	1996	Mach 0.9	27
10	Boeing 777	Jet transport	1994	Mach 0.87	31.6
11	B-2A Spirit	Strategic bomber	1989	Mach 0.95	33
12	MD-11	Jet transport	2001	Mach 0.945	35
13	Boeing 747	Jet transport	1969	Mach 0.92	37° 30′
14	Airbus 340	Jet transport	1991	Mach 0.9	30
15	F-16	Fighter	1974	>Mach 2	40
16	F/A-18	Fighter	1992	>Mach 1.8	28
17	Mig-31	Fighter	1991	Mach 2.83	40
18	Su-34	Fighter	1996	Mach 2.35	42
19	Eurofighter Typhoon	Fighter	1986	Mach 2	53
20	Mirage 2000	Fighter	1975	Mach 2.2	58
21	Concorde	Supersonic jet transport	1969	Mach 2.2	75 inboard 32 outboard
22	Space Shuttle	Spacecraft (flies in air during return mission)	1981	Mach 21	81 inboard 44 outboard

Wing dihedral angle (Γ) gives lateral stability to an aircraft. However, too much stable aircraft results in a reduction in rolling controllability. Wing sweep and high-wing configuration gives naturally positive dihedral whereas, low wing gives naturally negative dihedral effect.Table 2.6 [8] gives hint for the dihedral angle selection. Considering aircraft wing sweep selection, wing configuration and aerial target requirements dihedral angle is chosen as 0 degrees.

Table 2.8 Dihedral angle values for different wing configurations [8]

No.	Wing	Low wing	Mid-wing	High wing	Parasol wing
1	Unswept	5 to 10	3–6	−4 to −10	−5 to −12
2	Low-subsonic swept	2 to 5	−3 to +3	−3 to −6	−4 to −8
3	High-subsonic swept	3 to 8	−4 to +2	−5 to −10	−6 to −12
4	Supersonic swept	0 to −3	1 to −4	0 to −5	NA
5	Hypersonic swept	1 to 0	0 to −1	−1 to −2	NA

High lift devices did not added to the decoy design since, this type of UAV does not take off and land. Designed high speed decoy is launched by special apparatus and landed via parachute.

2.5.2 Fuselage geometry

For initial guess, fuselage length can be initially estimated by the following formula assuming jet fighter coefficients[5];

$$l_{fuselage} = aW_0^c \tag{2.32}$$

However, the actual length of the aerial targets have higher length compared to the calculated values. Some examples are given in the following table;

Table 2.9 Aerial Target Length Deviation Table

Aerial target Name	W_0(kg)	Calculated Length(m)	Actual Length(m)	Difference
BQM-167A	929.86	5.5928	6.09	8.89%
Firejet	145.15	2.71	3.28	21.03%
Banshee Jet	95	2.30	2.95	28.26%
Şimşek	75	2.095	2.30	9.78%
Yperion	45	1.71	2.45	43.27%
Nemisis	33	1.521	2.20	44.64%

Average length difference is calculated as 26%. Therefore, for the calculated W_0 , the aircraft length is calculated approximately as 9.03 ft

Another important parameter for fuselage design is the slenderness ratio value (f). This is the ratio of fuselage length to the maximum diamater of fuselage.

$$f = \frac{l_{fuselage}}{d} \tag{2.33}$$

Slenderness value is chosen as 11 from previous successful aerial target designs which have similar design requirements. Slenderness value of 11 is also close to the jet fighter designs.

2.5.3 Tail Geometry

Tail has three main functions. It provides stability, control and trim. Trim refers to generation of the lift force, by acting through some tail moment arm about the C.G, balances some other moment generated by aircraft[5].

Different tail configurations have been considered. The T-tail configuration has been selected due to simplicity. T-tail offers advantage to have a wake free horizontal tail.Whereas, it offers to have a heavy vertical tail structure to carry the horizontal tail. Fighter tail volume coefficient values are selected from table 2.8[8] assuming that decoy aircraft shows similar characteristics with fighter aircrafts(i.e. Manuever capabilities). Note that as volume coefficient decreases, stability of the aircraft also decreases and therefore, controllability increases.

Table 2.10 Horizontal and Vertical tail volume coefficients [8]

No.	Aircraft	Horizontal tail volume coefficient ($\overline{V}_H$)	Vertical tail volume coefficient ($\overline{V}_v$)
1	Glider and motor glider	0.6	0.03
2	Home-built	0.5	0.04
3	GA single prop-driven engine	0.7	0.04
4	GA twin prop-driven engine	0.8	0.07
5	GA with canard	0.6	0.05
6	Agricultural	0.5	0.04
7	Twin turboprop	0.9	0.08
8	Jet trainer	0.7	0.06
9	Fighter aircraft	0.4	0.07
10	Fighter (with canard)	0.1	0.06
11	Bomber/military transport	1	0.08
12	Jet transport	1.1	0.09

Horizontal tail and vertical tail has been arranged that, part of rudder is out of the wake of horizontal tail.

Tail location can be estimated from following table [8]. This table shows the relation between the total aircraft length and the tail arm.

Table 2.11 Typical values of $l/l_{(fuselage)}$ for different configurations[8]

No.	Aircraft configuration/type	l/L
1	An aircraft whose engine is installed at the nose and has an aft tail	0.6
2	An aircraft whose engine(s) are installed above the wing and has an aft tail	0.55
3	An aircraft whose engine is installed at the aft fuselage and has an aft tail	0.45
4	An aircraft whose engine is installed under the wing and has an aft tail	0.5
5	Glider (with an aft tail)	0.65
6	Canard aircraft	0.4
7	An aircraft whose engine is inside the fuselage (e.g., fighter) and has an aft tail	0.3

From previous table,

$$L_{HT} = 0.3 l_{fuselage} \tag{2.34}$$

$$L_{VT} = 0.3 l_{fuselage} \tag{2.35}$$

2.5.3.1 Horizontal Tail

Horizontal tail generates aerodynamic force to trim the aircraft longitudinally in other words, it is responsible for balancing the moment which is done by the wing.

Horizontal tail is chosen movable tail. Leading edge sweep has been chosen 35 degrees, 5 degrees more than the wing sweep to ensure that critical mach number to avoid elevator control loss because of shock formation. The t/c ratio of airfoil section is selected thinner than the wing t/c to reduce the flow mach number at tail section.

The Aspect ratio of the horizontal tail is selected lower than the wing because, the stall characteristics of a low AR are more smooth as in figure 2.9 Ref[8]. Moreover, bending moment is lower when elevator is deflected. Lower bending moment is desirable.

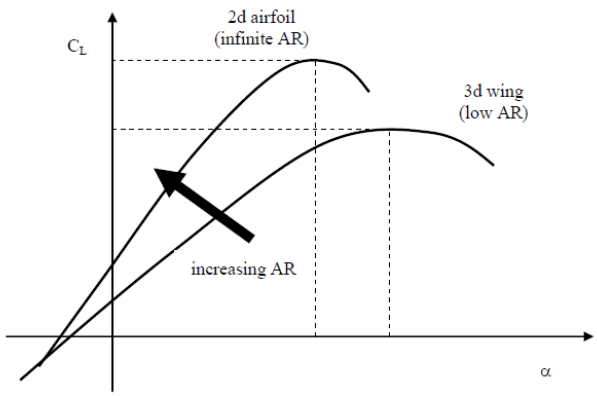

Figure 2.8 Effect of aspect ratio on C_L vs α [8]

Horizontal tail AR;

$$AR_{HT} = \frac{{l_{HT}}^2}{S_{HT}}$$

(2.36)

Horizontal tail AR can be estimated from wing AR as follows[8].

$$AR_{HT} = \frac{2}{3} AR_{wing} \quad (2.37)$$

Horizontal tail volume coefficient is assumed as 0.4 from fighter aircraft assumption from volume coefficients table[8]. The horizontal tail surface area is calculated in appendix A6.1 as 0.152 m^2 and the formula is given below[5];

$$S_{HT} = \frac{c_{HT}\bar{C}_W S_W}{L_{HT}} \quad (2.38)$$

Horizontal tail Mean Aerodynamic Chord;

$$\overline{C_{HT}} = (\frac{2}{3}) c_{rHT} \frac{1+\lambda_{HT}+{\lambda_{HT}}^2}{1+\lambda_{HT}} \quad (2.39)$$

Horizontal taper ratio is selected smaller than wing taper ratio to lower the tail weight. Horizontal tail taper ratio is selected 1/3 and formula of horizontal tail taper ratio is given as;

$$\lambda_{HT} = \frac{C_{t\,HT}}{C_{r\,HT}} \tag{2.40}$$

2.5.3.2 Vertical Tail

Vertical tail generates aerodynamic force to trim the aircraft directionally. Rather than (yawing)directional stability, rudder is a movable part of vertical tail. Therefore, directional control and maneuvering the aircraft is done by vertical tail. Vertical tail and horizontal tail combination should be designed that, at least a third of rudder should be out of the wake for spin recovery.

Like horizontal tail, vertical tail also should have high sweep angle to increase M_{crit} and avoid problems due to shock formation. The vertical tail airfoil section t/c ratio is selected same as horizontal tail to reduce the vertical tail mach number. High lift curve slope airfoil is selected since directional stability derivative is directly related to the lift curve slope of the airfoil of the vertical tail.

Vertical tail AR is chosen as 1.3 from previous fighter aircrafts and Vertical tail AR formula is given as;

$$AR_{VT} = \frac{{l_{VT}}^2}{S_{VT}} \tag{2.41}$$

Vertical tail volume coefficient is assumed as 0.07 from fighter aircraft assumption[8]. The vertical tail surface area is calculated in Appendix A6.2 the calculation formula is given as[5];

$$S_{VT} = \frac{c_{VT} b_W S_W}{L_{VT}} \tag{2.42}$$

Vertical tail mean aerodynamic chord;

$$\overline{C_{VT}} = (\frac{2}{3}) c_{rVT} \frac{1+\lambda_{VT}+{\lambda_{VT}}^2}{1+\lambda_{VT}} \tag{2.43}$$

Taper ratio of vertical tail;

$$\lambda_{VT} = \frac{C_{t\,VT}}{C_{r\,VT}} \tag{2.44}$$

The calculations of geometrical parameters are given in Appendix A4-5-6. Final geometrical parameters of decoy UAV is given below.

Table 2.12 UAV final geometrical parameters(British Units(ft, ft^2, deg, lb))

Wing Parameters:		**Horizontal Tail Parameters:**		**Vertical Tail Parameters:**		**Fuselage Parameters:**	
AR	5	**AR(HT)**	3.33	**AR(VT)**	1.3	Length(ft)	9.03
S(ft^2)	8.1	**S_{HT}**	1.634	**S_{VT}**	1.36	Diameter(ft)	0.821
Cr(ft)	1.87	**Cr $_{HT}$**	1.06	**Cr $_{VT}$**	1.52	Slenderness	11
Ct(ft)	0.674	**Ct $_{HT}$**	0.353	**Ct $_{VT}$**	0.506	**TOGW(lb)**	188
b $_{wing}$(ft)	6.36	**b $_{HT}$**	2.332	**b $_{VT}$**	1.316		
λ Wing	0.36	**λ $_{(HT)}$**	1/3	**λ $_{(VT)}$**	1/3		
M.A.C (wing)(ft)	1.366	**M.A.C $_{(HT)}$**	0.758	**M.A.C $_{(VT)}$**	1.095		
Spanwise Direction(ft)	1.342	**Λ $_{LE\ HT}$**	35	**Λ $_{LE\ VT}$**	35		
Λ $_{LE}$	30	**Λ $_{Maxt\ HT}$**	27.32	**Λ $_{Maxt\ VT}$**	24.82		
Λ $_{c/4}$	25.8	**Λ $_{c/2}$**	21.26				
Λ $_{tmax}$	23.11						

2.5.4 Control Surfaces

Control surfaces are movable parts of wing and tail and these surfaces are used to control the aircraft. These control surfaces also contributes to trim.

Stability and controllability are the two key factors when designing control surfaces. Manueverability is significant for fighter aircrafts and high speed decoy UAV's. Therefore, the controllability should be focused on more than stability. Primary control surfaces are ailerons, elevators and rudders. In fact, the design of these control surfaces are complicated. Therefore, the fighter aircraft coefficients and previous high speed target UAV design coefficients were considered.

2.5.4.1 Aileron

The rolling moment generated by ailerons are related to its size, deflection and distance from the centerline of the fuselage. From historical guidelines figure, the span and chord of the aileron can be estimated.

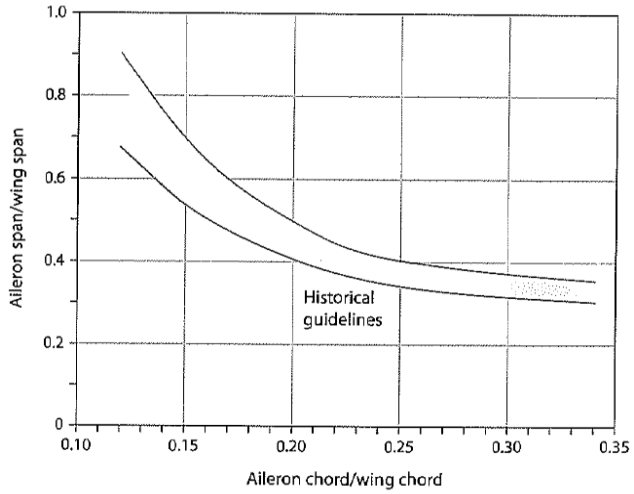

Figure 2.9 guidelines of the span and chord of ailerons [5]

Although previous figure gives hint, estimated parameters of previous high speed aerial target designs helps to finalize the parameters. The Firejet[9] and Yperion[25] aerial target have $C_{aileron}/C$ an approximate handwriting calculation from aircraft pictures have value of 0.266 and 0.2465 respectively and $b_{aileron}/b_{wing}$ value of 0.38 and 0.313 respectively.

From the combination of the informations given by the curve and successful aerial target designs, the $C_{aileron}/C$ value is chosen 0.25 and $b_{aileron}/b_{wing}$ is chosen 0.38.

2.5.4.2 Elevator and Rudder

Elevators are the movable part of the horizontal tail. The longitudinal control is handled by elevators. when elevators are deflected, the pitch rate of the aircraft is changed. Rudders on the other hand, are the movable part of the vertical tail. When rudders are deflected, yawing moment is generated. Therefore, the directional control can be achieved.

Table 2.10 from Ref[5] suggests rudder and elevator size estimations. After making Fighter assumption,

Table 2.13 Elevator and Rudder chord values[5]

Aircraft	Elevator(C_e/C)	Rudder C_r/C
Fighter/attack	0.30	0.30
Jet Trainer	0.35	0.35
Jet Transport	0.25	0.32

The high speed decoy has a movable horizontal tail, there is no need for elevators. The aerial targets such as, Yperion, BQM-167A, BQM-177A and Nemisis have also no elevators.

To check the 0.3 estimation by fighter assumption, C_{rudder}/C of the Firejet and BQM-167A have been approximately calculated. Firejet and BQM-167A C_{rudder}/C value is approximately 0.315 and 0.25 respectively. Therefore 0.3 assumption can be used for new high speed decoy design.

Control surface parameters calculation is given in Appendix A7. The final control surface parameters are given as;

Table 2.14 Control Surface Parameters of High Speed Decoy UAV

Aileron:		**Rudder:**	
b $_{aileron}$(ft/m)	2.42/0.736	**l $_{rudder}$(ft/m)**	0.921/0.28
c $_{aileron}$(ft/m)	0.342/0.1	**C $_{rudder}$(ft/m)**	0.274/0.08

2.5.5 Airfoil Selection

Airfoil effects the aircraft performance such as cruise speed, stall speed, handling qualities and overall aerodynamic efficiency[5]. Airfoil can be defined as the 2-D profile of the wing. Optimum pressure distribution can be achieved on the upper and lower surfaces by choosing the right airfoil. Right airfoil can be chosen if the design lift coefficient $C_{l(ideal)}$, $C_{l(max)}$, operating Reynolds number (RE) and design Mach

number is known. $C_{l(ideal)}$ and $C_{l(max)}$ are calculated by using the formula for a given wing loading,

$$W = L = qSC_L \tag{2.45}$$

$$C_{L(ideal)} = \frac{1}{q_{(cruise)}}\left(\frac{W}{S}\right) \tag{2.46}$$

Since, wing sweep lowers the lift distribution for a 3-D wing, higher airfoil design lift coefficient is needed. The ideal lift coefficient is calculated as 0.236 in Appendix A9

$$C_{L_{ideal}} = 0.9C_{l_{ideal}}cos\Lambda_{0.25c} \tag{2.47}$$

$$C_{l_{ideal}} = \frac{C_{L_{ideal}}}{0.9cos\Lambda_{0.25c}} \tag{2.48}$$

To gel maximum lift coefficient the stall velocity condition is considered.

$$C_{L_{max}} = \frac{1}{q_{stall}}\left(\frac{W}{S}\right) \tag{2.49}$$

After finding C_{Lmax}, the airfoil lift coefficient is found from the formula

$$C_{L_{max}} = 0.9C_{l_{max}}cos\Lambda_{0.25c} \tag{2.50}$$

$$C_{l_{max}} = \frac{C_{L_{max}}}{0.9cos\Lambda_{0.25c}} \tag{2.51}$$

Reynolds number and Mach number are given as,

$$Re_{cruise} = \frac{\rho\, V\, \bar{c}}{\mu} = \frac{V\, \bar{c}}{\nu} \tag{2.52}$$

$$M = \frac{v}{a} \tag{2.53}$$

Airfoil thickness(t/c) and Drag coefficient parameter(C_d) values are also considered when choosing an airfoil, thinner airfoils show less drag values for given high mach numbers and therefore reduces critical mach number(M_{crit}). Figure 2.11 shows the drag values for different t/c ratio as mach number increases.

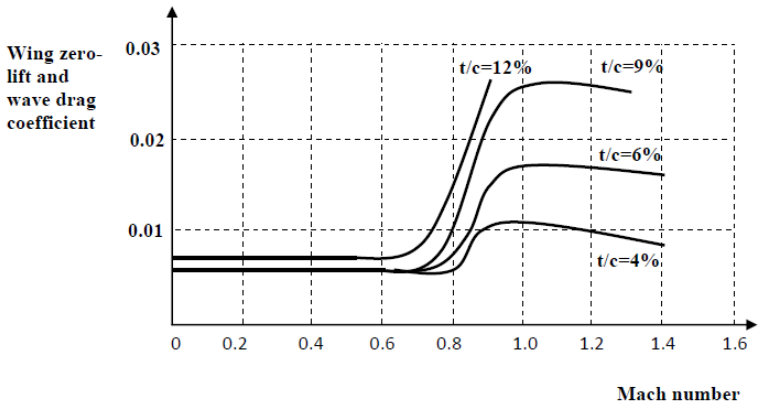

Figure 2.10 Airfoil Drag Rise Data [10]

For our case, thickness ratio is chosen 12% from historical trendline. Given in Fig2.12[5].

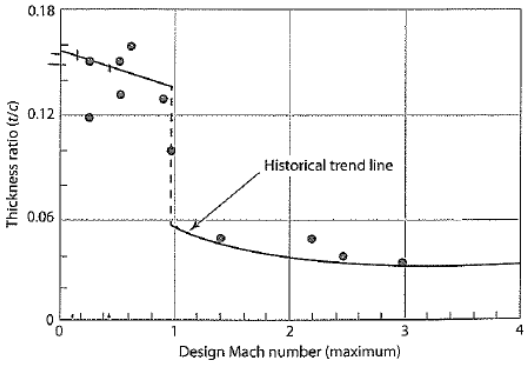

Figure 2.11 Historical trendline for t/c ratio [5]

Total force coefficients(C_l and C_d) and moment coefficient(C_m) results the total integrated pressure distribution[2]. In this section, different airfoil performances were compared by using XFLR5 programme after calculating and choosing $C_{l(design)}$, t/c, $C_{l(max)}$,$C_{l(ideal)}$ for given M and Re values. XFLR5 is a airfoil design and analysis programme like XFoil. In Fact, XFOIL was translated from Fortran language to the C++ language and integrated in the program XFLR5[27].

$C_{d(min)}$, C_m, stall angle (α_{stall}), C_l/C_d, and stall smoothness have been considered during the airfoil selection proces.

The comparison is given in table 2.11 Due to high $(C_l/C_d)_{max}$,high $C_{l(\alpha)}$,high $C_{l(Max)}$ and accurate $C_{l(ideal)}$ value which is calculated as 0.3 in Appendix A9.1.2, NACA 63-412 Airfoil has been selected. NACA 63-412 airfoil has a maximum thickness at 34.9% of the chord and it has a 2.2% maximum camber at 50% of the chord.

Table 2.15 Airfoil Comparison Table

Airfoil	$NACA64_{(1)}$-112	$NACA65_{(1)}$-212	NACA65-210	$NACA66_{(1)}$-212	$NACA65_{(1)}$-412	NACA63-412
$C_{l(\alpha)}(deg^{-1})$	0.12	0.10667	0.10667	0.10715	0.12	0.12
$C_{d(min)}$	0.01	0.009	0.009	0.0096	0.007	0.005
$(C_l/C_d)_{max}$	60-80	60-80	55-75	55-70	70-90	70-90
$(t/c)_{max}$	12%	12%	10%	12%	12%	12%
$C_{l(Max)}$	1.19-1.3	1.19-1.3	1.05-1.3	1.1-1.25	1.3-1.5	1.36-1.55
C_m	-0.0234	-0.04	-0.04	-0.035	-0.08	-0.08
$C_{l(ideal)}$	0.1	0.2	0.2	0.2	0.35	0.35

For horizontal and vertial tail, a symmetric airfoil NACA 0009 smoothed has been selected.

Table 2.16 Airfoils of Wing and Tails of the Highspeed Decoy UAV

	Wing	**Horizontal Tail**	**Vertical Tail**
Airfoil Type	**NACA 63-412**	**Naca 0009 sm-il**	**Naca 0009 sm-il**
Thickness to Chord Ratio	**0.12**	**0.09**	**0.09**
Max Thickness Location	**34.9%**	**30.9%**	**30.9%**

2.6 Aerodynamics

2.6.1 Lift Coefficient

At airfoil choosing section, lift coefficient calculations were considered. The ideal and maximum lift coefficient values are given as,

$$C_{L_{ideal}} = 0.9C_{l_{ideal}} cos\Lambda_{0.25c} \tag{2.47}$$

$$C_{L_{max}} = 0.9C_{l_{max}} cos\Lambda_{0.25c} \tag{2.50}$$

2.6.2 Lift curve slopes

The lift curve slope of the wing is given as;

$$C_{L_\alpha} = \frac{2\,\pi\,(AR)}{2+\sqrt{4+\frac{(AR)^2\,\beta^2}{\eta^2}\left(1+\frac{tan^2(\Lambda_{max\,t})}{\beta^2}\right)}} \left(\frac{S_{exposed}}{S_{ref}}\right) F \tag{2.54}$$

Where,

$$\beta = \sqrt{1-M^2} \tag{2.55}$$

$$M = \frac{V}{a} \tag{2.53}$$

$$F = 1.07\,(1+\frac{D_{fuselage}}{l_{fuselage}})^2 \tag{2.56}$$

$$\eta = 0.95$$

Lift curve slope is varied with mach number,

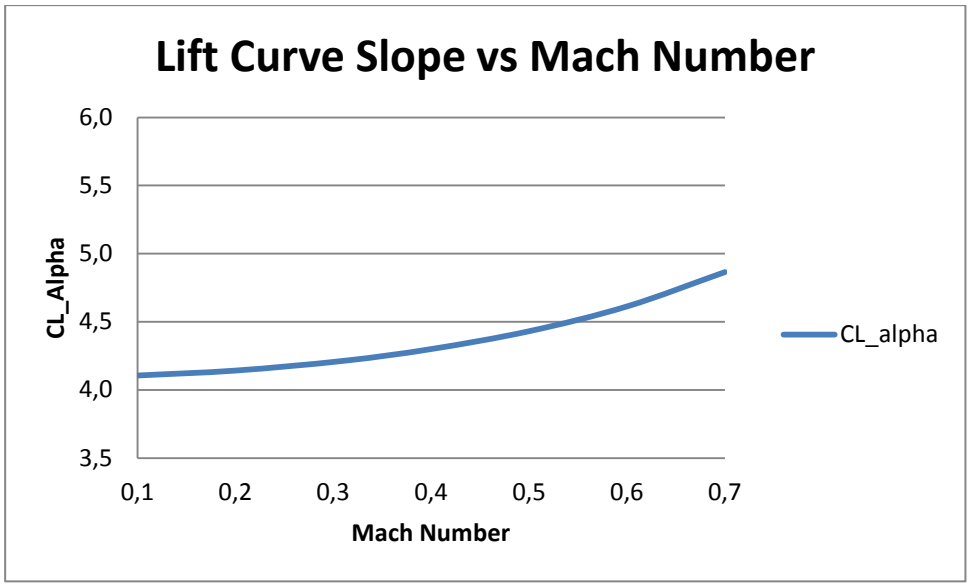

Figure 2.12 Lift Curve Slope versus Mach Number

The lift curve slope of horizontal tail is given as;

$$C_{L_{\alpha\,HT}} = \frac{2\,\pi\,(AR_{HT})}{2+\sqrt{4+\frac{(AR_{HT})^2\,\beta^2}{\eta^2}\left(1+\frac{tan^2\left(\Lambda_{c/2HT}\right)}{\beta^2}\right)}}\left(\frac{S_{exposed\,HT}}{S_{refHT}}\right)F \tag{2.57}$$

2.6.3 Drag coefficient

Total drag coefficient value can be found by summing the parasitic drag and the drag due to lift.

$$C_D = C_{D_0} + K{C_L}^2 \tag{2.58}$$

Drag due to lift component can be found

Where, K is the oswald span efficiency factor,

2.6.3.1 Parasitic Drag coefficient

For parasitic drag C_{D0} estimation, there are two methods, initially equivalent skin friction method has been used because the geometry of the aerial target was unknown. Assuming the(equivalent skin friction coefficient (C_{fe}) value 0.0035(air force fighter assumption) [5] , the initial parasitic drag value has been calculated as 0.014 in Appendix A1 and formula is given below ;

$$C_{D_0} = C_{f_e} \frac{S_{wet}}{S_{ref}} \tag{2.59}$$

Other method to determine the parasitic drag coefficient is the component buildup method. Formula for subsonic aircrafts is given as[5];

$$C_{D_0} = \frac{\sum(C_{f_c} FF_c Q_c S_{wet_c}}{S_{ref}} + C_{D_{misc}} + C_{D_{L\&P}} \tag{2.60}$$

For the high speed aerial target, wings,tails and fuselage are assumed to have turbulent flow. Therefore, for turbulent flow, flat plate skin friction coefficient formula is given as[5];

$$C_f = \frac{0.455}{(log_{10}R)^{2.58}(1+0.144M^2)^{0.65}} \tag{2.61}$$

Form factor (FF) for wing, tail, strut and pylon is found from following formula[5];

$$FF = \left[1 + \frac{0.6}{\left(\frac{x}{c}\right)_m}\left(\frac{t}{c}\right) + 100\left(\frac{t}{c}\right)^4\right][1.34M^{0.18}(cos\Lambda_m)^{0.28}] \tag{2.62}$$

Form factor(FF) for fuselage and smooth canopy;

$$FF = (1 + \frac{60}{f^3} + \frac{f}{400}) \tag{2.63}$$

Where f is the slenderness ratio.

In the high speed decoy, there is no flaps and landing gear. Therefore, their drag components are neglected. The parasitic drag coefficient is initially calculated as 0.0196 for 0.31M cruise velocity and the calculation is given in Appendix A9.3. In

fact, parasitic drag alters for different mach numbers. Parasitic drag vs mach number at cruise altitude is given in the next figure.

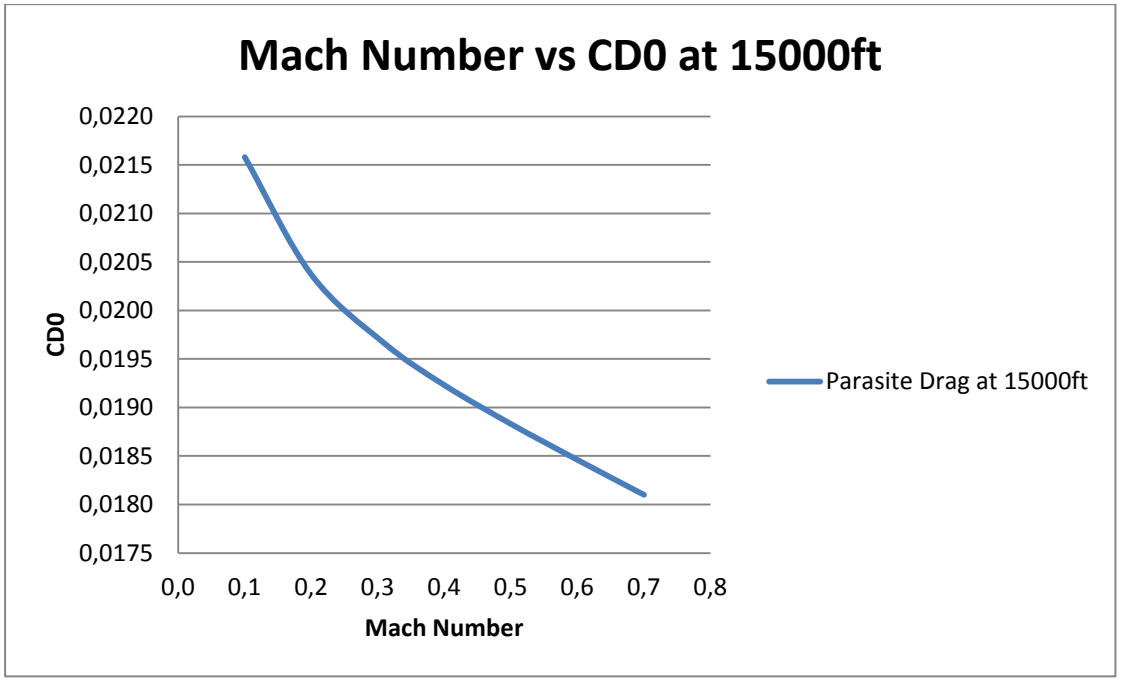

Figure 2.13 Parasite Drag Coefficient vs Mach Number at Cruise Altitude

2.6.3.2 Drag Due To Lift

For initial estimation, K value can be calculated from Oswald span efficiency method.

$$K = \frac{1}{\pi(AR)e} \tag{2.64}$$

K value is approximated as 0.079. The calculation is given in Appendix A1.

Better approximation can be made from the leading edge suction method[5]. In this method, K varies with C_L value. K value ranges between K_0 and K_{100} according to the equation below.

$$K = SK_{100} + (1 - S)K_0 \tag{2.65}$$

Where,

$$K_{100} = \frac{1}{\pi AR} \tag{2.66}$$

$$K_0 = \frac{1}{C_{L_\alpha}} \tag{2.67}$$

Where S is leading edge suction factor, S values are chosen from figure below.

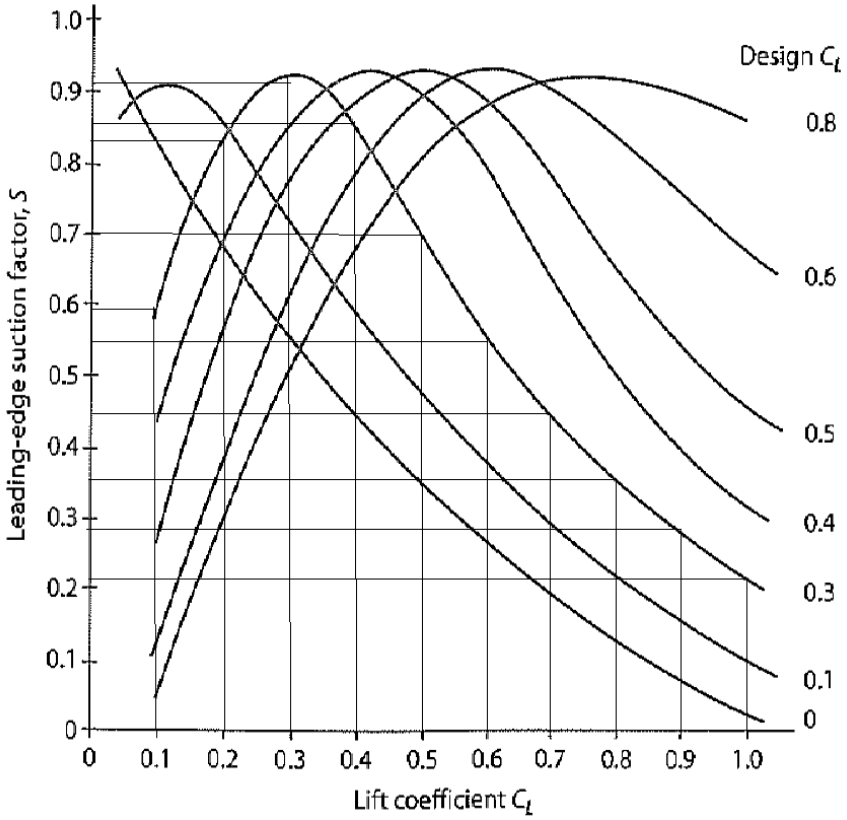

Figure 2.14 Typical design goal values for supersonic aircraft, leading edge suction vs C_L [4]

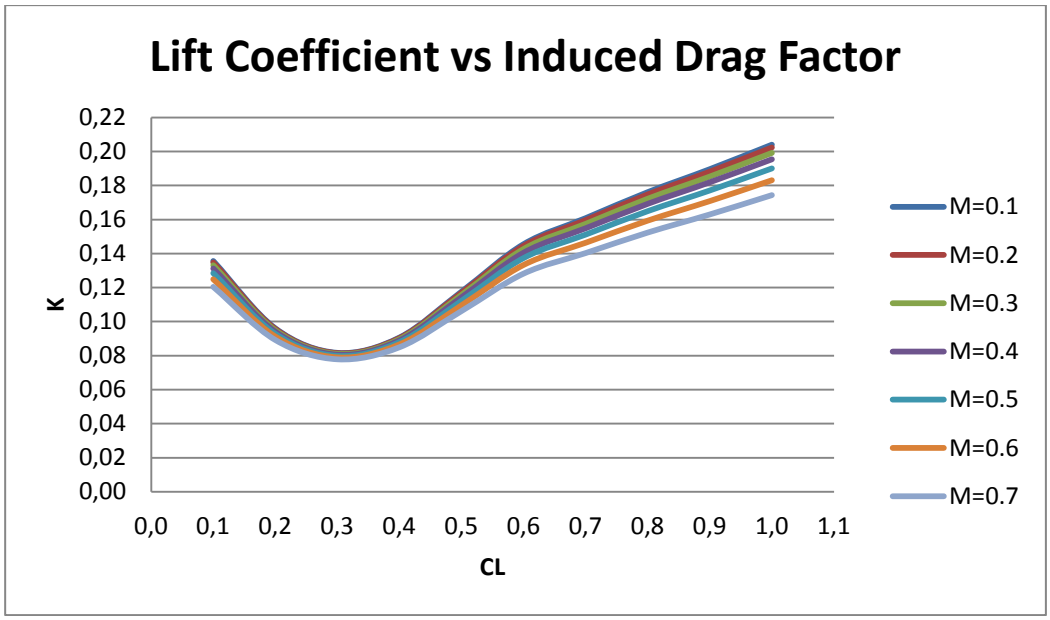

Figure 2.15 Lift Coefficient versus Induced Drag Factor for Different Mach Numbers

Since the parasite drag CD0 vs mach number and induced drag factor K vs mach number are found, total drag is found from leading edge suction method K values and the drag polar curve is plotted at cruise altitude.

$$C_D = C_{D_0} + K{C_L}^2 \tag{2.58}$$

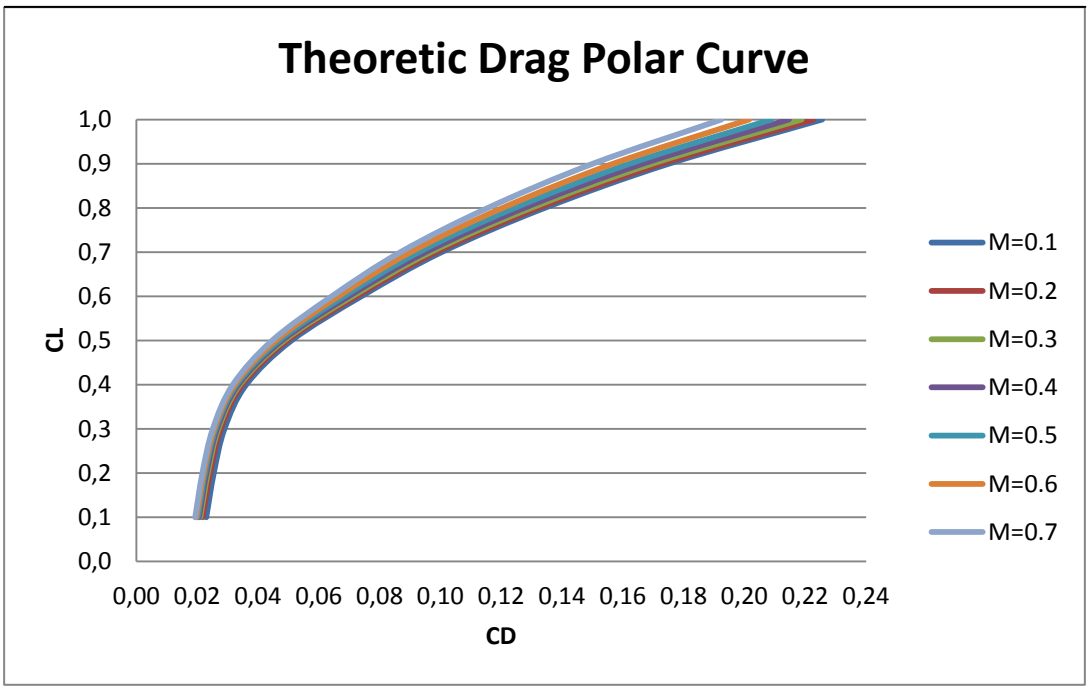

Figure 2.16 Theoretic Drag Polar Curve for Different Mach Numbers

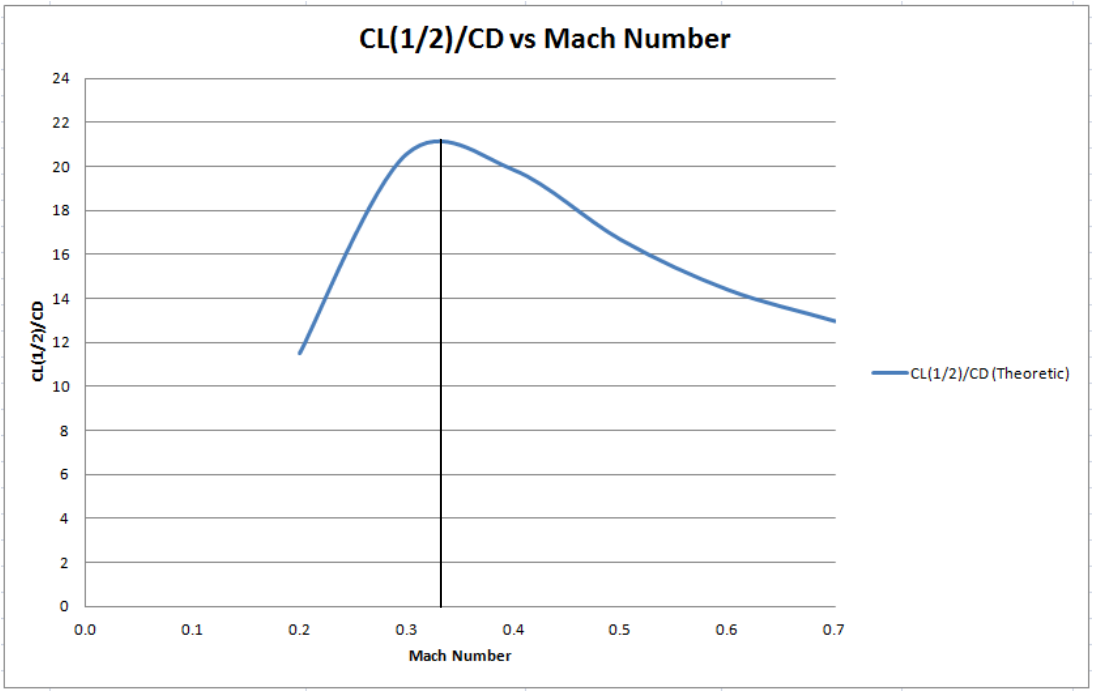

Figure 2.17 Theoretic CL(1/2)/CD curve for Different Mach Numbers

Theoretical curves claim that 0.32 M is the most efficient cruise velocity.

2.6.4 Downwash Factor

$\frac{\partial \varepsilon}{\partial \alpha}$ arises due to wing trailing vortex contributions to the downwash of the tail. This will be computed using Appendix A9.2.3 in Ref[11].

$$\frac{\partial \varepsilon}{\partial \alpha} = 4.44[K_A * K_\lambda * K_H * \left(Cos\Lambda_{\frac{c}{4}}\right)^{0.5}]^{1.19} \tag{2.68}$$

Where,

$$K_A = \frac{1}{A} - \frac{1}{1+A^{1.7}} \tag{2.69}$$

$$K_\lambda = \frac{10-3\lambda}{7} \tag{2.70}$$

$$K_H = \frac{1-\frac{h_{HT}}{b}}{(\frac{2*L_{HT}}{b})^{\frac{1}{3}}} \tag{2.71}$$

Aerodynamic calculations are given in Appendix A5, the aerodynamic parameters of UAV are given below.

Table 2.17 Aerodynamic Parameters of UAV

$C_{l\ cruise}$	**0.291**	**$C_{L\alpha}$ (deg^{-1})**	**0.078**	**V_{stall} (ft/s)(KTS)**	**143.46/84.7**
$C_{l\ max}$	**1.173**	**$C_{l\alpha}$ (deg^{-1})**	**0.12**	**V_{loiter} (ft/s)(KTS)**	**238.44/141**
C_{D0}	**0.0196**	**$C_{Ldesign}$**	**0.236**	**V_{cruise} (ft/s)(KTS)**	**323.232/191.4**
$C_{D\ cruise}$	**0.024**	**C_{Lmax}**	**1.0935**	**V_{max}(ft/s)(KTS)**	**759.5 / 450**
L/D cruise	**9.86**	**L/D_{max}**	**12.72**	**V_{combat}(ft/s)(KTS)**	**452 / 267**
$W/S_{(take\ off)}$	**23.209**	**$T/W_{(take\ off)}$**	**0.635**		

2.7. Performance

2.7.1 Thrust Required and Available Thrust

In order to calculate the required thrust, one should equate it to drag. Formula is given as[4],

$$D = T = \frac{1}{2}\rho V^2 S C_D \tag{2.72}$$

The available thrust is the given Nike turboengine thrust in Ref[12].

2.7.2 L/D Ratio

L/D ratio is given as;

$$\left(\frac{L}{D}\right) = \frac{\frac{1}{2}\rho V^2 S C_L}{\frac{1}{2}\rho V^2 S C_D} = \frac{C_L}{C_D} = \frac{C_L}{C_{D_0} + \frac{{C_L}^2}{\pi(AR)e}} \tag{2.73}$$

L/D ratio during cruise is found from polar curve. It alters for different cruise mach number.

2.7.3 Stall Velocity

From previous wing loading calculations, stall velocity can be obtained as[4];

$$V_{stall} = \sqrt{\frac{2}{q_{stall}}\left(\frac{W}{S}\right)\frac{1}{(C_{L_{max}})}} \tag{2.74}$$

2.7.4 Rate of Climb (ROC)

ROC is given as the excess power divided by the aircraft weight, ROC is given as[4];

$$ROC = \frac{Excess\ power}{W} = \frac{(T-D)V_{\infty}}{W} \tag{2.75}$$

The maximum rate of climb is given as;

$$ROC_{max} = \sqrt{\frac{\left(\frac{W}{S}\right)Z}{3\rho_{\infty}C_{D_0}}}\left(\frac{T}{W}\right)^{\left(\frac{3}{2}\right)}\left[1 - \frac{Z}{6} - \frac{3}{2\left(\frac{T}{W}\right)^2\left(\frac{L}{D}\right)_{max}^{\ 2}Z}\right] \tag{2.76}$$

Where $Z = 1 + \sqrt{1 + \frac{3}{\left(\frac{L}{D}\right)_{max}^{\ 2}\left(\frac{T}{W}\right)^2}}$

2.7.5 Turn Performance

2.7.5.1 Load Factor

The load factor (n) is defined as the ratio of lift to weight. The load factor formula is given as[4];

$$n = \frac{L}{W} = \frac{\frac{1}{2}\rho V^2 C_L S}{W} \tag{2.77}$$

The maximum load factor is found from same formula at maximum lift coefficient;

$$n_{max} = \frac{\frac{1}{2}\rho V^2 C_{L_{max}} S}{W} \tag{2.78}$$

Maximum load factor for a given (T/W), (W/S) and velocity V is given as[4];

$$n_{max} = \sqrt{[\frac{\frac{1}{2}\rho V^2}{K(\frac{W}{S})}\left[\left(\frac{T}{W}\right)_{max} - \frac{1}{2}\rho V^2 \frac{C_{D_0}}{(\frac{W}{S})}\right]]} \quad (2.79)$$

The corner velocity at given altitude is given as;

$$V^* = \sqrt{\frac{2n_{max}}{\rho(C_{L_{max}})}\frac{W}{S}} \quad (2.80)$$

2.7.5.2 Minimum Turn Radius

Minimum Turn Radius formula is given as[4];

$$R_{min} = \frac{{V_{combat}}^2}{g*\sqrt{n^2-1}} \quad (2.81)$$

2.7.5.3 Maximum Sustained Turn Rate

Maximum turn rate is given as[4];

$$\omega_{max} = \frac{g*\sqrt{n^2-1}}{V_{combat}} \quad (2.82)$$

2.7.5.4 Pull up and Pull down Instantaneous Turn Rate Manuevers

For pull up manuever,

Turn radius is given as[4];

$$R = \frac{V^2}{g(n-1)} \quad (2.83)$$

Instantaneous turn rate;

$$\omega = \frac{g(n-1)}{V} \quad (2.84)$$

Corner velocity;

$$V_{corner} = \sqrt{\frac{2n_{max}}{\rho * C_{L_{max}}} * (\frac{W}{S})_{combat}} \quad (2.85)$$

For pull down manuever,

Turn radius is given as;

$$R = \frac{V^2}{g(n+1)} \tag{2.86}$$

Instantaneous turn rate;

$$\omega = \frac{g(n+1)}{V} \tag{2.87}$$

Table 2.18 Performance Values of the High Speed Decoy UAV

Max Rate of Climb (ft/s) / (m/s)	**188.85 / 57.561**	**Pull up instantaneous turn rate(rad/s) / (deg/s)**	**0.57 / 32.658**
Min.Turn Radius in combat:(ft) / (m)	**1074/ 409 m**	**Pull up instantaneous turn radius(ft) / (m)**	**996.08 / 303.605**
Max Turn rate at combat (rad/s)/(deg/s)	**0.42 / 24.115**	**Pull down instantaneous turn rate(rad/s) / (deg/s)**	**0.711 / 40.737**
Max. Load factor for sustained turn rate	**6**	**Pull down instantaneous turn radius(ft) (m)**	**635 / 193.55**
Max. Load factor for instantaneous turn rate	**9**	**Corner Velocity(ft/s) / (m/s)**	**450 / 137**

2.8 C.G and Stability

2.8.1 C.G Determination

Designed UAV has been drawn in Catia v5 software. The coordinate system reference point(0.0.0) is located on the nose. Because of this reason, location of Y_{cg} is 0 for inner components of the aircraft.

Placement of the components were made and shown below:

Table 2.19 X_{cg} and Y_{cg} location for different components of Full aircraft

Components	Weight (lbs) / (kg)	Location of X_{cg} (*ft*) / (m)	Location of Y_{cg} (*ft*) / (m)
Wings	26.121 / 11.85	5.255 / 1.601	0.026 / 0.008
Payload+Avionics	26.47 / 12	1.23 / 0.375	0 / 0
Fuselage	9.27 / 4.205	4.577 / 1.395	-0.075 / -0.023
Engine	23.32 / 10.58	8.234 / 2.51	0 / 0
Vertical Tail	2.787 / 1.264	8.24 / 2.511	0.766 / 0.233
Horizontal Tail	2.3 / 1.05	8.80 / 2.682	1.268 / 0.3865
Fuel Tank	11.55 / 5.238	4.475 / 1.364	0 / 0
Fuel	71.345 / 32.361	4.475 / 1.364	0 / 0
All Else Empty	16.337 / 7.41	1.83 / 0.557	0 / 0
Total:	188.706 /	4.475 / 1.364	0.026 / 0.008

Fuel tank is placed on the C.G of the aircraft. Therefore, static margin will remain unchanged for full fuel and empty aircraft.

Table 2.20 X_{cg} and Y_{cg} location for different components of Empty aircraft

Components	Weight (lbs) / (kg)	Location of X_{cg} (*ft*) / (m)	Location of Y_{cg} (*ft*) / (m)
Wings	26.121 / 11.85	5.255 / 1.601	0.026 / 0.008
Payload+Avionics	26.47 / 12	1.23 / 0.375	0 / 0
Fuselage	9.27 / 4.205	4.577 / 1.395	-0.075 / -0.023
Engine	23.32 / 10.58	8.234 / 2.51	0 / 0
Vertical Tail	2.787 / 1.264	8.24 / 2.511	0.766 / 0.233
Horizontal Tail	2.3 / 1.05	8.80 / 2.682	1.268 / 0.3865
Fuel Tank	11.55 / 5.238	4.475 / 1.364	0 / 0
Fuel	0 / 0	4.475 / 1.364	0 / 0
All Else Empty	16.337 / 7.41	1.83 / 0.557	0 / 0
Total:	117.361 / 53.234	4.475 / 1.364	0.042 / 0.0128

2.8.2 Stability Analysis

In pitching moment stability analysis, neutral point is responsible for the aircraft is statically stable or not.

Aerial targets are very highly agile aircrafts and does not need to be stable. However, in our case, in prototype production, aircraft is preferred as stable. Therefore, initially the C.G has been arranged to achieve a stable aircraft.

Neutral point is calculated as[5];

$$\bar{X}_{np} = \frac{C_{L_\alpha}\bar{X}_{acw} - C_{m_{\alpha fus}} + \eta_h \frac{S_h}{S_w} C_{L_{\alpha h}} \frac{\partial \alpha_h}{\partial \alpha} \bar{X}_{ach}}{C_{L_\alpha} + \eta_h \frac{S_h}{S_w} C_{L_{\alpha h}} \frac{\partial \alpha_h}{\partial \alpha}} \quad (2.88)$$

Where, fuselage factor is calculated as;

$$C_{m_{\alpha fus}} = \frac{K_{fus} * {W_f}^2 * L_f}{\bar{c} * S_w} \quad (2.89)$$

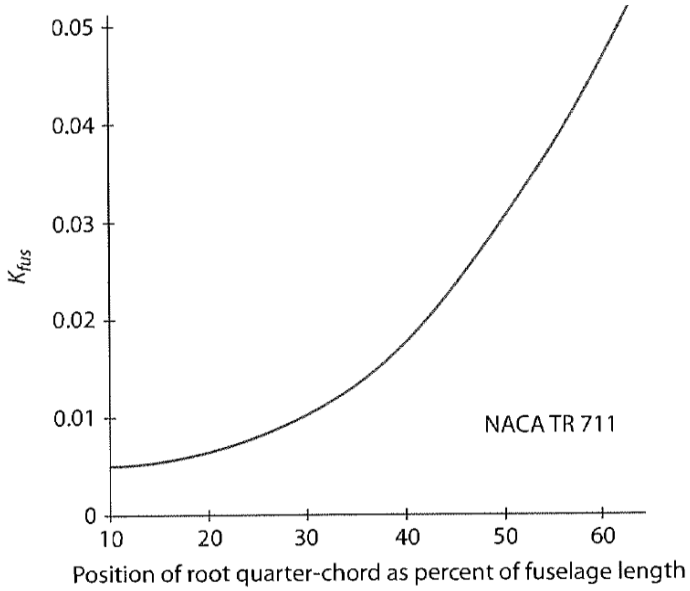

Figure 2.18 Fuselage Moment Term [5]

From figure above, Moment term is selected as 0.055 deg $^{-1}$. Maximum width of fuselage is 1.1 ft.

The $C_{L\alpha wing}$ and $C_{L\alpha wing}$ were calculated as 0.077 deg $^{-1}$ and 0.028 deg $^{-1}$ in aerodynamics chapter. Fuselage term is calculated as 0.0543 deg $^{-1}$. The fuselage term and static margin calculation is given in the Appendix A11.

$C_{L\alpha}$ values vary with mach number as a result, the static margin also varies with mach number.

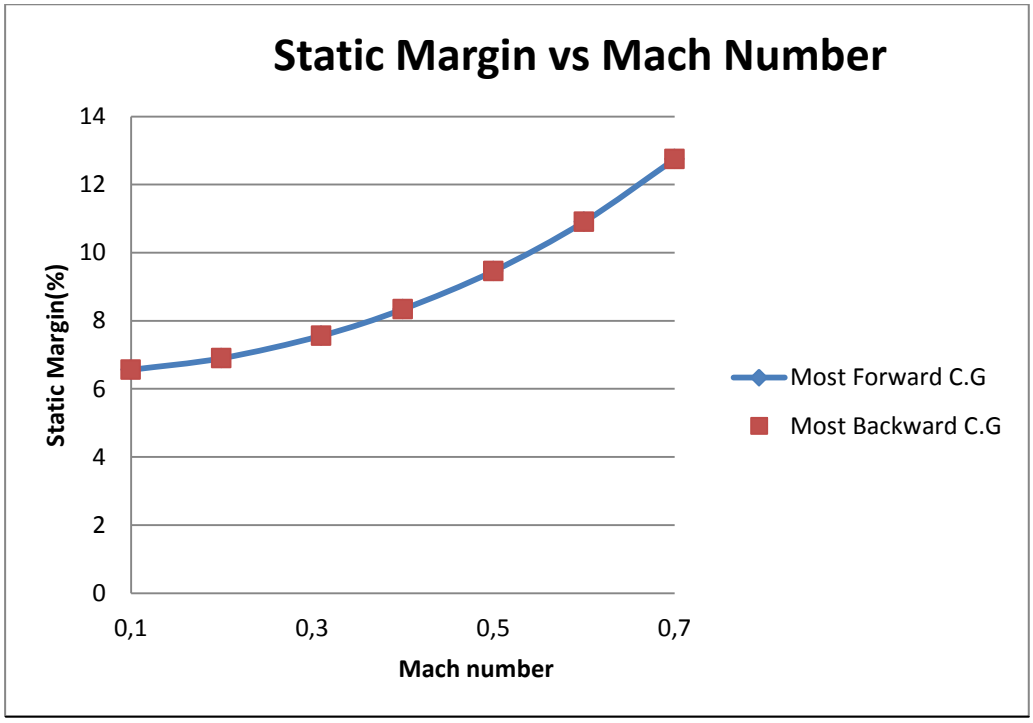

Figure 2.19 Static Margin vs Mach Number

2.9 Propulsion

2.9.1 Fuel Tank Design

Fuselage shape of the high speed decoy UAV is cylindrical. Therefore, the fuel tank shape of this UAV is chosen as cylindrical shape to fit the fuselage shape. The fuel weight was calculated as 32.6 kg and volume of the fuel was calculated in appendix A6 as ;

$$V_f = \frac{W_f}{\rho_f} \tag{2.90}$$

The fuel volume is calculated as 0.0402 m^3

The designed Fuel tank dimensions are given in the next table:

Table 2.21 Fuel Tank Dimensions

Length (m)	1.018
Radius (m)	0.116

Fuel tank is drawn in Catia-v5 software and CAD drawing is shown in the next figure.

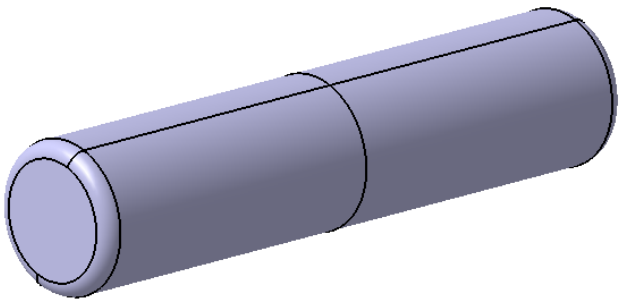

Figure 2.20 Fuel Tank Catia-v5 CAD Drawing

2.9.2 Inlet Design

Air inlet place for the engine has been selected as the under of the fuselage so that for high values of angles of attack, engine can get enough air to operate.

In order to prevent boundry layer occurance, small gap has been left between inlet and fuselage body. The inlet shape of the high speed decoy model is shown in the next figure.

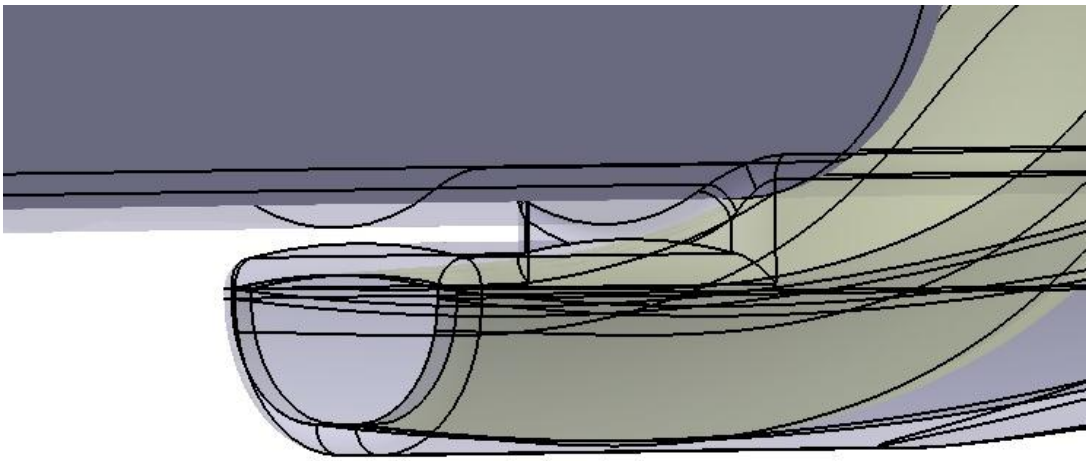

Figure 2.21 Inlet Shape of High Speed Decoy UAV

Capture area for pitot-tube inlet should also be calculated. The capture area is calculated for the worst condition, that is stall condition. The capture area at stall condition becomes,

$$A_c = \frac{\dot{m}_{engine}}{\rho_{stall} V_{stall}} \tag{2.91}$$

Mass flow rate is 0.3 kg/s, stall velocity is 40.6m/s and the density of air is 1.225 kg/m^3. Then, A_c becomes 0.006 m^2.

2.9.3 Engine Selection

The Nike engine, created by AMT-NL has been selected due to low weight and high thrust properties. This engine has a single radial compressor and an axial flow turbine.

Figure 2.22 Nike Turbojet Engine [13]

The technical drawing of the Nike engine is given below,

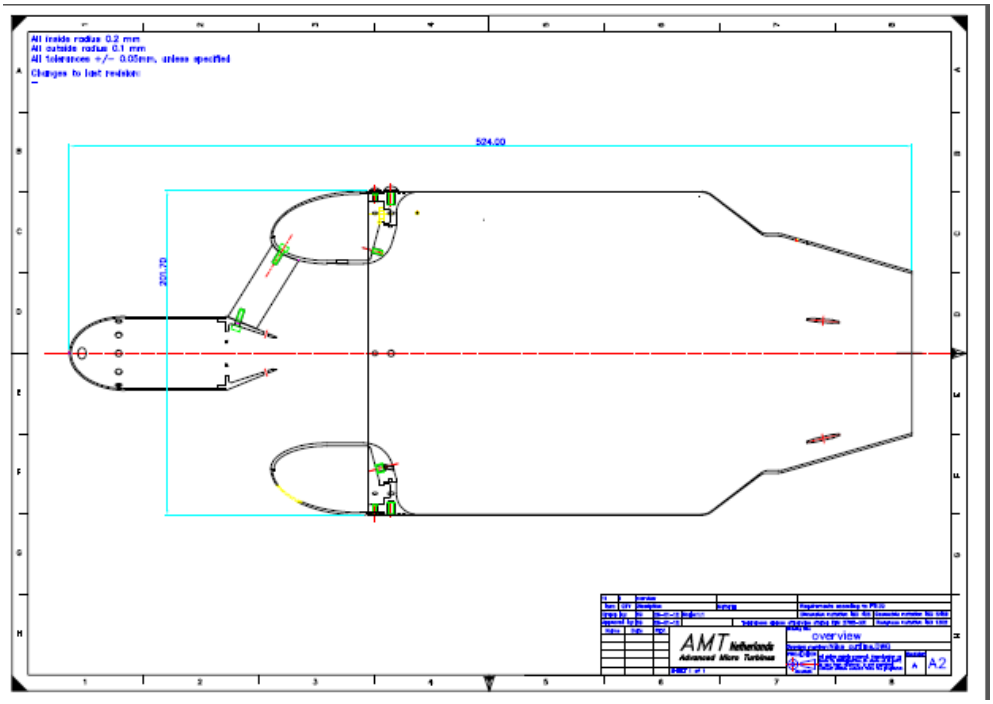

Figure 2.23 The technical 2-D drawing of the Nike engine [13]

From technical drawing, the Nike Jet Engine CAD model has been drawn in Catia-v5 CAD software and integrated to the high speed decoy UAV.

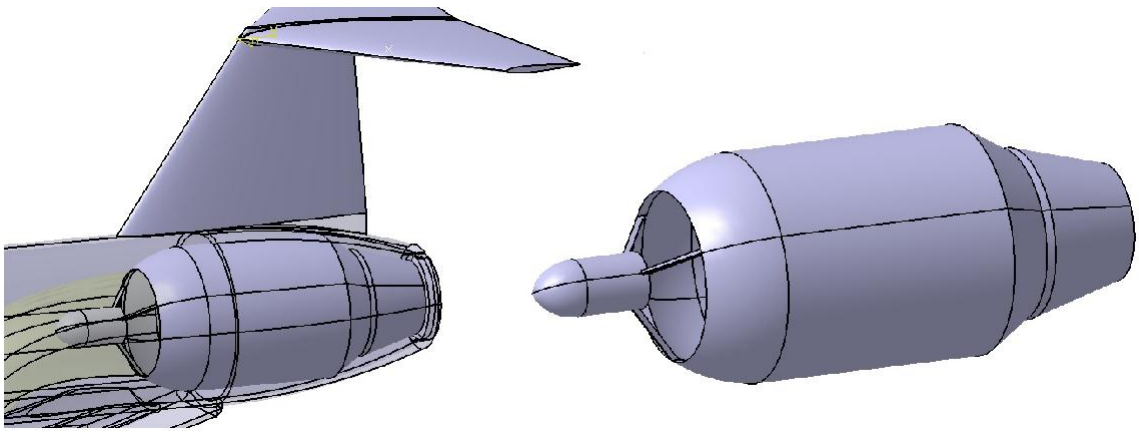

Figure 2.24 Nike Jet Engine CAD Drawing and installation to the UAV Model

The specifications of the Nike turbojet engine is given in the following table 2.22;

Table 2.22 Specifications of the Nike Turbojet Engine [13]

Engine diameter	201 mm / 7.9 Inch
Engine length	524 mm / 20.6 Inch
Engine weight	8770 Gr / 19.3 Lb
System airborne weight*	10580 Gr / 23.3 Lb
Thrust at max RPM at S.T.P.	784 N / 176.2 Lbf
Maximum allowed RPM	60000 / 60000
Thrust at idle RPM	40 N / 9 lbf
Pressure ratio at max RPM	4:1 / 4:1
Mass flow	1100 Gr/sec / 2.42 Lb/sec
Normal EGT(internal EGT probe	760 Deg C / 1400 Deg F
Max EGT	800 Deg C / 1472 Deg F
Fuel consumption	1740 Gr/min / 61.37 oz/min
Specific fuel consumption	36.9gr/(Kn*sec) / 1.30 (lb/lbf*hr)
Starting method	Direct kerosene system
*Total weight of ; Engine, ECU, Pump, Lipo battery, Thermosensor, valves, Mounting straps	

The thrust and specific fuel consumption values of the engine are related to velocity and altitude of the aircraft. Therefore, during calculations, these values were chosen from the thrust and specific fuel consumption curves which are given below Figure2.17[13].

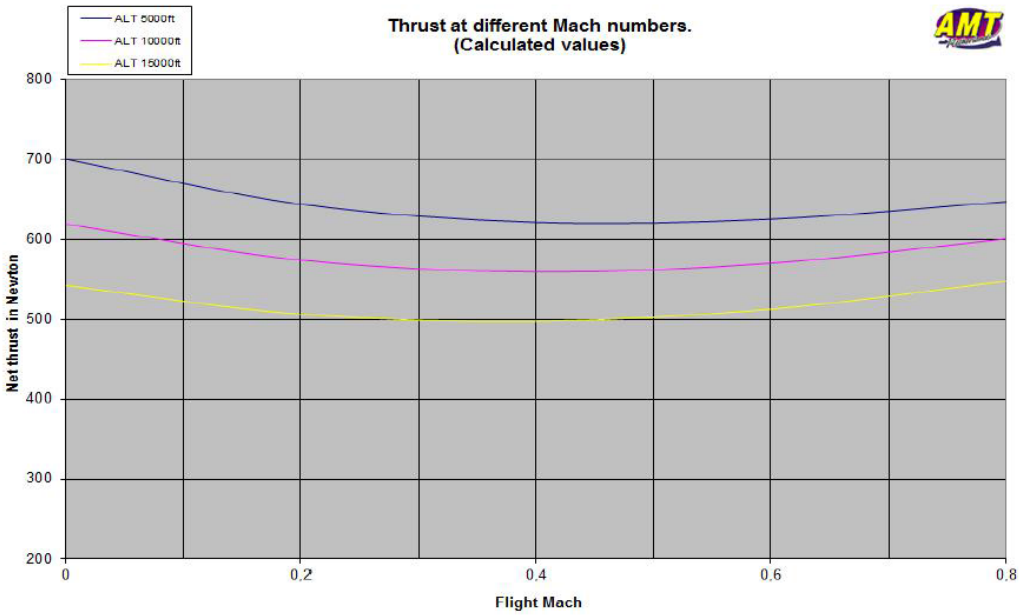

Figure 2.25 Thrust(T) at different velocity and altitude[13]

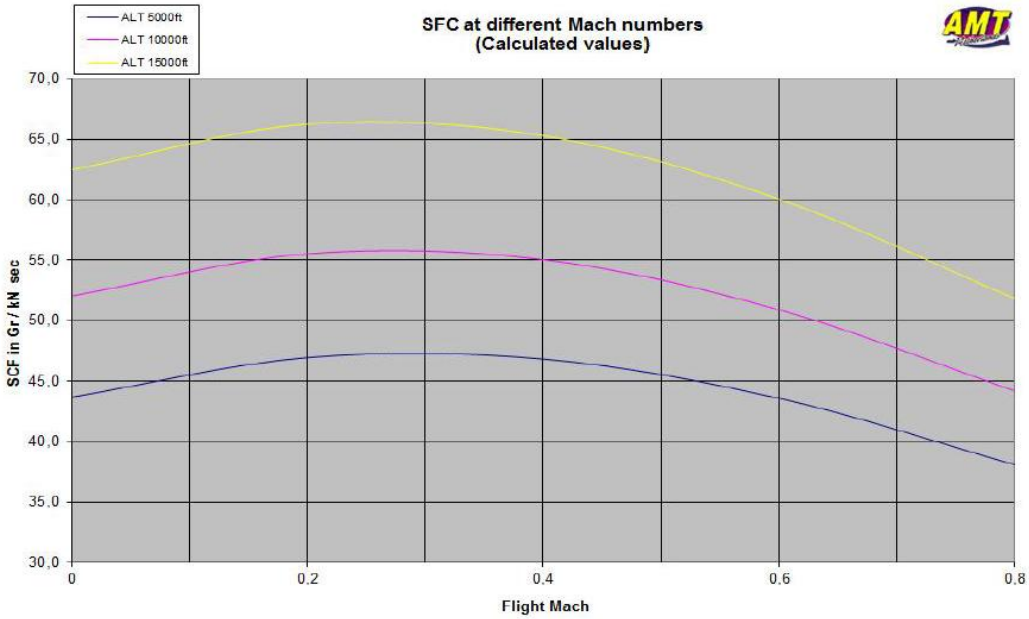

Figure 2.26 Specific Fuel consumption(C) at different velocity and altitude[13]

2.9.4 Installed Thrust

Thrust values are given in previous section. In fact, when the engine is installed to the aircraft, some portion the gained thrust is lost because of bleed air, pressure

recovery and inlet. In this section, the installed net thrust is calculated by approximations.

2.9.4.1 Bleed Air

For UAV's thrust loss from bleed air occurs because of anti icing. Bleed air loss percentage is calculated from following formula[5],

$$\%\ thrust\ loss\ from\ bleed\ air = C_{bleed}\left(\frac{bleed\ mass\ flow}{engine\ mass\ flow}\right) * 100 \qquad (2.92)$$

C_{bleed} is approximated as 2 and bleed mass flow is approximated as 1% [5]. The total thrust loss percentage becomes 2%.

2.9.4.2 Pressure Recovery

Thrust loss from pressure recovery is calculated from following formula[5],

$$\%\ thrust\ loss\ from\ pressure\ recovery = C_{ram}\left(\left(\frac{P_1}{P_0}\right)_{ref} - \left(\frac{P_1}{P_0}\right)_{act}\right) * 100 \qquad (2.93)$$

There is no information about C_{ram} of the Nike Jet engine. Therefore, C_{ram} can be approximated as 1.35 because this will be a subsonic flight[5]. $(P_1/P_0)_{ref}$ becomes 0 because flight will be below mach 1. At M=0.7, $(P_1/P_0)_{actual}$ is approximated as 0.985. Thrust loss from pressure recovery becomes 2.025%.

2.9.4.3 Inlet Drag

From Ref[5] the inlet drag becomes

$$T_{inlet\ drag} = \left(\frac{D/q}{A_c}\right) * q * A_c \qquad (2.94)$$

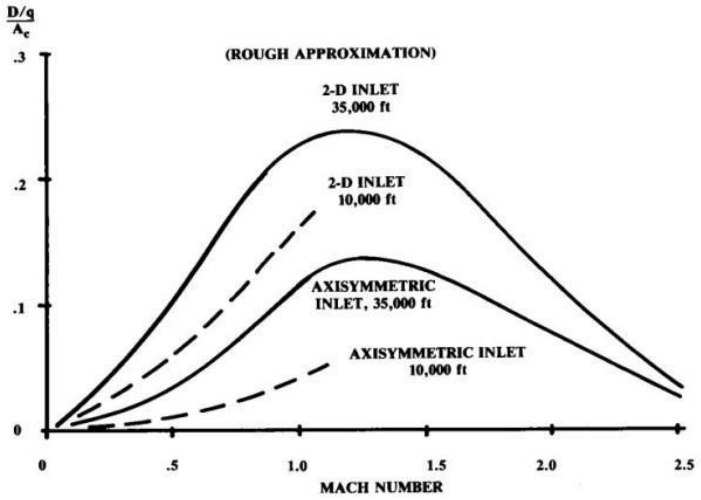

Figure 2.27 Inlet Drag Trends[5]

The inlet $\frac{D/q}{A_c}$ is approximated 0.013 from the previous figure, thrust reduction becomes:

2.9.4.4 Total Installed Thrust

Installed thrust is calculated as;

$$T_{installed} = T_{uninstalled} - T_{uninstalled}\left(Per.loss_{bleed\ air} + Per.loss_{p.rec.}\right) * 100 - T_{inlet\ drag} \quad (2.95)$$

Installed thrust at operation altitude curve is given in the next figure.

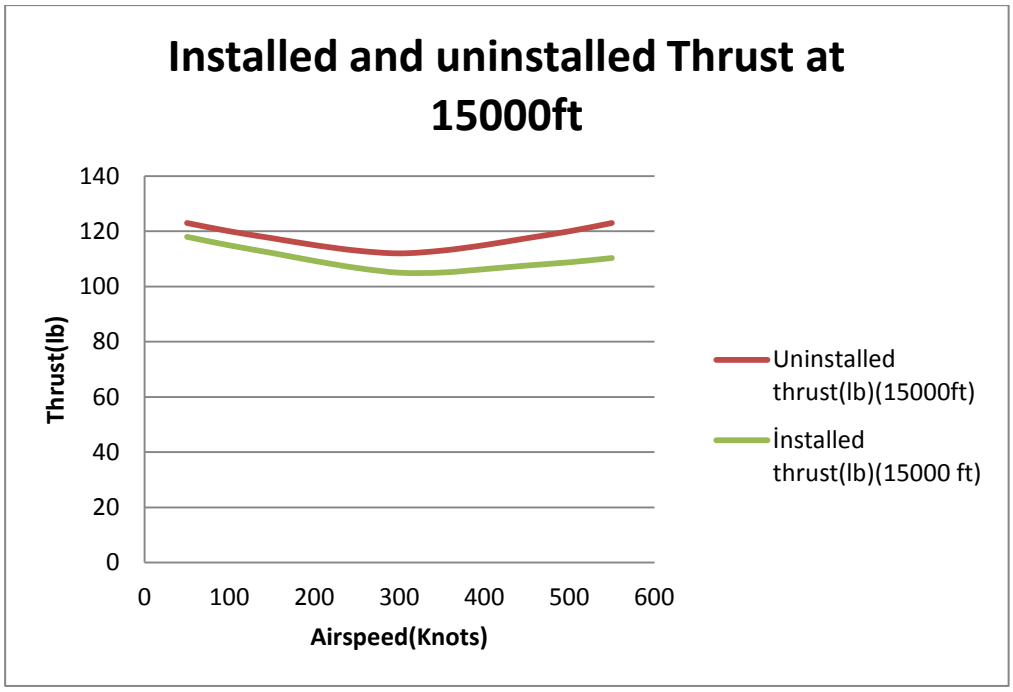

Figure 2.28 Installed and Uninstalled Thrust at 15000ft altitude

2.10. Launch and Recovery Systems

2.10.1 Launch system

Rail launchers are commonly used for the aircrafts which are less then 500 lb. Therefore, pneumatic rail launcher system is selected for the designed decoy UAV. Pneumatic rail launcher uses pneumatic pistons to accelerate the UAV to the desired flight velocity.

The rail launcher size is chosen according to the amount of energy which is transferred to the UAV.

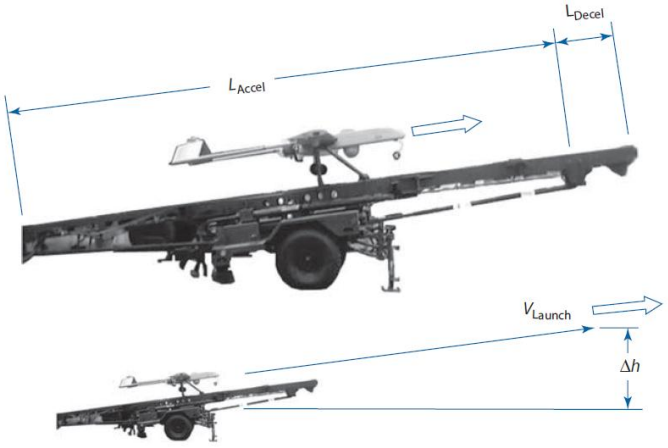

Figure 2.29 Rail launcher geometry [1]

Launch system is not going to be designed. It is selected from previous aerial target launchers. The launch velocity of the Twinjet Meggit Banshee and the specifications of its launcher is very appropriate to the designed aerial target launch velocity. Meggit Banshee weight is also similar to the designed decoy UAV Therefore, the Hercules launcher[14] is selected. The specifications of the Hercules launcher is given below in the table.

Table 2.23 Hercules Pneumatic Launcher Specifications [14]

Length(towing config. with rail folded)	36ft 5 in / 11.06 m
Length(with rail extended)	53ft 5 in / 16.28 m
Width	7ft 5 in / 2.26 m
Height	9ft 6 in / 2.9 m
Weight	16535 lbs / 7500 kg
Max launch velocity	107 KTS / 55 m/s
Max air vehicle mass	551 lbs / 250 kg
Max launch pressure	145 pounds/in^2 /10 bar
Rate of pressurisation	1 bar/min

2.10.2 Recovery system

Parachute recovery system is used for Aerial targets. Governing equations are used to calculate the parachute variables [12].

$$W_{recovery} = D = \frac{1}{2}\rho {V_T}^2 C_{D_{parachute}} S_{parachute} \quad (2.96)$$

From previous calculation, terminal Rate Of Decent(V_T) is given as;

$$V_T = \sqrt{\frac{2W_{recovery}}{\rho C_D S_{parachute}}} \quad (2.97)$$

ROD is directly related to canopy loading (CL). For required ROD value, canopy loading is estimated from following table 2.16 [12]

Table 2.24 Canopy loading ROD relation [12]

Canopy Loading (PSF)	Multiply 29.0 Times	ROD (ft/sec)
0.25	0.50	14.5
0.50	0.71	20.5
1.00	1.00	29.0
2.00	1.41	41.0
4.00	2.00	58.0
8.00	2.83	82.0

After the estimation of Canopy loading(CL), the drag area is given as;

$$C_D S_{parachute} = \frac{W_{recovery}}{CL} \quad (2.98)$$

Assuming the drag efficiency (C_{eff}) 50 ft^2/lb, the canopy weight (W_P) is calculated as;

$$W_P = \frac{C_D S_{parachute}}{C_{eff}} \quad (2.99)$$

Traditional Hand Pack method is selected. Therefore, we have 25 PCF pack density. The volume required for packing is given as,

$$Volume\ Required = \frac{W_P}{25\ PCF} \tag{2.100}$$

Since $S_{parachute}$ is given as $\pi/4 * (D_{parachute})^2$, the parachute diameter is given as;

$$D_{parachute} = \sqrt{\frac{8W_{recovery}}{\pi\rho {V_T}^2 C_{D_{parachute}}}} \tag{2.101}$$

Parachute drag coefficient ($C_{D\ parachute}$) ranges between 0.7 to 1.3. Taking parachute drag coefficient ($C_{D\ parachute}$) value as 1.1 , parachute diameter is found as approximately 12 ft.

CHAPTER 3

CONFIGURATIONS OF DECOY UAV

3.1 Wing and Tail Location Options

Baseline high speed decoy UAV has been designed in the previous chapter. However, what if other configurations were had been chosen at design process? What would be the aerodynamic difference between them? In order to find the best configuration, other possible configuration variations is going to be designed.

3.1.1 Wing vertical location options

Wing vertical location effect the performance directly. It alters the C.G of the aircraft and therefore, the stability.

Baseline high speed decoy UAV has been designed as Mid-wing due to reasons stated at previous chapter. In this section, low and high wing configurations have been designed.

3.1.1.1 Low Wing

Low wing configuration yields that, wings are closer to the inlet of the decoy UAV and C.G becomes higher than the wing. Low wing advantages and disadvantages are as follows[8]:

1-It has less ground clearance.

2-Low wing tends to be less laterally stable. On the other hand, it enables better lateral control.

3-Theoretically, It produces less lift and less induced drag.

3-Wing has less downwash to tail. Therefore, tail is more effective.

4- Low wing configuration is structurally lighter than high wing.

3.1.1.2 High Wing

At high wing configuration, the wings are far away from inlet and the C.G becomes lower than the wing.

High wing advantantages and disadvantages are as follows[8]:

1-It has more ground clearance.

2-It tends to be more laterally stable than other configurations due to dihedral effect.On the other hand, it reduces lateral control.

3-Theoretically, this configuration tends to produce more lift. Therefore, produces more lift induced drag.

4-High wing configuration becomes structurally more heavy.

3.1.2 Horizontal Tail vertical location Options

T-tail configuration had been selected for baseline design. In fact, T-tail helps to get rid of the wing wake, wing vortices and engine exit flow. However, T-tail makes heavy vertical tail and has a big disadvantage at stall condition. That is, Wing wake blocks the airflow to the elevators and results in deeps stall. This dangerous situation may even lead to the crush of the decoy UAV. Following figure shows the deep stall situation.[8]

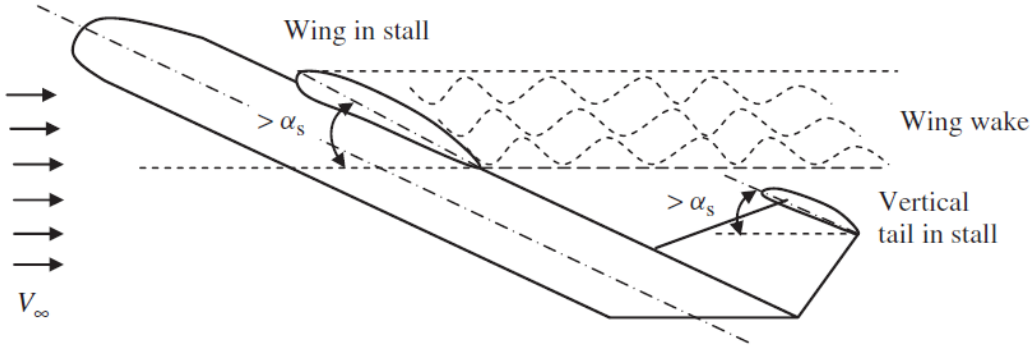

Figure 3.1 Deep stall situation in T-tail configuration [8]

In this section, other tail configurations have been designed.

3.1.2.1 Cruciform Tail

Cruciform tail is the combination of the T-tail and the Conventional tail. Cruciform tail enables lighter vertical tail and help preventing deep stall.

3.1.2.2 Conventional Tail

Conventional tail is the third tail option.Vertical tail is the lightest structure of all three tail combinations. Because vertical tail do not need to carry the horizontal tail.

The wing wake can disturb horizontal tail in this tail configuration. Expecially with high wing combination.

3.2 Configuration CAD Models

Some combinations of different wing and tail configurations were designed. In order to find the most efficient configuration, Computational fluid dynamics(CFD) analysis will be performed.

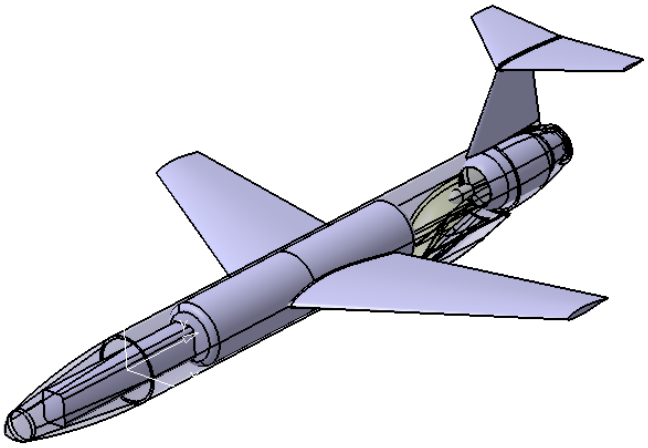

Figure 3.2 Baseline High Speed Decoy Design CAD model

After the baseline design, all possible combinations of wing and tail configurations were designed in CAD software. The configuration matrix is given below.

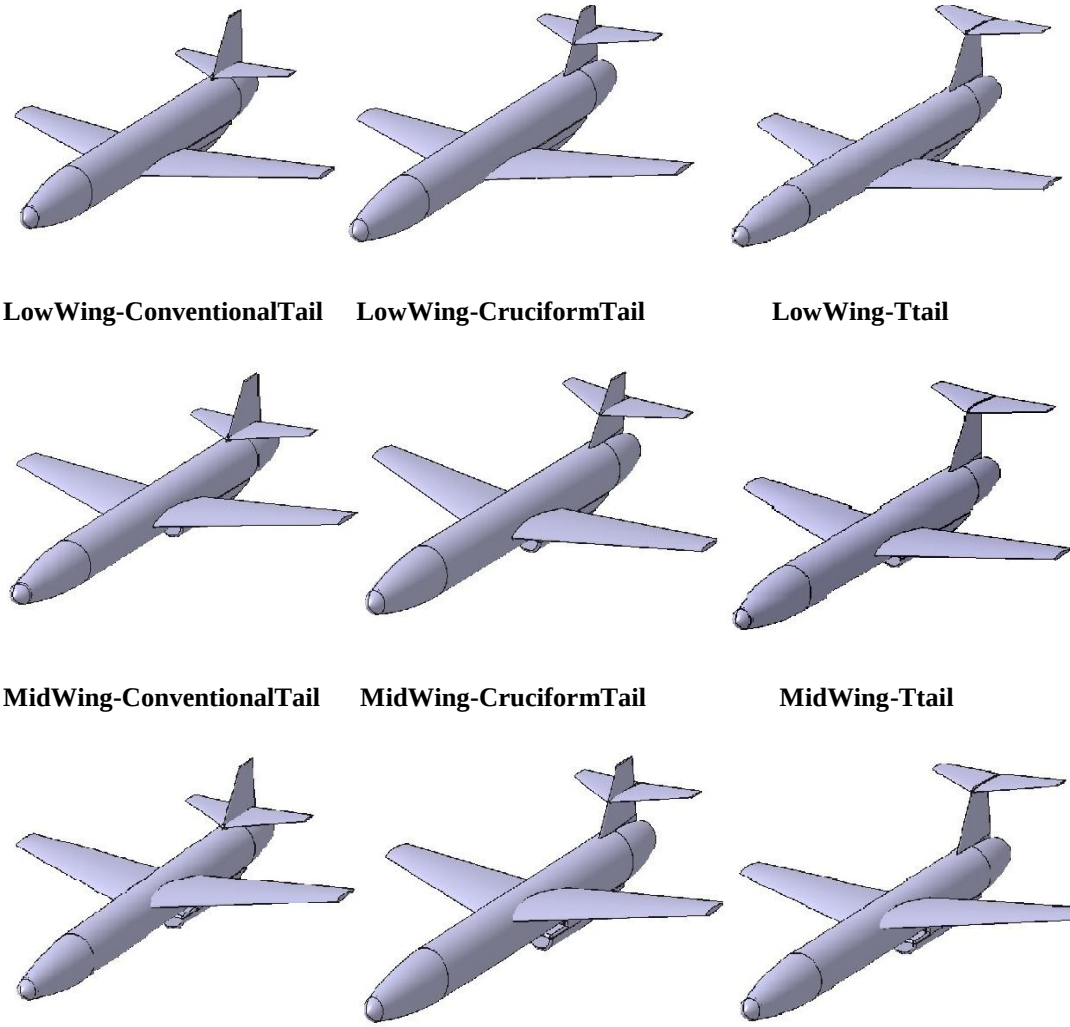

Figure 3.3 High Speed Decoy Configuration Matrix

The purpose of the design of the various configurations is to observe the flowfield of the wing wake and to investigate deep stall effect, to observe the fuselage interference effects on wing and to reveal the performance differences between these configurations. The theoretic advantages and disadvantages of the different geometries given above, are going to be observed.

CHAPTER 4

CFD ANALYSES

4.1 Introduction to CFD and CFD Methodology

Computational Fluid Dynamics (CFD) tool helps to simulate the aircraft for the given atmospheric condition and velocity. Nowadays, CFD simulations contribute more and more significantly to the Commercial/military aircraft and UAV design. Unsuccessful designs can be easily understood and altered by the use of CFD.

The reasons why CFD is used in this thesis are given below:

a) In fact, the wind tunnel test with a prototype gives the most accurate results related to a conceptual design. However, to create a turbojet powered prototype decoy UAV in this size requires great deal of financial support. Therefore, CFD analysis has been performed in this thesis to justify the conceptual design is successful.

b) In this thesis, Midwing-Ttail configuration was chosen at conceptual design phase. However, different configuration combinations related to the different vertical positions of the wing and tail were also designed to discuss the wing fuselage body interference. CFD analysis is used to check the deep stall effects of the wing on the tail. Moreover, CFD analysis is used to compare the lift and drag efficiency of these configurations and to choose the decoy UAV which yields the best aerodynamic outputs.

c) The decoy UAV is supposed to operate at M = 0.7 . This is a critical mach number for the shock occurance. If the flow velocity at the upper surface of the wing exceeds M = 1, shock wave occurs and the magnitude of the generated drag rises significantly. As a result, the decoy UAV can not reach its maximum speed. CFD

analysis is used to test the occurance of the shock wave at the upper surface of the wing when operating at M=0.7. If shock wave occurs, the location of the shockwave will be revealed and shock strength will be calculated from pressure loss. Boundary layer interaction with shockwave and flow separation will also be discussed.

CFD methodology of FloEFD software in the next figure.

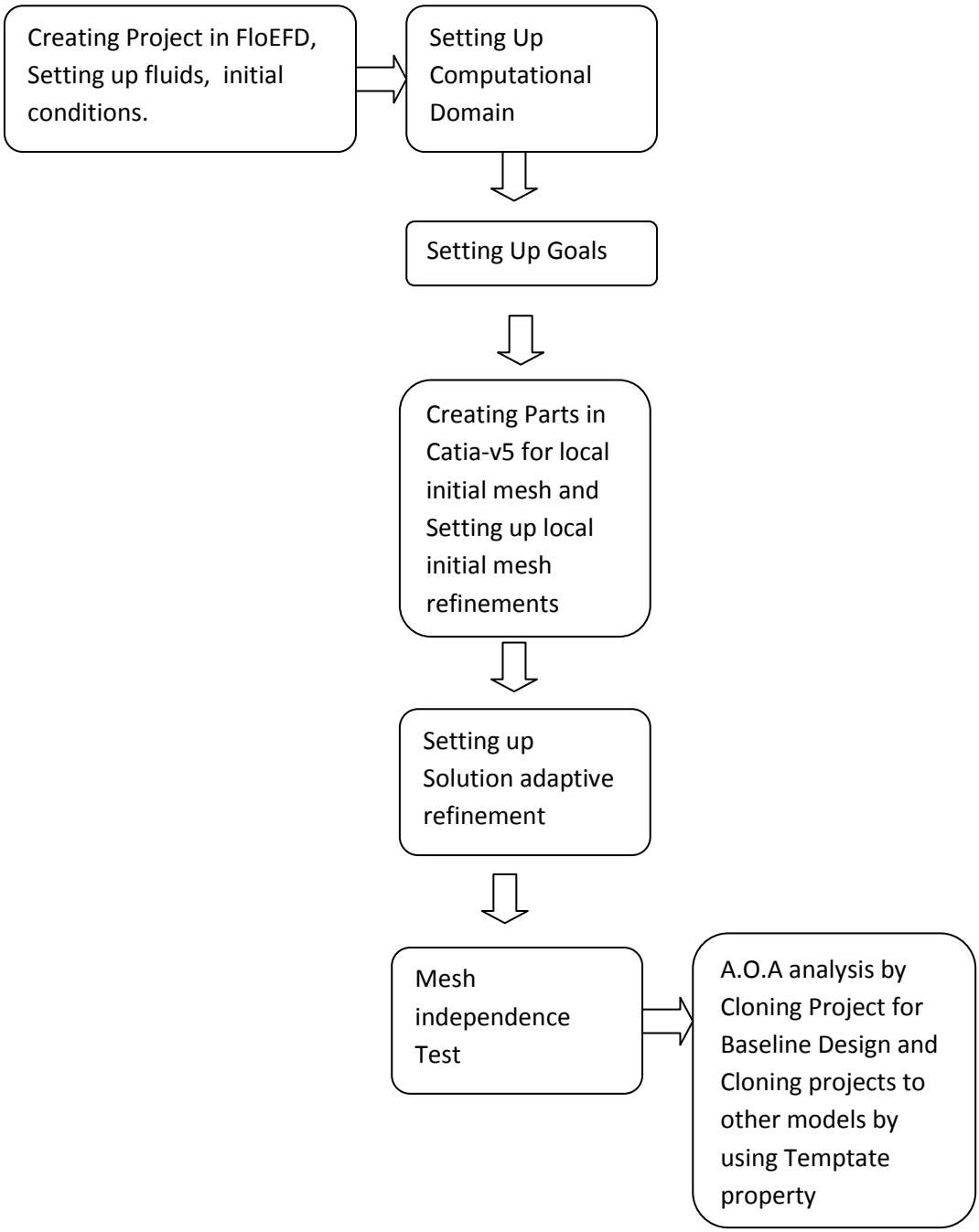

Figure 4.1 CFD Methodology in FloEFD

4.2 CAD-Embedded FloEFD Software

FloEFD is a modern CFD software which successfully proved itself in lots of areas including aerodynamics. FloEFD provides several advantages, some advantages are given below:

a) Unlike other CFD softwares, FloEFD is embedded to CAD softwares such as Catia-v5, Solidworks, Siemens-NX and Creo. Therefore, CFD engineer do not need to transfer the geometry from CAD software to CFD software.

b) FloEFD is equipped with a new partial cell technology. FloEFD is able to solve solid-fluid boundies in a single cell these cells are called partial cells.

c) FloEFD offers to clone projects which were previously used. One can alter the parameters such as boundry conditions and mesh settings and make a batch run. Moreover, template property helps to clone a project to a completely different model.

d) Parametric study enables to solve different cases with batch run.

e) FloEFD has automatic meshing capabilities and solution adaptive mesh refinement technology. It refines mesh at the alteration points of the flow.

4.2.1 Meshing Strategy of FloEFD

Body fitted algorithms are usually used by mesh generators for traditional CFD softwares.

Generally, unstructural mesh grids are used for complicated body geometries.

Ref[22] states that, "The EFD technology is based upon the use of Cartesian-based meshes and Meshing Technology is one of the key elements of the CAD/CFD bridge for CAD-embedded CFD."

Since cartesian based mesh are used, there are cells which are located in solid body(solid cells), fluid body(fluid cells) and cells which consists from solid and fluid control volumes(partial cells)[22].

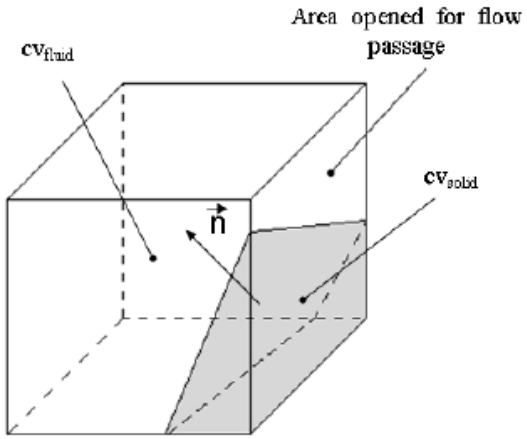

Figure 4.2 Partial Cell containing two control volumes inside [22]

Cartesian cells with partial cell technology and new boundary layer treatment led to achieve unexpectedly successful results with much lower cell number compared to other CFD tools. Society of Automative Engineers of Japan conducted a benchmark study to compare CFD tools with test data on a new car shape[7].

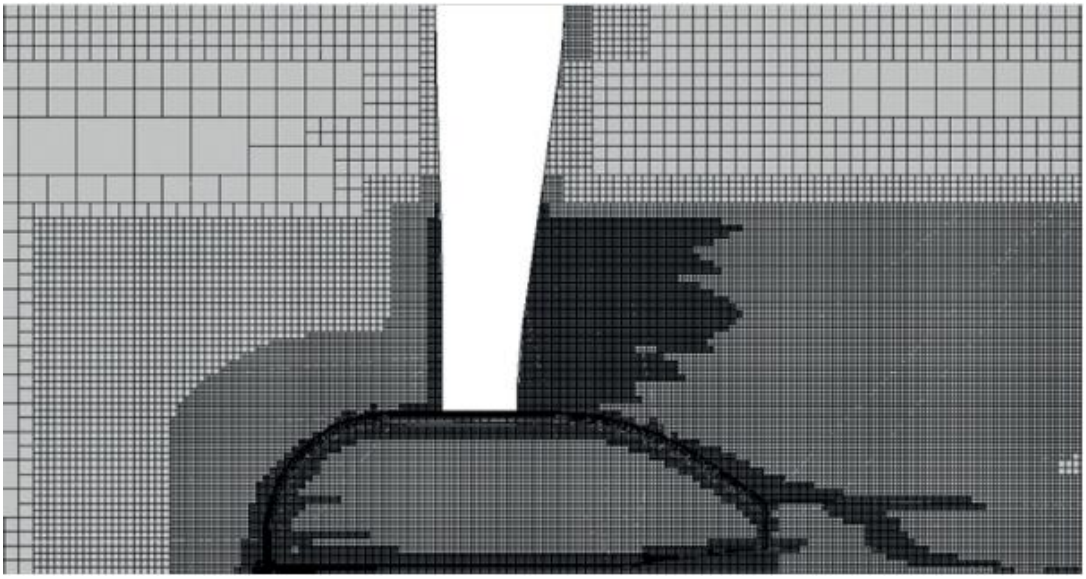

Figure 4.3 Computational Mesh used by FloEFD for JSAE benchmark model [7]

Table 4.1 Participant companies and CFD codes in the JSAE blind automotive aerodynamic benchmark [7]

Software	Mesh Type	Number of Cell Layers in the Boundary Layer	Number of Cells Without Rear Flat Panel (Case 1)	Number of Cells With Rear Flat Panel (Case 2)	Mesher Used
AcuSolve	Tetrahedral mesh	7	24,755,000	25,795,000	AcuConsole1.8b
ANSYSFluent R14.5	Unstructured grid	17	16,000,000	16,700,000	ANSYSMeshing R14, TGridR14
FloEFD	Cartesian mesh based on octree technology	-	3,520,000		FloEFD
iconCFD	Hexahedral dominant mesh	7	37,640,000	38,300,000	foamProMesh
PAM-FLOW	Tetrahedral mesh	6	38,260,000		PAMGEN3D
SCRYU/Tetra (DES, SAS)	Tetrahedral mesh with prisms	10	27,000,000		SCRYU/Tetra
STAR-CCM+ v7.06 (IDDES, SST k-ω)	Hexahedral dominant mesh	20	16,690,000	16,835,000	STAR-CCM+ v7.06

Test was conducted for two different cases, case 1 was car without additional part and case 2 was car with additional part.

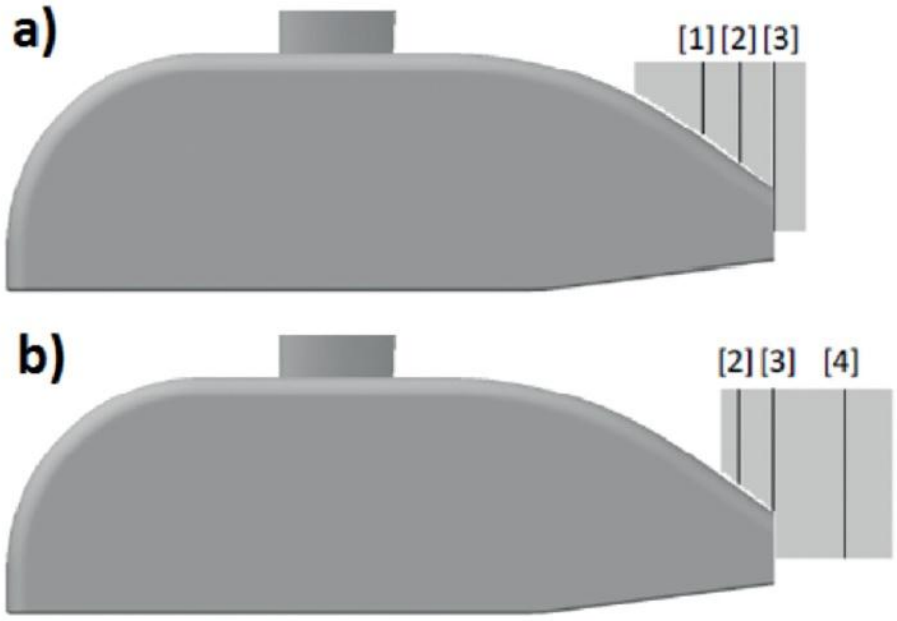

Figure 4.4 Wake measurements at y/W = 0.0 for the JSAE car body: a) the case without the additional part and b) thecase with the additional part [7]

CL and CD results of the FloEFD were given in the next figures

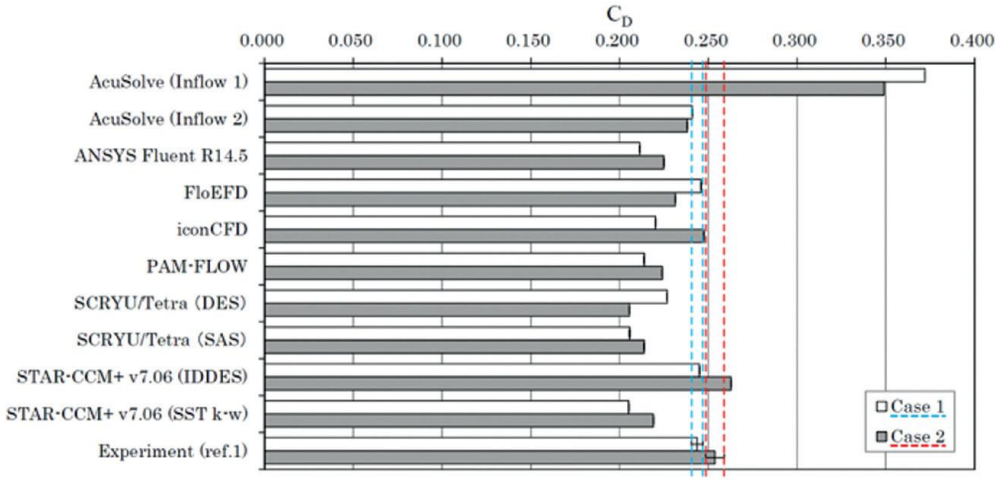

Figure 4.5 Drag coefficients for all CFD codes for cases 1 and 2 with experimental test data error in blue dashed lines (Case 1) and red dashed lines (Case 2) [7]

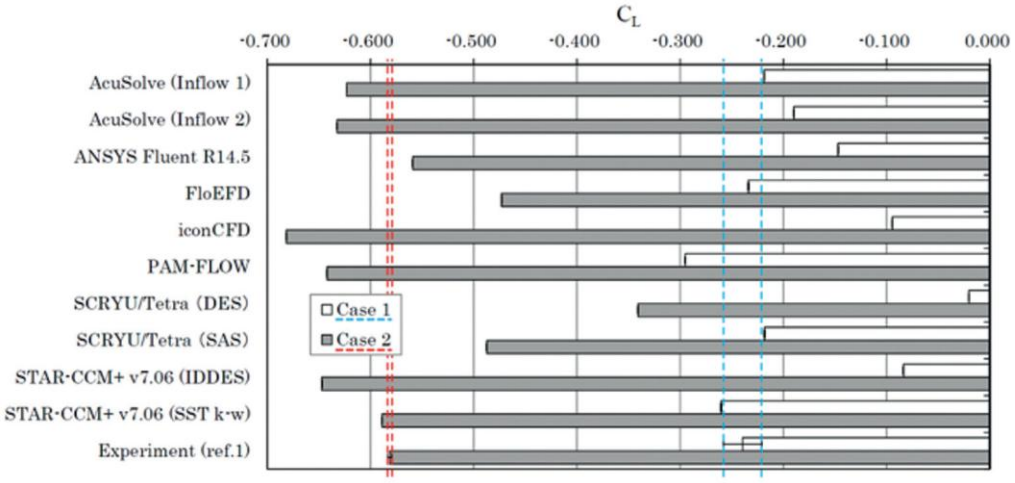

Figure 4.6 Lift coefficients for all CFD codes for cases 1 and 2 with experimental test data error [7]

This test proves that FloEFD can succeed with its meshing system with lower mesh numbers compared to other CFD software packages. Low mesh number enables to save CPU time significantly.

4.2.2 Basic Equations used by FloEFD

FloEFD calculates two kinds of physical phenomena within solid regions, heat conduction and direct electric current. In this aerodynamics analysis, these phenomenas are disabled. Therefore, they are not calculated.

In fluid regions, N-S equations are used, they are composed of mass, momentum and energy conservation equations[22].

$$\frac{\partial \rho}{\partial t} + \frac{\partial (\rho u_i)}{\partial x_i} = 0 \tag{4.1}$$

$$\frac{\partial (\rho u_i)}{\partial t} + \frac{\partial}{\partial x_j}\left(\rho u_i u_j\right) + \frac{\partial P}{\partial x_i} = \frac{\partial}{\partial x_j}\left(\tau_{ij} + \tau_{ij}^R\right) + S_i \tag{4.2}$$

$$\frac{\partial \rho H}{\partial t} + \frac{\partial \rho u_i H}{\partial x_i} = \frac{\partial}{\partial x_i}\left(u_j\left(\tau_{ij} + \tau_{ij}^R\right) + q^i\right) + \frac{\partial P}{\partial t} - \tau_{ij}^R \frac{\partial u_i}{\partial x_j} + \rho\varepsilon + S_i u_i + Q_H \tag{4.3}$$

$$H = h + \frac{u^2}{2} \tag{4.4}$$

FloEFD can detect the flow is laminar or turbulent automaticly. To predict turbulent flows, Fawre averaged N-S equations are used. In these equations, time average effects of turbulences are calculated[22].

When there is high speed compressible flow and shock wave in the analysis, following energy equation is used[22].

$$\frac{\partial \rho E}{\partial t} + \frac{\partial \rho u_i (E + \frac{P}{\rho})}{\partial x_i} = \frac{\partial}{\partial x_i}\left(u_j\left(\tau_{ij} + \tau_{ij}^R\right) + q^i\right) - \tau_{ij}^R \frac{\partial u_i}{\partial x_j} + \rho\varepsilon + S_i u_i + Q_H \tag{4.5}$$

4.2.3 Turbulence Model and Boundry Layer Calculation in FloEFD

FloEFD uses new type of a turbulence model which is called Enhanced Turbulence Model(ETM). ETM consists of the combination of the classical k-ε model with two-scale wall function(2SWF).

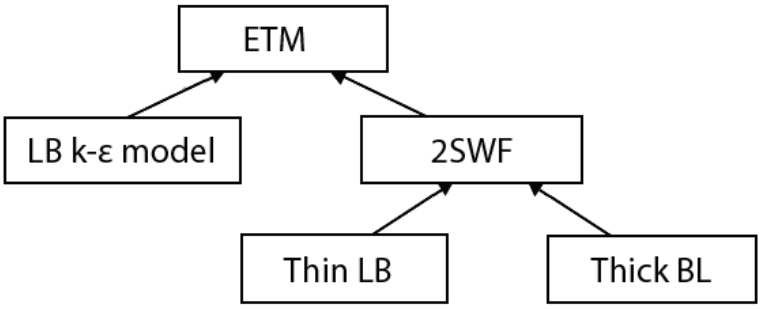

Figure 4.7 Structure of ETM approach used in FloEFD CFD software[27]

"To solve the Navier-Stokes equations with a two-equation *k-ε* turbulence model without resolving the near-wall fluid boundary layer would require a very fine computational mesh, hence a "wall function" approach had been proposed by Launder and Spalding (1972, 1974) to reduce mesh sizes. According to this now classical approach, the fluid wall frictional resistance and heat fluxes from the fluid to the wall are used to calculate the wall boundary conditions for solving the Navier-Stokes equations."[23]

In order to calculate the skin friction and heat flux at the wall, the Prandtl approach for boundry layers is used. "FloEFD uses novel and original two scale wall function approach which consists of two methods of coupling the B.L calculation with the solution of bulk flow"[22].

Thin boundary layer approach is used when mesh number across the B.L is too coarse.

Thick boundary layer approach is used when mesh number across the B.L is too fine to resolve the B.L.

Hybrid approach is the compilation of the two approach.

"In the thin-boundary-layer approach the Prandtl boundary layer equations already integrated along the normal to the wall. If the boundary layer is laminar, these equations are solved with a method of successive approximations based on the Shvetz trial functions technology. If the boundary layer is turbulent or transitional, a

generalization of this method employing the Van Driest hypothesis about the mixing length in turbulent boundary layers is used."[22].

"When the number of cells across the boundary layer is sufficient (more than ~10) the simulation of laminar boundary layers is done via Navier-Stokes equations as part of the core flow calculation. For turbulent boundary layers a modification of the well-known wall function approach is used. However, instead of the classical approach where the logarithmic velocity profile is used, the EFD technology uses the full profile proposed by Van Driest(1956)"[22].

4.3 Preparing the model, Boundry conditions and Calculation options

The model has been prepared following the instructions given in Ref[15].

External analysis option has been selected in the analysis wizard. Air has been selected for the fluid material. Internal space of the decoy is excluded and Exclude cavities without flow conditions option is selected so that the internal cavities is not taken into account and the number of cells is reduced.

For the initial conditions, 98.66 m/s airflow in the y direction with density 0.771kg/m^3 and 57205 Pa outside air pressure has been selected considering that the cruising altitude is 15000ft. For Oncoming flow direction, aerodynamic angle option is selected and longitudinal plane is selected as XY plane and Longitudinal axis is selected as Y coordinate. This means, at 0 angle of attack, flow direction is along +Y coordinate.

Flow type option is selected as laminar and turbulent, with this option laminar/turbulent transition is calculated automaticly.

High mach number flow option is disabled since flow is subsonic or transonic. According to Ref[15], high mach number option is needed for Mach numbers greater than 5.

4.4 Adjusting Computational Domain

Ref[15] yields that computational domain should be at least 10 times larger than the characteristic size in each directions. Taking this into account, computational domain has been configured as;

X = 0 / 10m Total 20m (symmetry)

Y = 23m / -10m Total 33m (downstream is larger)

Z = 10m / -10m Total 20m

4.5 Setting Up Goals

FloEFD has a special property. The designer can set up a goal and can input the convergence criteria to an individual goal. The convergence criteria for every goal is initially set up by FloEFD software automaticly and can be updated during solution by designer.

Goals has been set up according to the Ref[16]. First of all, a point has been assigned at the upstream region. The point location is in meters (0 ,-9.6 ,0) in the coordinate system. Point goals have attributed to this point in upstream. Then global goals are Constructed. Force global goals are the sum of forces in a given direction on every surfaces. Note that actual force should be found by multiplying all the forces with 2 since symmetric B.C are added. If needed, new global goals may be constructed later on. After global goals and point goals are constructed, equation goals should be set up.

Equation goals are set up according to the Ref[16]. Ref[16] uses force surface goals to calculate force coefficients. However, using global force goals can give the same coefficients as well. The equations are given below.

$$Normal\ Force\ Coefficient = \frac{GG\ Force(Z)}{\frac{1}{2}*(PG\ Density\ (fluid))*(PG\ Velocity)^2*S} \quad (4.6)$$

$$Axial\ Force\ Coefficient = \frac{GG\ Force(Y)}{\frac{1}{2}*(PG\ Density\ (fluid)*(PG\ Velocity)^2*S} \quad (4.7)$$

$$Lift\ Coefficient\ = (Normal\ Force\ Coefficient * \frac{PG\ Velocity\ (Y)}{PG\ Velocity}) -$$

$$(Axial\ Force\ Coefficient * \frac{PG\ Velocity\ (Z)}{PG\ Velocity})$$

(4.8)

$$Drag\ Coefficient\ =$$

$$(Axial\ Force\ Coefficient * \frac{PG\ Velocity\ (Y)}{PG\ Velocity}) + (Normal\ Force\ Coefficient * \frac{PG\ Velocity\ (Z)}{PG\ Velocity})$$ (4.9)

$$Pitching\ Moment\ Coefficient = \frac{GG\ Torque(Z)}{\frac{1}{2}*(PG\ Density\ (fluid))*(PG\ Velocity)^2*S*\bar{C}}$$ (4.10)

Note that, equation goals have no unit. Total goals are listed in the table below;

Table 4.2 Defined goals in FloEFD

Global goals	Point Goals	Surface Goals	Equation Goals
GG Maximum Mach Number	**PG Static pressure(Pa)**	**SG Avg Static Pressure(Pa)**	**Normal Force Coefficient**
GG Force (Y) (N)	**PG Density (fluid) (kg/m^3)**		**Axial Force Coefficient**
GG Force (Z) (N)	**PG Velocity (m/s)**		**Lift Coefficient**
GG Torque (Y)(N.m)	**PG Velocity (Y) (m/s)**		**Drag Coefficient**
GG Torque (Z)(N.m)	**PG Velocity (Z) (m/s)**		**Pitching Moment Coefficient**

4.6 Calibrating Mesh

4.6.1 Initial Mesh

The initial mesh has been constructed by using control planes. Initial mesh number for global domain has been selected as 49x102x42 cells according to NASA

Common Research Model(CRM) in Ref[17]. The control plane locations have been adjusted to the given high speed decoymodel computational domain. Mesh aspect ratios were also adjusted carefully to increase mesh numbers around aircraft and decrease at unimportant regions.

Mesh numbers were increased at X1, Y3 and Z2 planes. Initial mesh

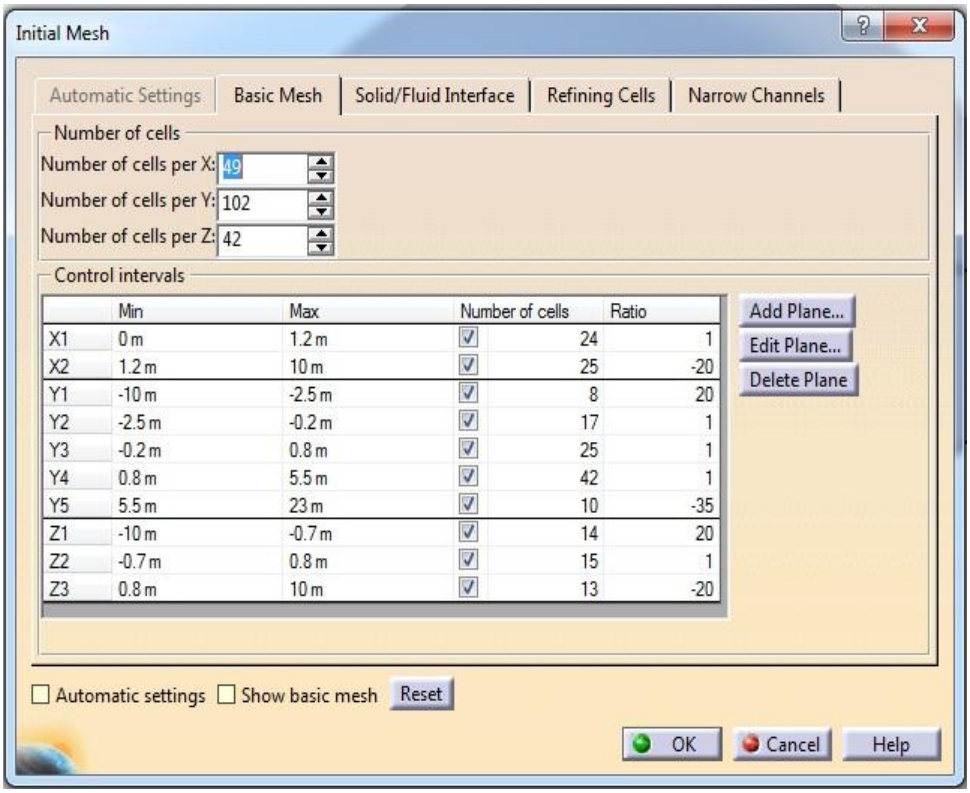

Figure 4.8 Global Domain Initial Mesh Settings in FloEFD

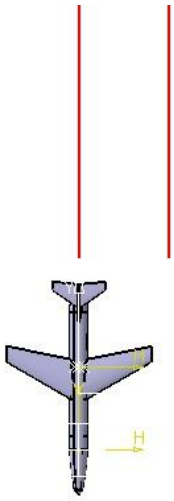

Figure 4.9 X1 Control Plane

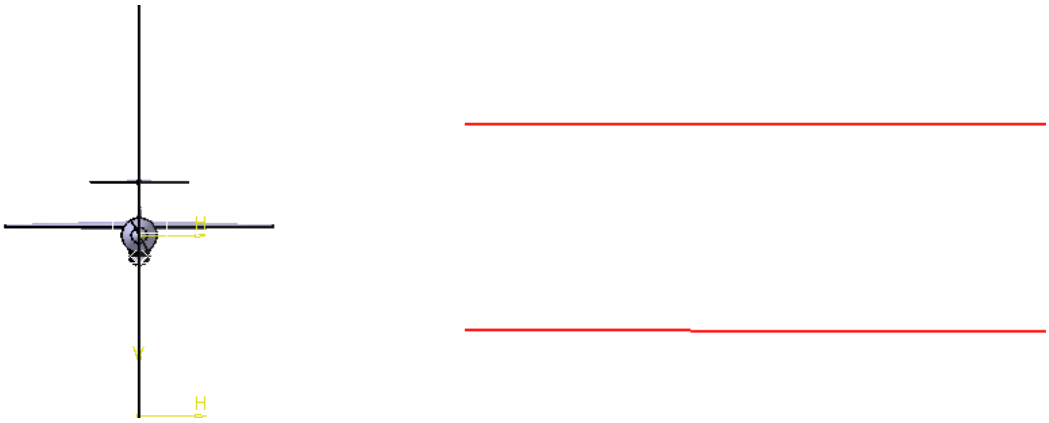

Figure 4.10 Z2 Control Plane

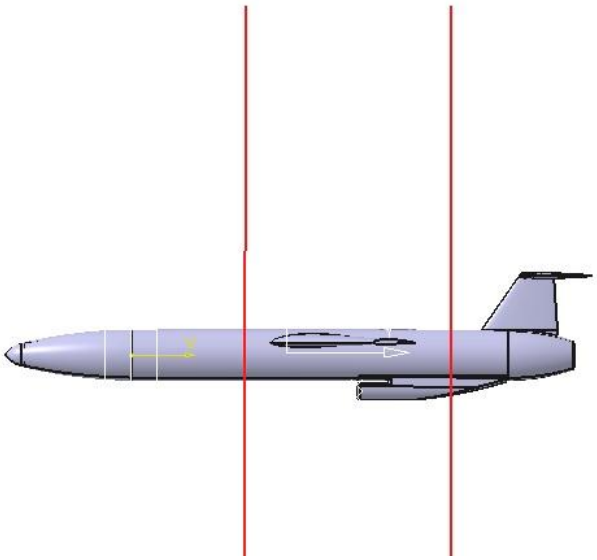

Figure 4.11 Y3 Control Plane

Initial mesh number is increased when the local initial mesh regions are included.

The initial mesh structure grid is given in the next figure. The vertical black spot is the wing control plane which is Y3 control plane region.

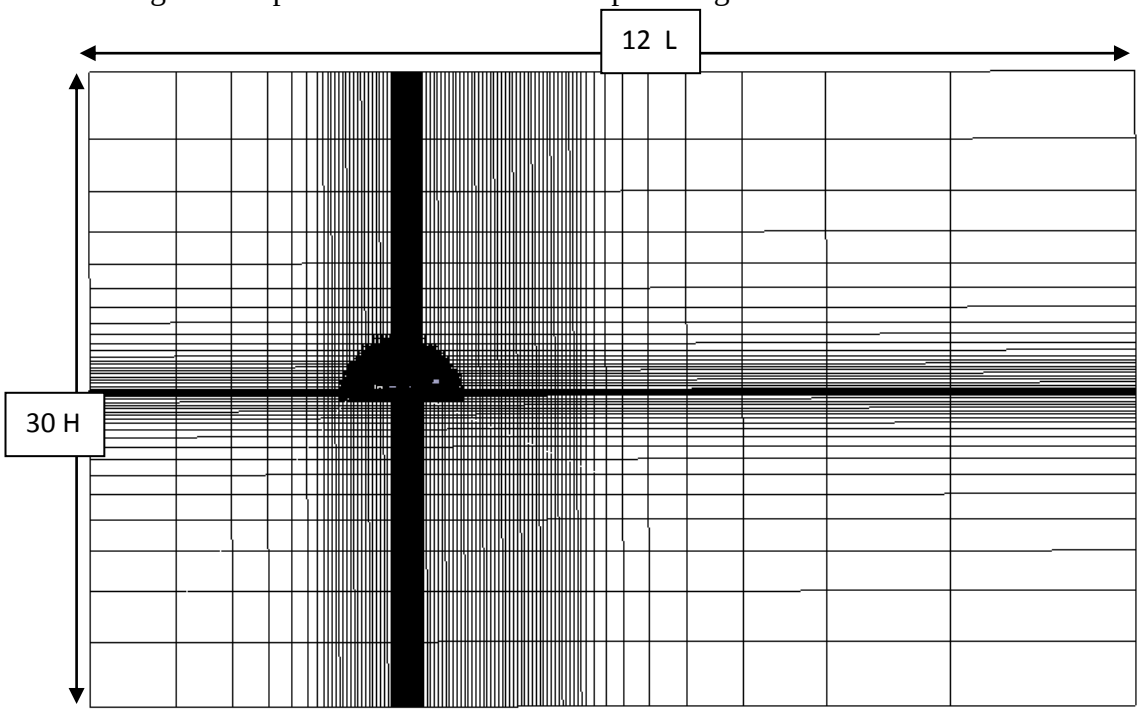

Figure 4.12 Computational Domain and Initial Mesh around aircraft

4.6.2 Local Initial Mesh Areas

For a given 3D aircraft aerodynamics problem,Suggested local mesh areas are given in the next figures[15].

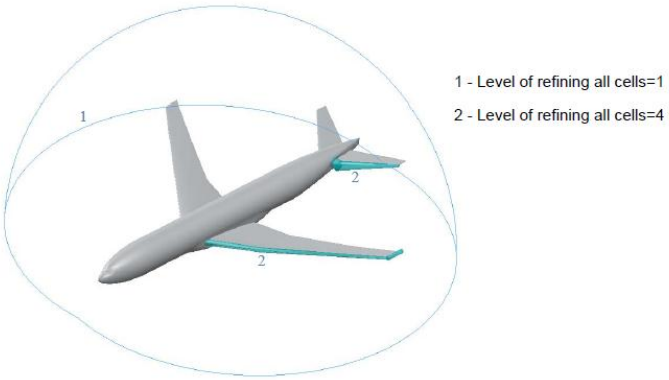

Figure 4.13 Local Mesh Regions And Settings [15]

In high speed decoy thesis 3 local mesh areas were constructed.

1- Outer hemisphere local Mesh (Part Created)

2- Wing Leading Edge and Trailing Edge Local Mesh (Part Created)

3- Tail Leading Edge and Trailing Edge Local Mesh (Part Created)

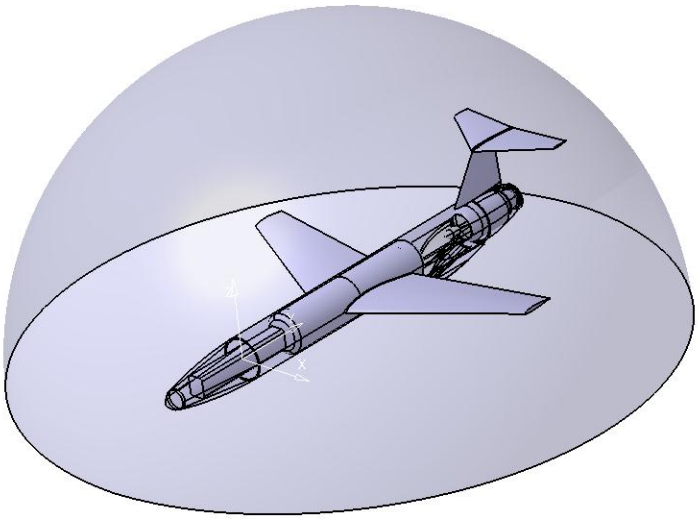

Figure 4.14 Hemisphere Local Initial Mesh Area of High Speed Decoy

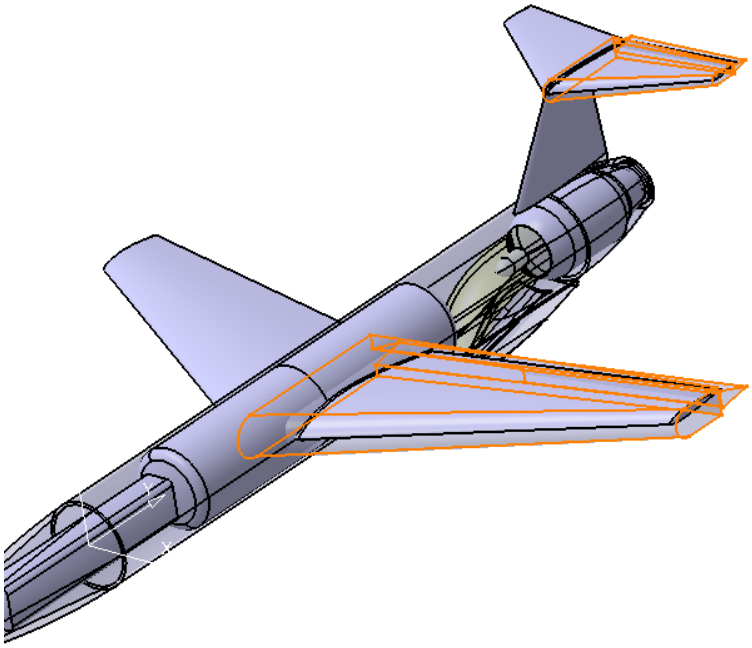

Figure 4.15 Wing and Tail Local Initial Mesh Areas of High Speed Decoy

Adviced local initial mesh all cell refining all cells is 1 for hemisphere and local initial mesh refinement for all cells for wing and tail local initial mesh locations is 4 [16]. However, these local mesh settings will be altered during mesh independence test. Local initial mesh on wing is shown in the next figure.

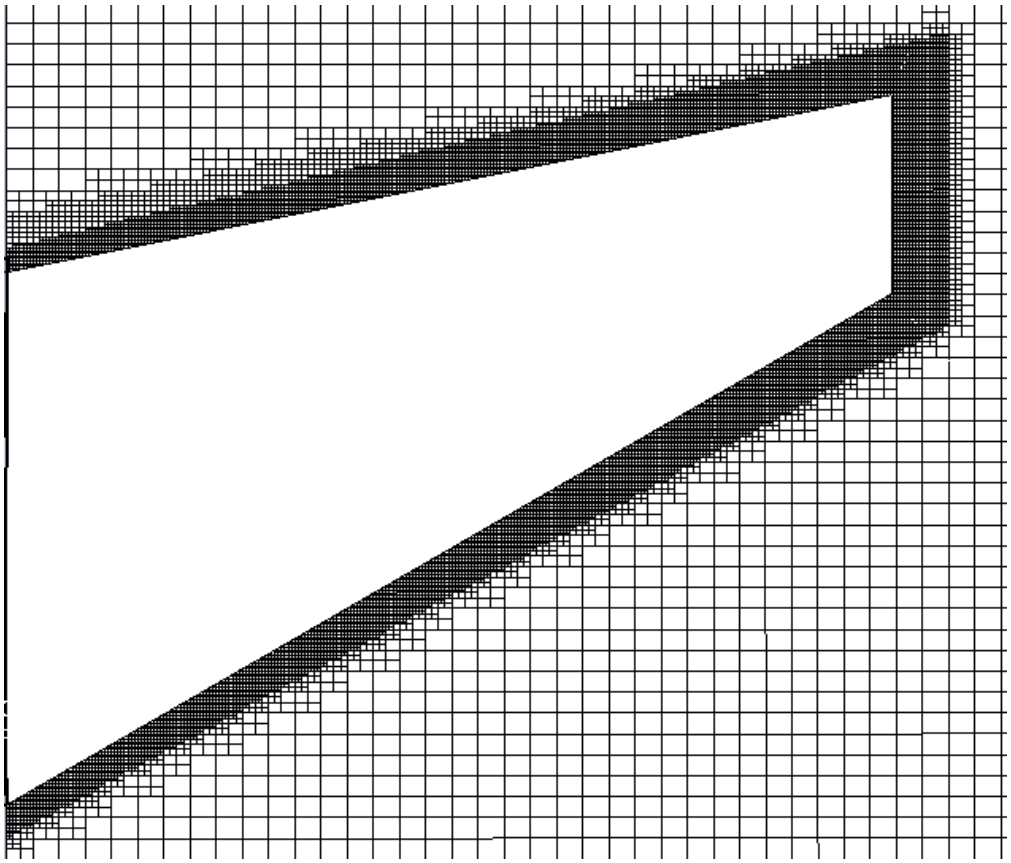

Figure 4.16 Local Initial Mesh Structure cut plot around Wing

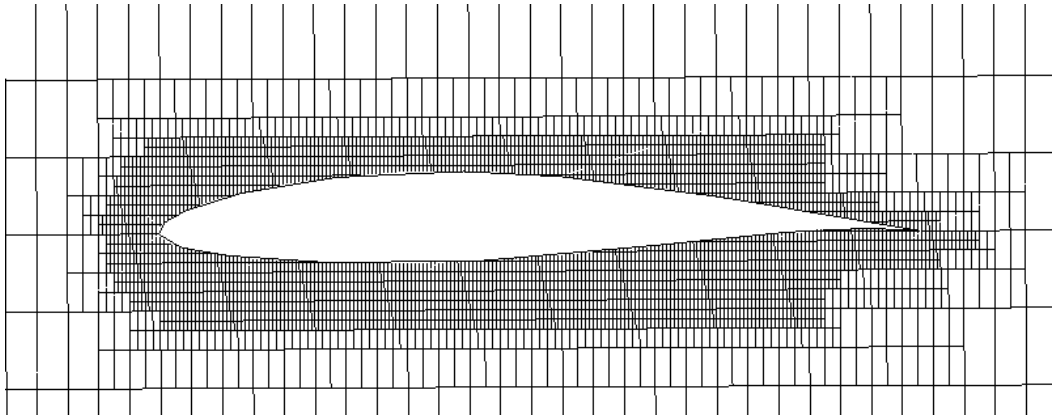

Figure 4.17 Local Initial Mesh Structure cut plot around airfoil

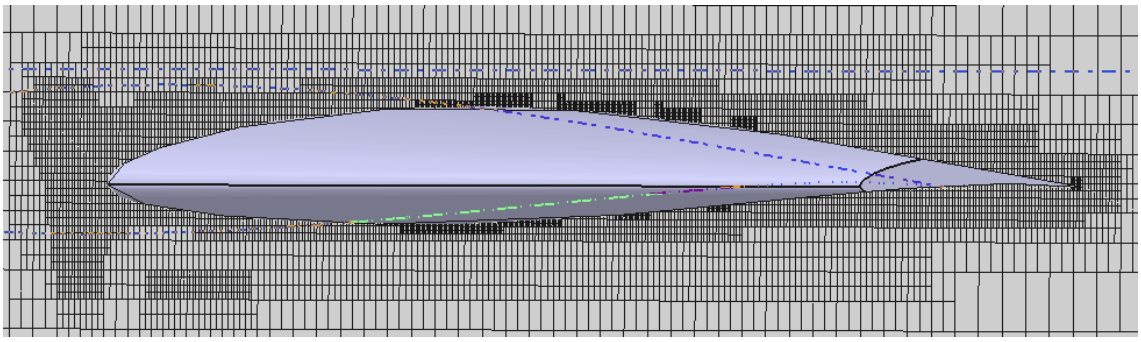

Figure 4.18 FloEFD Final Mesh cut plot around airfoil.

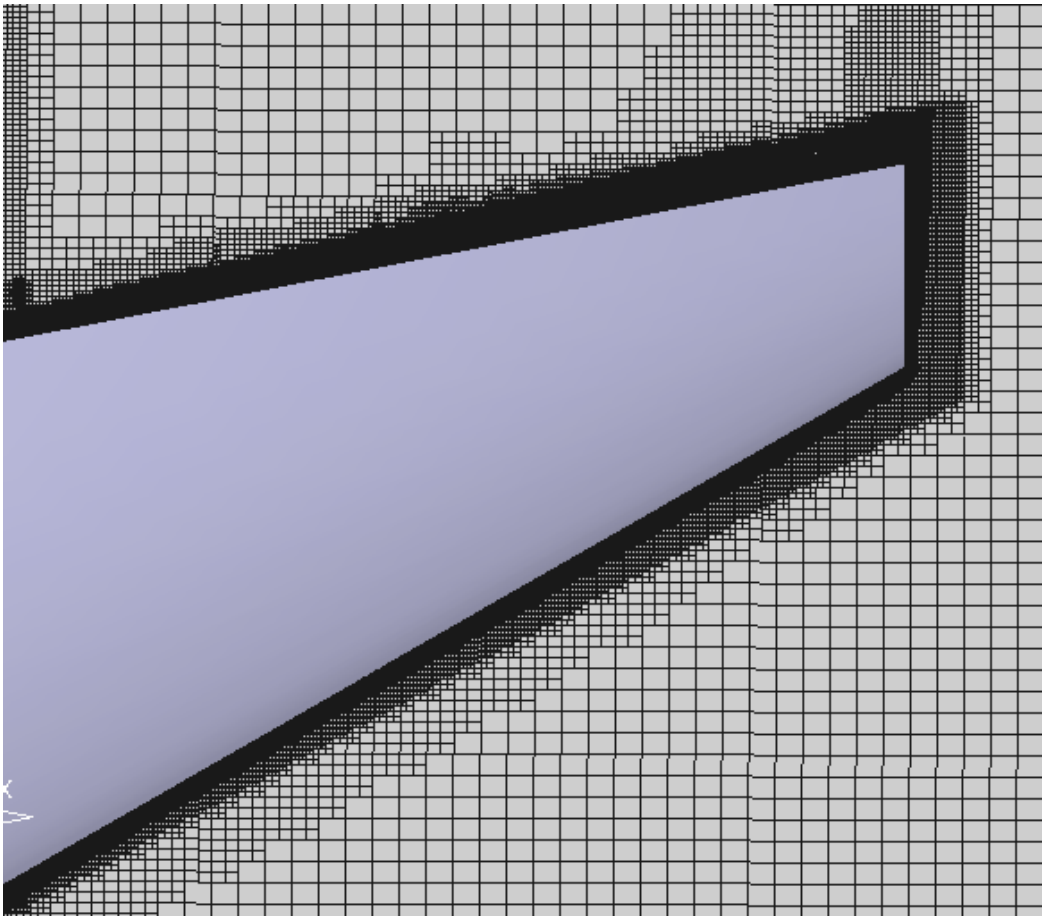

Figure 4.19 Final Mesh Structure cut plot around Wing

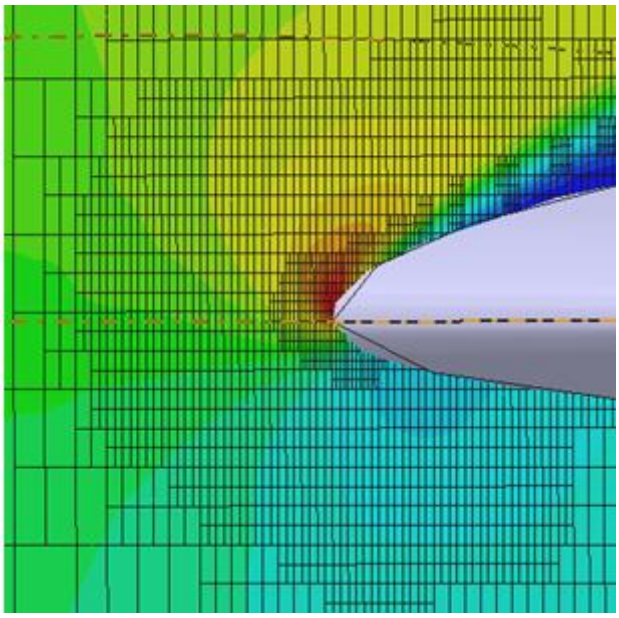

Figure 4.20 FloEFD Final Mesh at 16 A.O.A Solution adaptive Refinement example of the Leading Edge of Airfoil

4.6.3 Mesh Number and Mesh Independence Test

As mesh number increases, the solution becomes more and more realistic.Whereas, the computational time increases. In every CFD problem, it is very crucial to optimize the mesh areas and number. In this aerodynamic case,mesh number should be optimized. Mesh number should be tuned such that it should give an acceptable solution and the computation time should not last too long. In order to optimize the mesh number, the project has been cloned several times and all results were reported until the results do not alter in acceptable region.

In fact, this mesh optimization process does not require too much effort since, FloEFD has Solution Adaptive Mesh refinement system. According to Ref[16], For best calculation accuracy, one should activate solution adaptive mesh refinement and use local meshes at the same time.

Solution adaptive refinement was set in calculation control options, solution based refinement level was set to tabular refinement at travels 0.7, 1.5 and 2.2. Hemisphere local initial mesh solution adaptive refinement is set to level 3 and wing and tail local initial mesh solution adaptive refinement was set to 2.

The mesh dependence test results are given in the next figure;

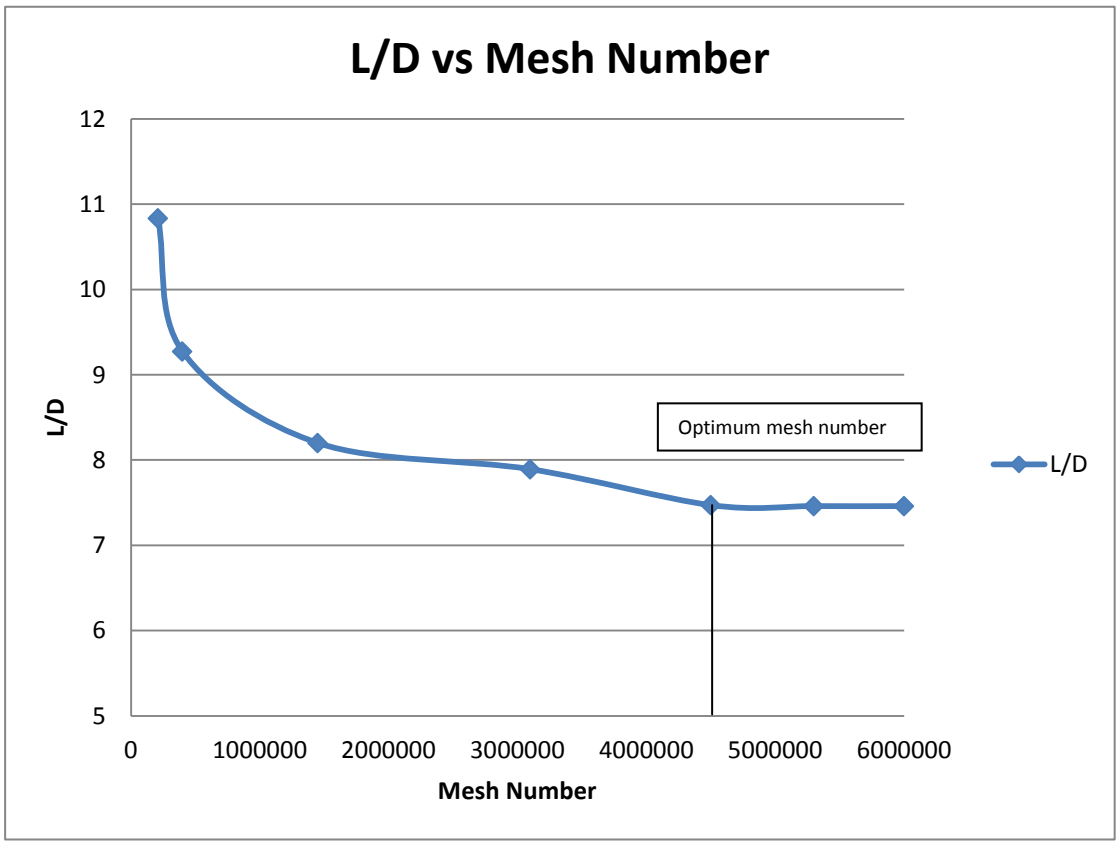

Figure 4.21 Mesh Dependence test results

Mesh number is converged at approximately 4,500,000 cells. The mesh dependence test is conducted for 98.5 m/s and for $\alpha=0^0$.

Solutions were converged and solver stopped after 700 iterations. The convergence of the results for baseline design at $\alpha=0^0$ is given in the next figure;

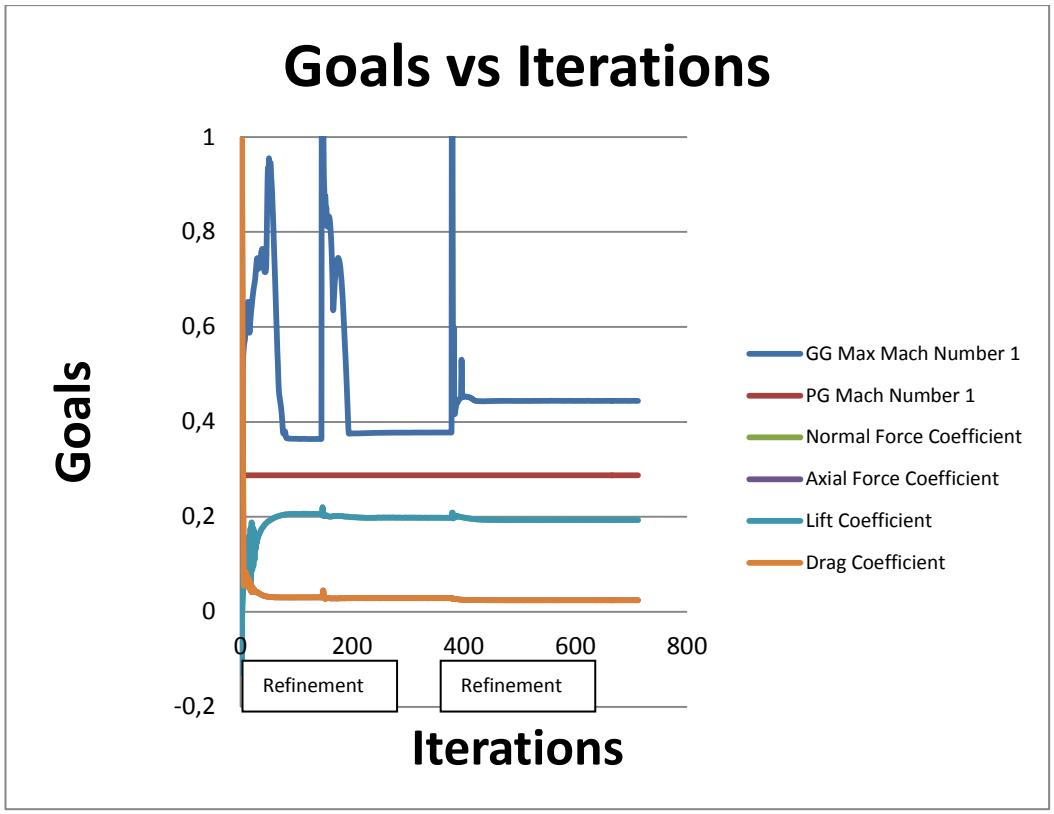

Figure 4.22 Goals Convergence Graph

The convergence criteria of all parameters are detected automaticly for every single parameter and this criteria alters during solution. This criteria can also be defined by user manually by calculation control options. Therefore, This software does not need to track residuals.

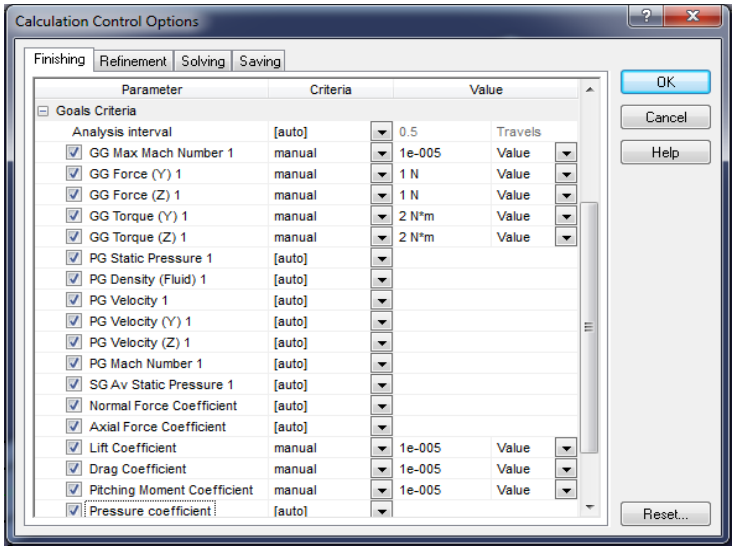

Figure 4.23 Convergence Criteria Options

4.7 Configuration Comparison CFD Results

4.7.1 Wing Comparison Results

High Wing, Mid Wing and Low Wing Configurations were compared. Whereas, tail configuration was kept as T Tail. That is, three configurations were High Wing-T tail, MidWing-Ttail and Low Wing-T tail.

4.7.1.1 Wing Comparison Cut Plot Results From 0.13m from Centerline

Cut plots for pressure and mach number are created to understand the fuselage effect on wing for different vertical positions. Contour plots are 0.13 m from centerline. This is a very close location to the fuselage.

0.13 m cut plot location is given in the next figure.

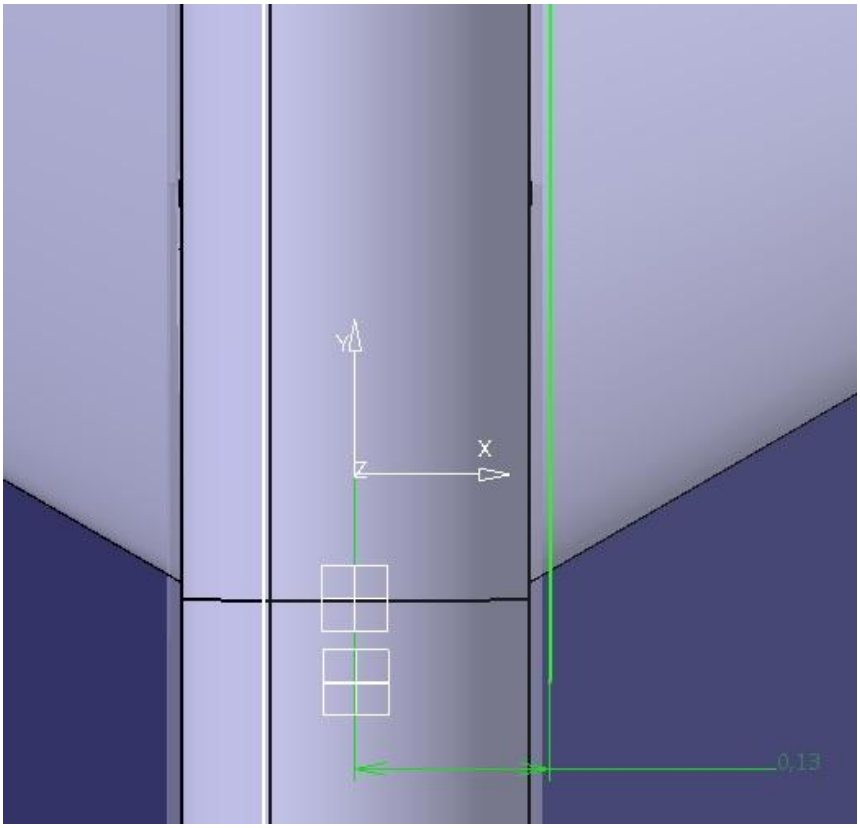

Figure 4.24 Vertical Cut plot location from 0.13m from centerline

4.7.1.1.1 Pressure Contours from 0.13m Spanwise Direction

$\alpha=2^0$

High wing Configuration

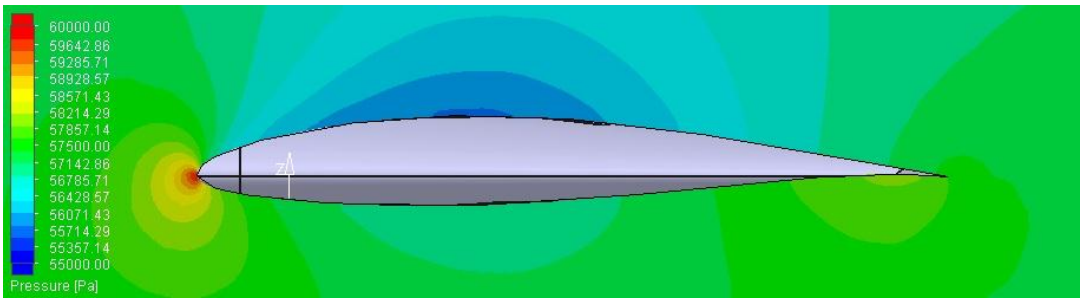

Mid wing Configuration

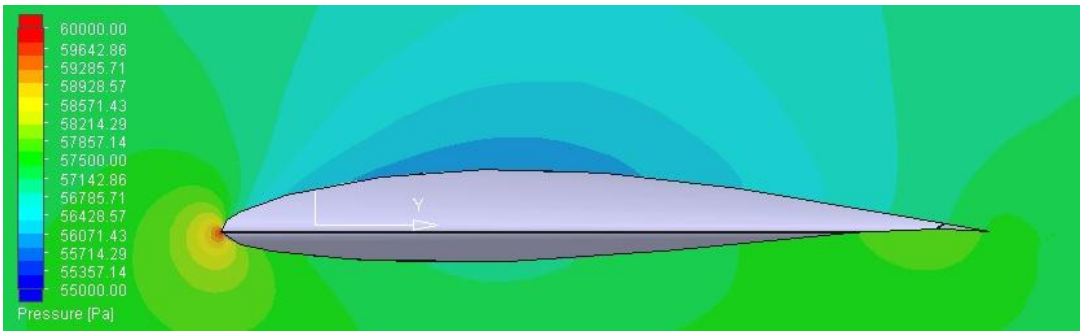

Low wing Configuration

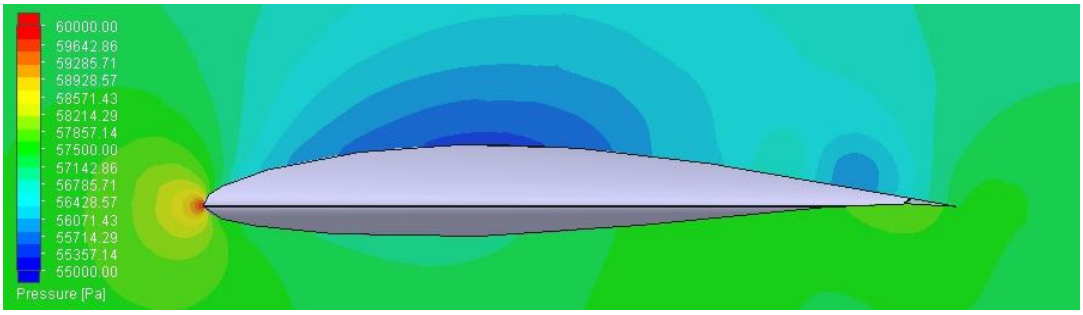

Figure 4.25 Pressure Contours 0.13m from centerline for High wing, Mid wing and Low wing Configurations at $\alpha=2^0$

$\alpha=6^0$

High wing Configuration

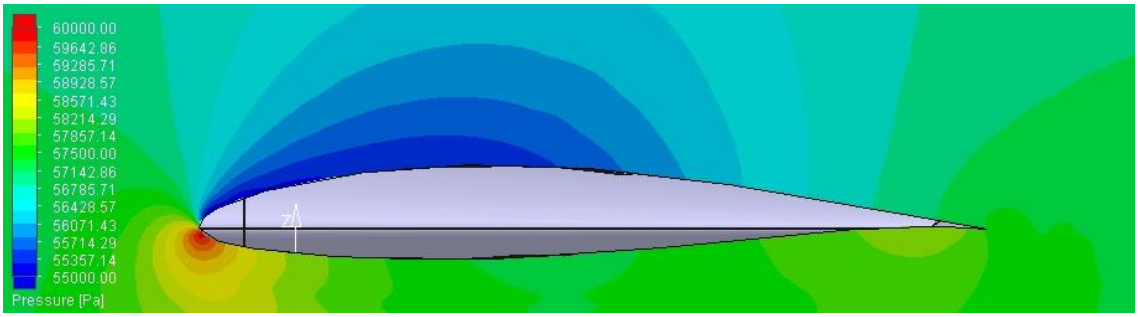

Mid wing Configuration

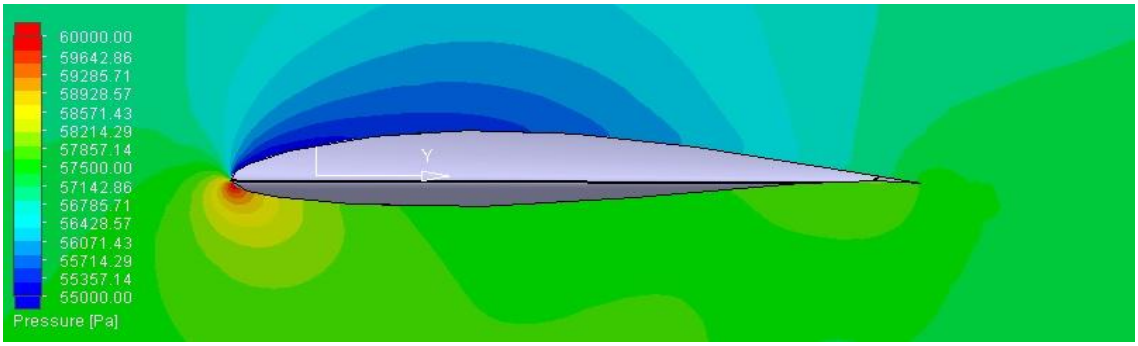

Low wing Configuration

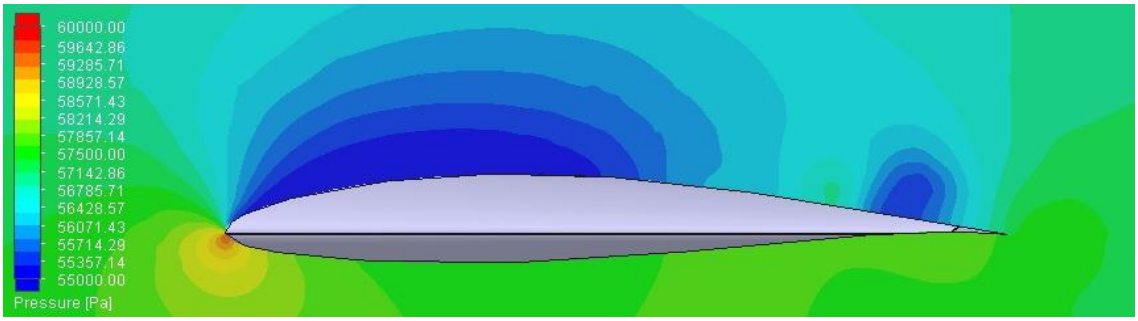

Figure 4.26 Pressure Contours 0.13m from centerline for High Wing, Mid wing and Low wing Configurations at $\alpha=6^0$

At 2 and 6 degrees of A.O.A, the high wing and mid wing configurations have similar pressure pattern whereas the low wing configuration has a pressure drop at the upper surface of the trailing of the airfoil. This shows a flow separation due to wing interference with fuselage.

$\alpha=14^0$

High wing Configuration

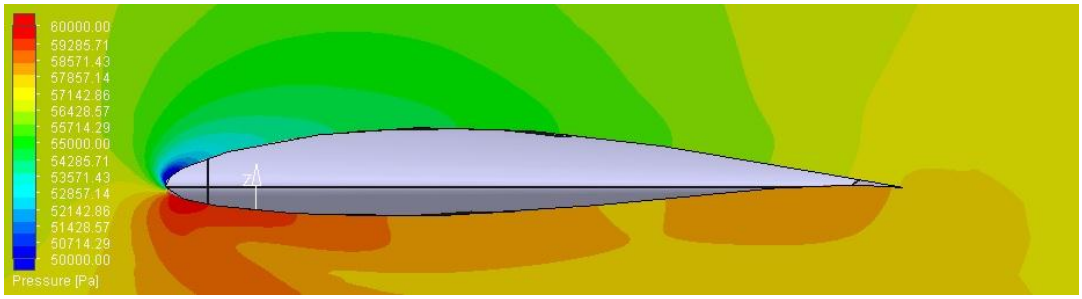

Mid wing Configuration

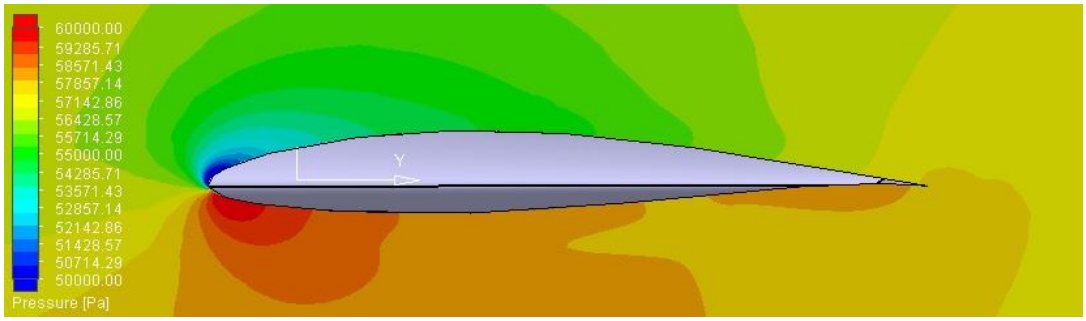

Low wing Configuration

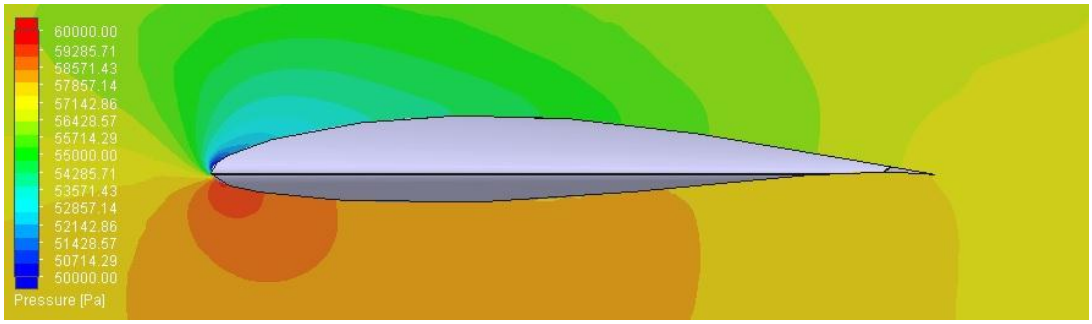

Figure 4.27 Pressure Contours 0.13m from centerline for High Wing, Mid wing and Low wing Configurations at $\alpha=14^0$

At $\alpha=14^0$, high wing pressure contours seems to have disturbed by the fuselage. However, the orange pressure area shows that high wing produces more lift than other configurations. This yields higher maximum lift coefficient than other wing configurations.

4.7.1.1.2 Mach Number Contours from 0.13m Spanwise Direction

$\alpha=2^0$

High wing Configuration

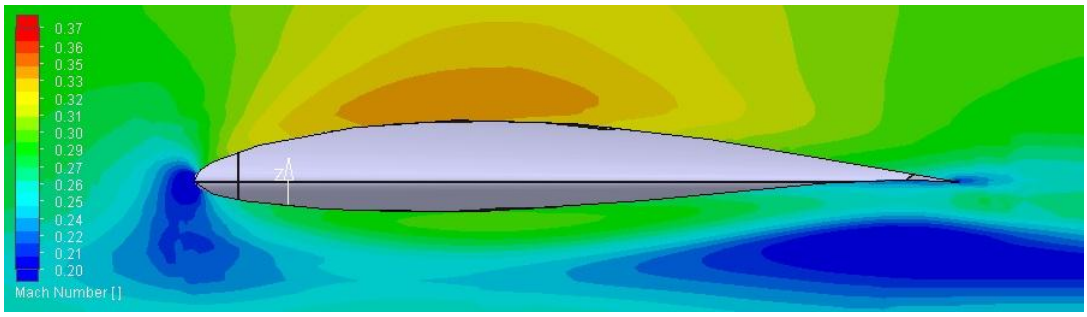

Mid wing Configuration

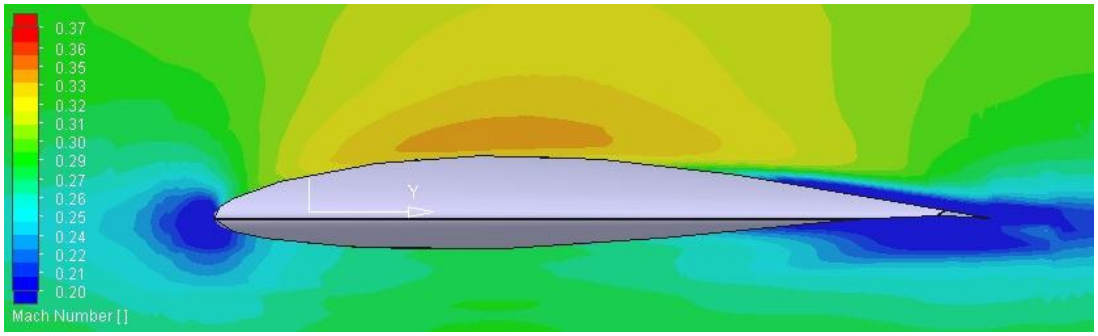

Low wing Configuration

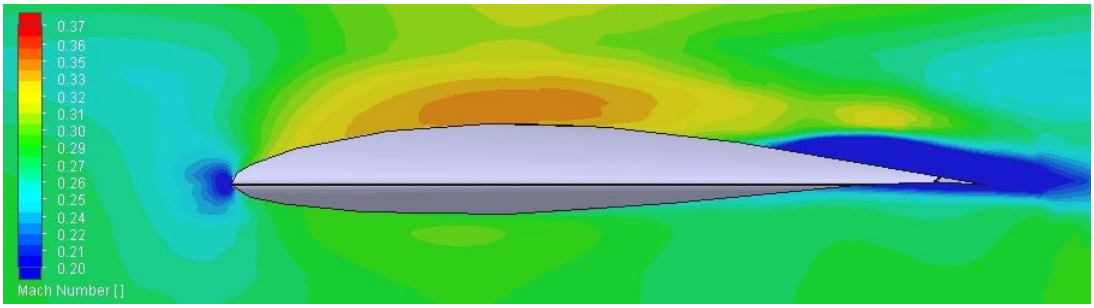

Figure 4.28 Mach Number Contours 0.13m from centerline for HighWing, Midwing and Lowwing Configurations at $\alpha=2^0$

While, Mid wing and Low Wing configurations there is a minimal flow separation at the trailing edge of the airfoil, the trailing edge of the airfoil is totally clear for High wing during $\alpha=2^0$ flight.

$\alpha=6^0$

High wing Configuration

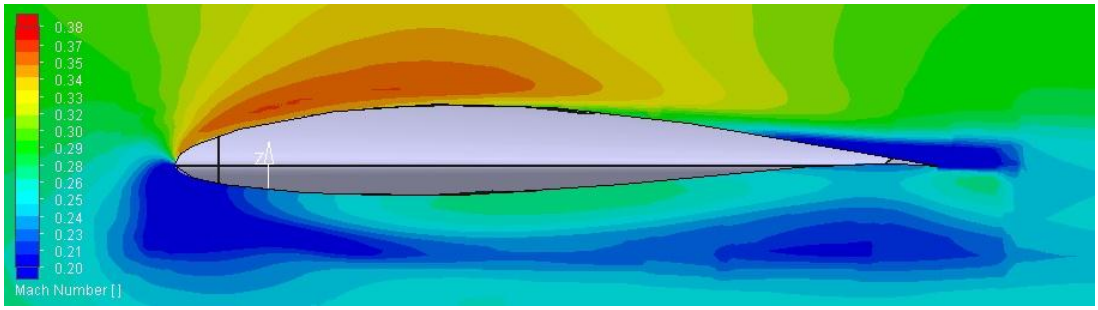

Mid wing Configuration

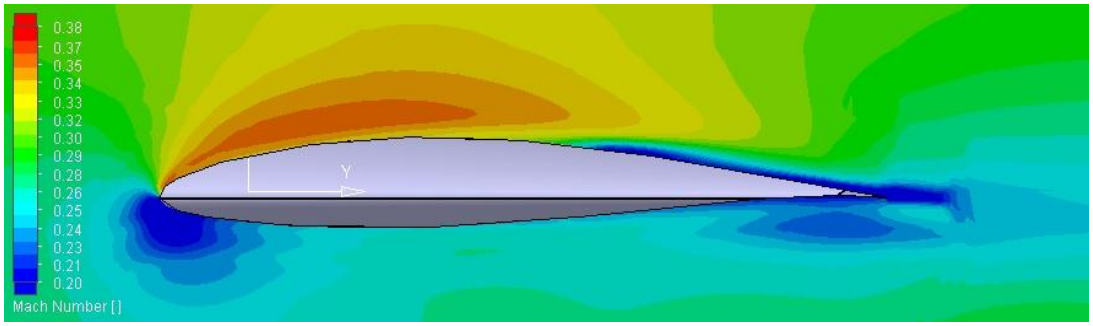

Low wing Configuration

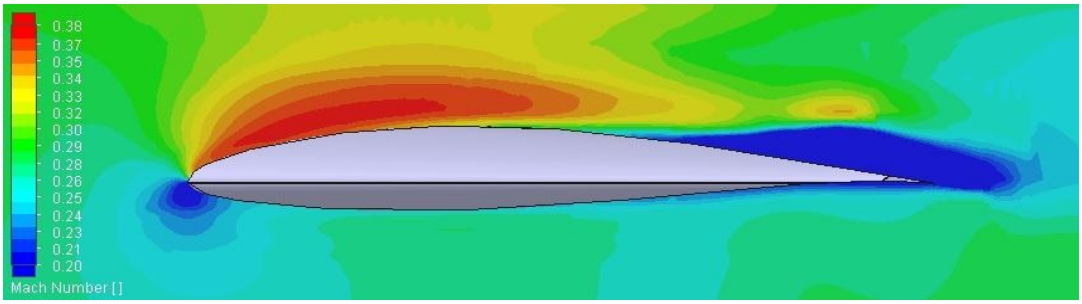

Figure 4.29 Mach Number Contours 0.13m from centerline for High wing, Mid wing and Low wing Configurations at $\alpha=6^0$

Mach number contours show that, flow separation occurs at the trailing edge of the airfoil of the Low wing configuration at $\alpha=2^0$ and $\alpha=6^0$. The reason is, the trailing edge upper surface of the airfoil is affected by the fuselage at low wing. For High wing, lower surface of the airfoil is affected by fuselage and this make more pressure difference and generates more lift. Moreover, flow separation is minimal for High wing configuration.

$\alpha=14^0$

High wing Configuration

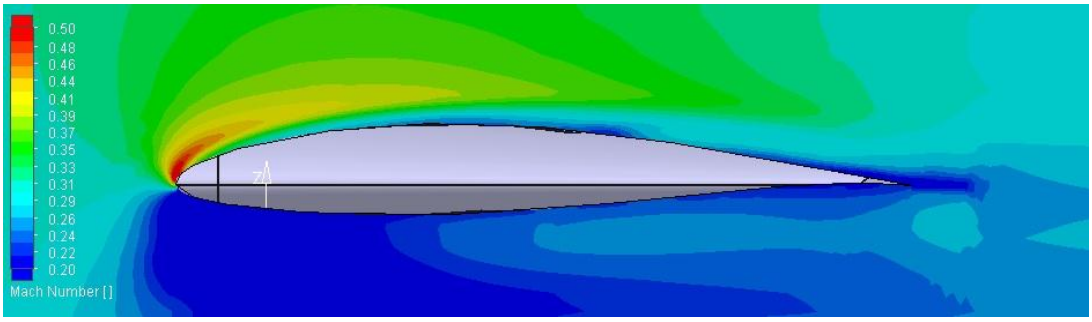

Mid wing Configuration

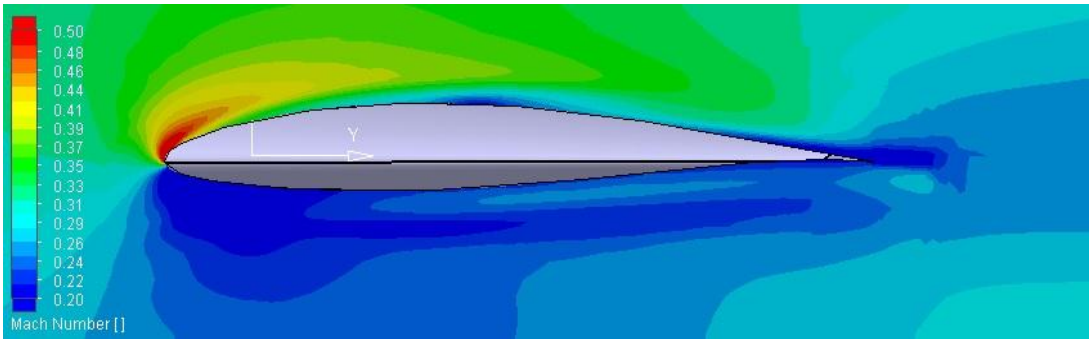

Low wing Configuration

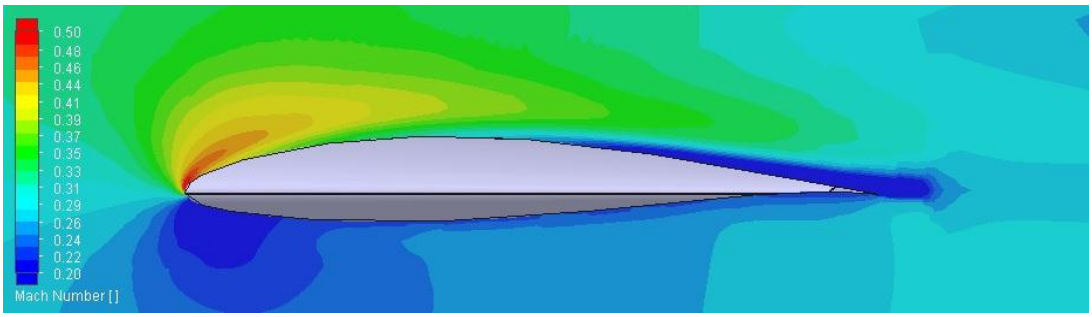

Figure 4.30 Mach Number Contours 0.13m from centerline for HighWing, Midwing and Lowwing Configurations from at $\alpha=14^0$

At $\alpha=14^0$, for High wing configuration, the air at lower surface of the airfoil is slowed by fuselage interference, this situation results in a higher pressure difference between upper and lower surface and this generates extra lift.

4.7.1.2 Wing Comparison Cut Plot Results From 0.417m from Centerline

Pressure and mach number contour cut plots were made for wing aerodynamic center spanwise direction which is located at 0.417 m from centerline.

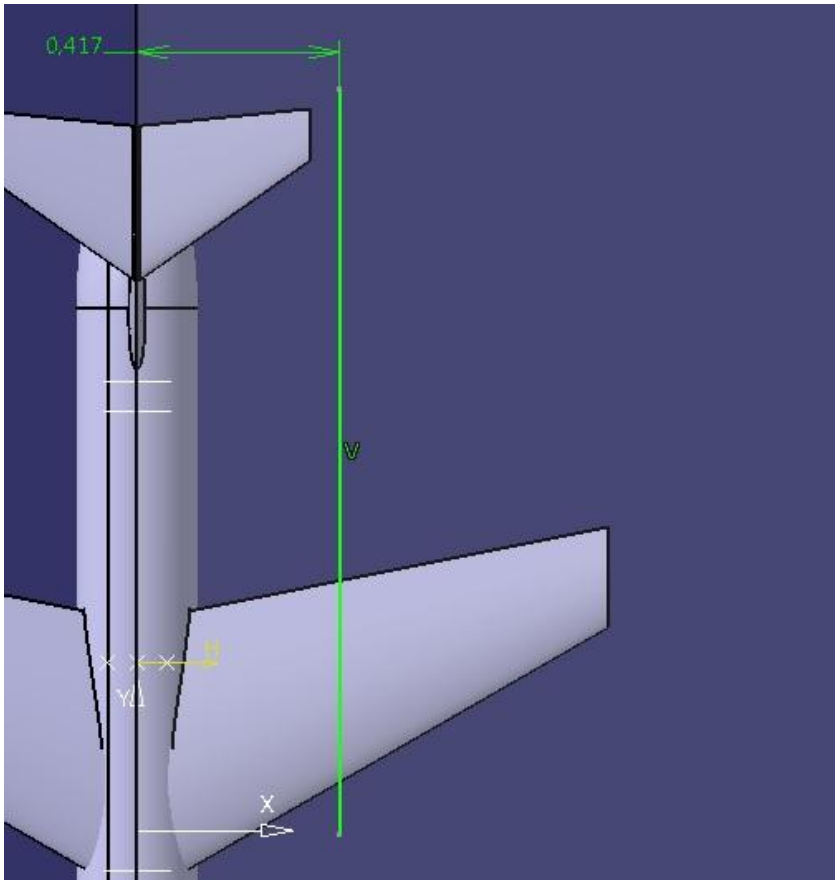

Figure 4.31 Vertical Plane Cut plot location 0.417m from centerline

Results are shown for 3 different A.O.A values 2, 6 and 14 degrees, 20 different colours were used for contours.

4.7.1.2.1 Pressure Contours from 0.417m Spanwise Direction

$\alpha=2^0$

High wing Configuration

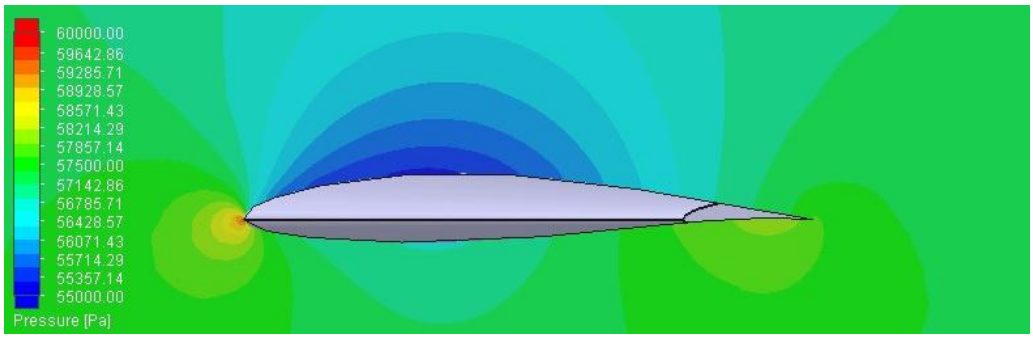

Mid wing Configuration

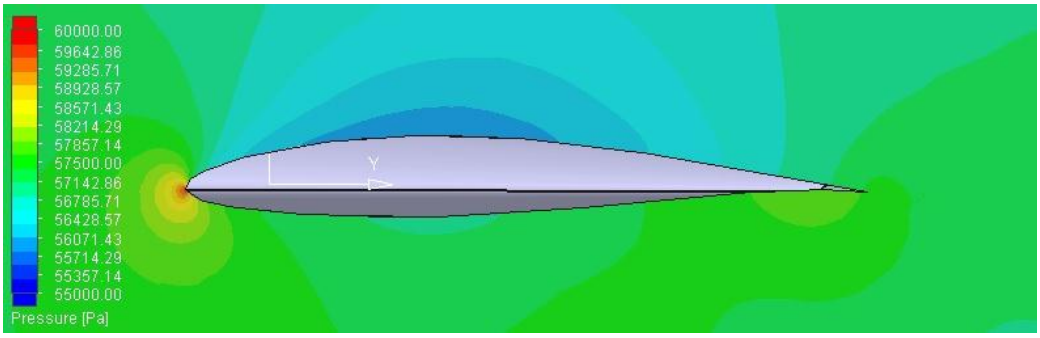

Low wing Configuration

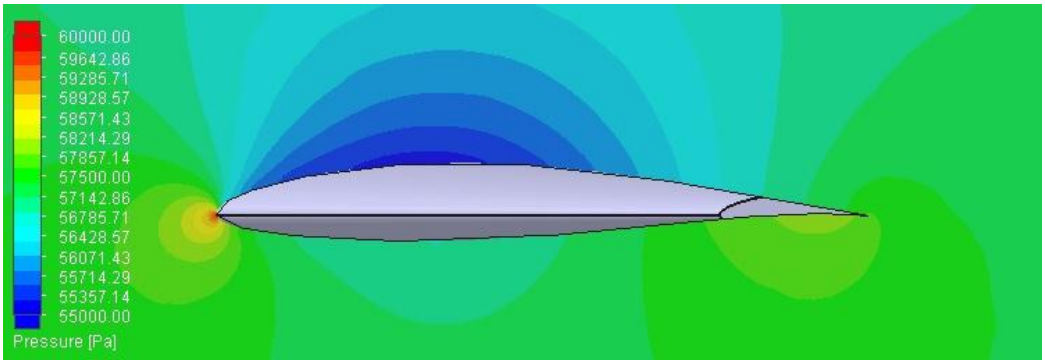

Figure 4.32 Pressure Contours 0.417m from centerline for High Wing, Mid wing and Low wing Configurations at $\alpha=2^0$

$\alpha=6^0$

High wing Configuration

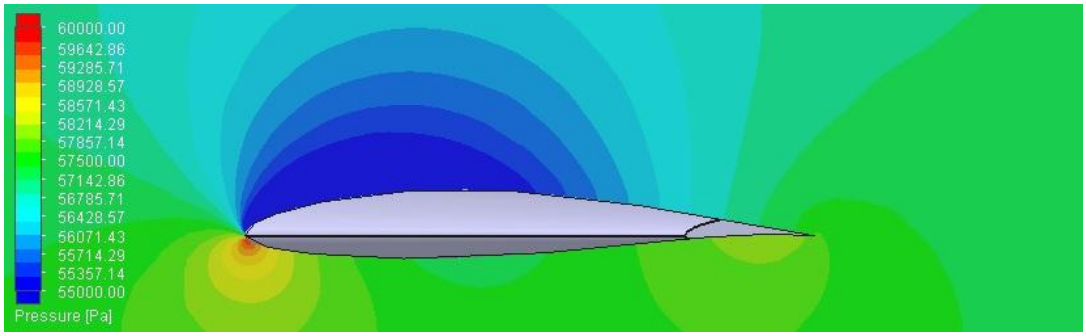

Mid wing Configuration

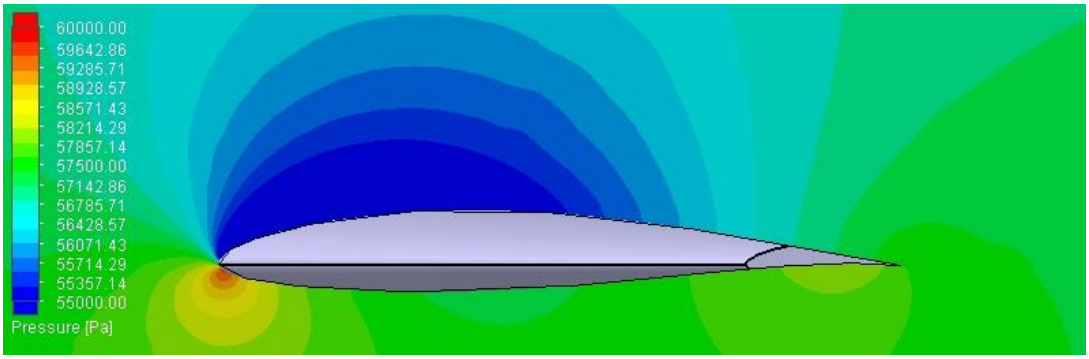

Low wing Configuration

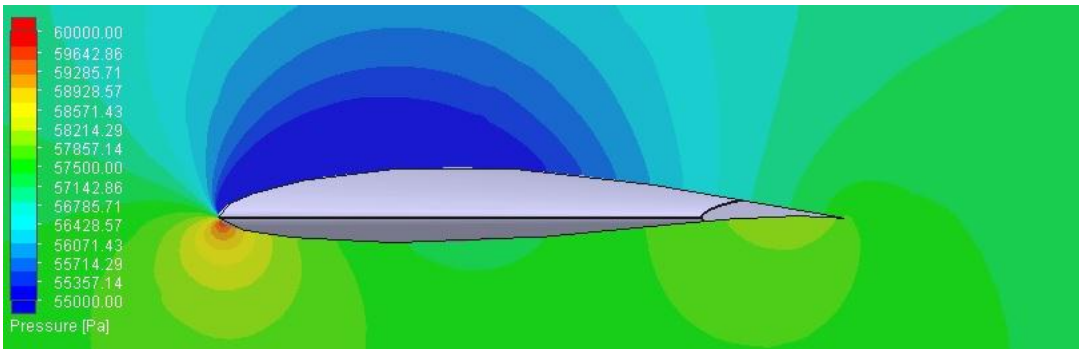

Figure 4.33 Pressure Contours 0.417m from centerline for High Wing, Mid wing and Low wing Configurations at $\alpha=6^0$

During $\alpha= 2^0$ and $\alpha= 6^0$ values, 0.417m cut plots are similar to each other. This cut plots imply that fuselage interference is not significant at these degrees of alpha.

$\alpha=14^0$

High wing Configuration

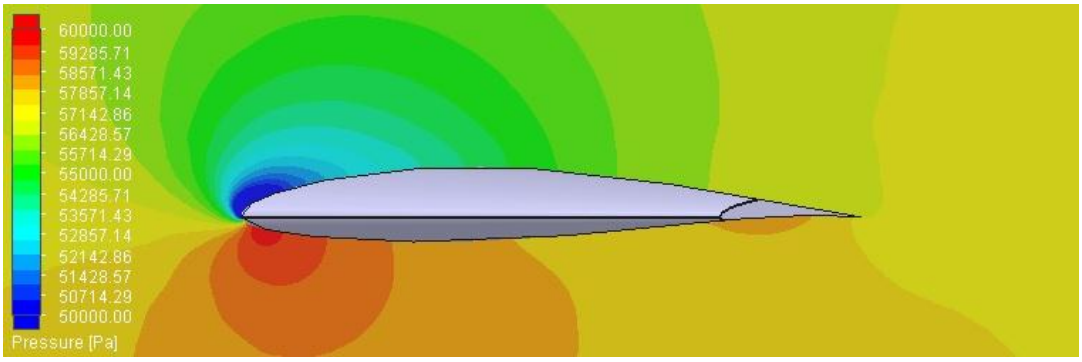

Mid wing Configuration

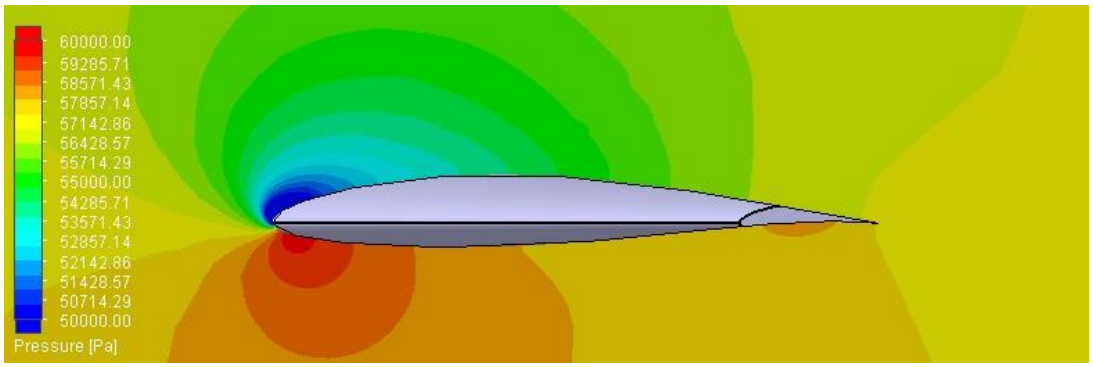

Low wing Configuration

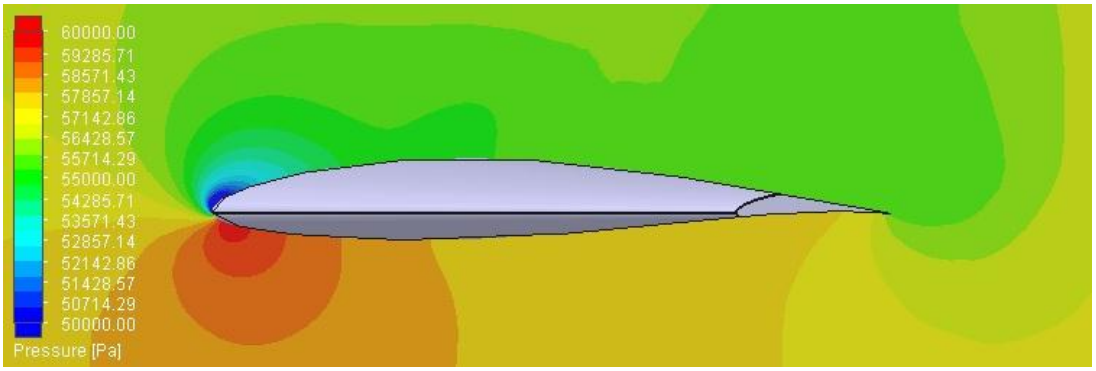

Figure 4.34 Pressure Contours 0.417m from centerline for High Wing, Mid wing and Low wing Configurations at $\alpha=14^0$

The pressure difference in low wing is lower than mid wing and high wing it means that low wing generates less lift and it is more prone to stall at $\alpha=14^0$

4.7.1.2.2 Mach Number Contours from 0.417m Spanwise Direction

$\alpha=2^0$

High wing Configuration

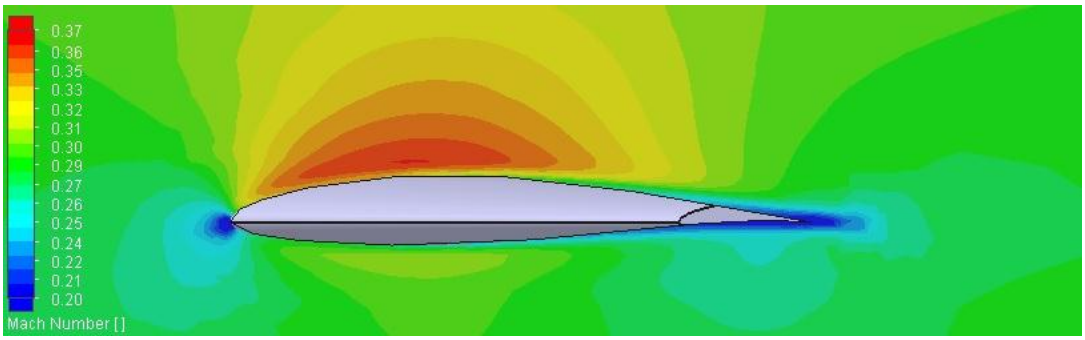

Mid wing Configuration

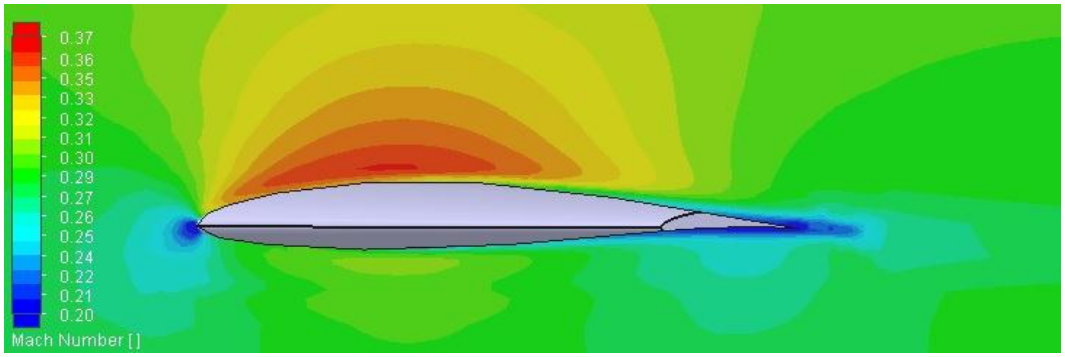

Low wing Configuration

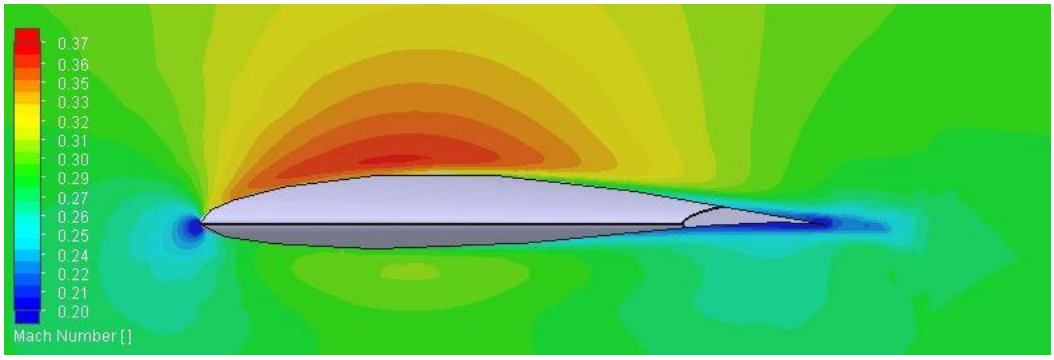

Figure 4.35 Mach Number Contours 0.417m from centerline for High Wing, Mid wing and Low wing Configurations at $\alpha=2^0$

$\alpha=6^0$

High wing Configuration

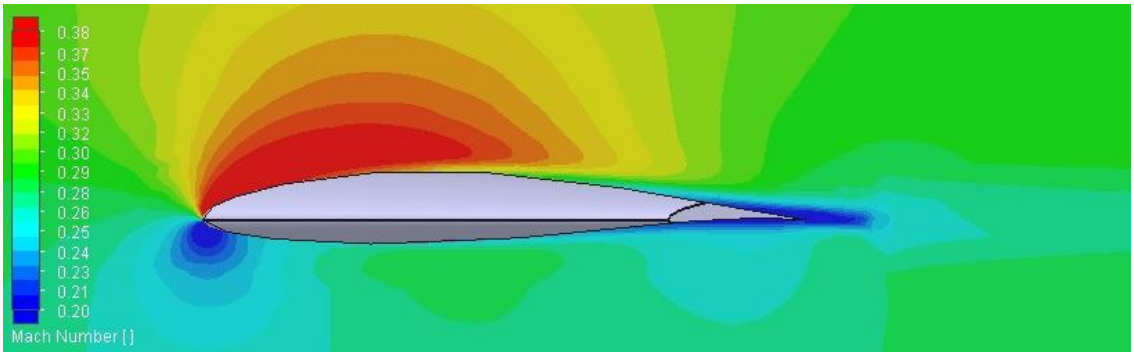

Mid wing Configuration

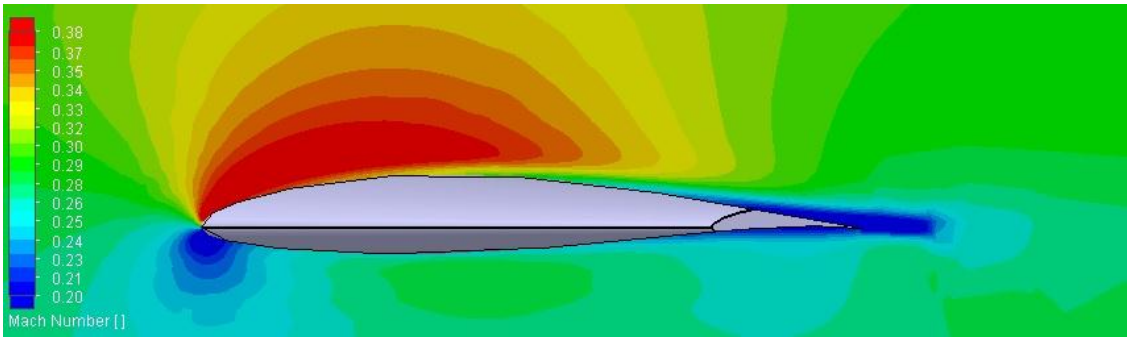

Low wing Configuration

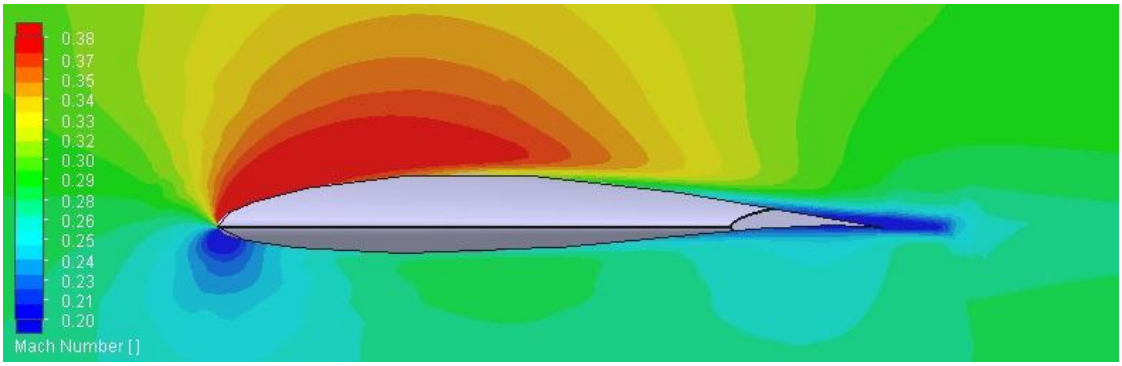

Figure 4.36 Mach Number Contours 0.417m from centerline for High Wing, Mid wing and Low wing Configurations at $\alpha=6^0$

Mach number contours are similar for $\alpha= 2^0$ and $\alpha=6^0$, the fuselage interference seems to be insignificant at this spanwise location.

$\alpha=14^0$

High wing Configuration

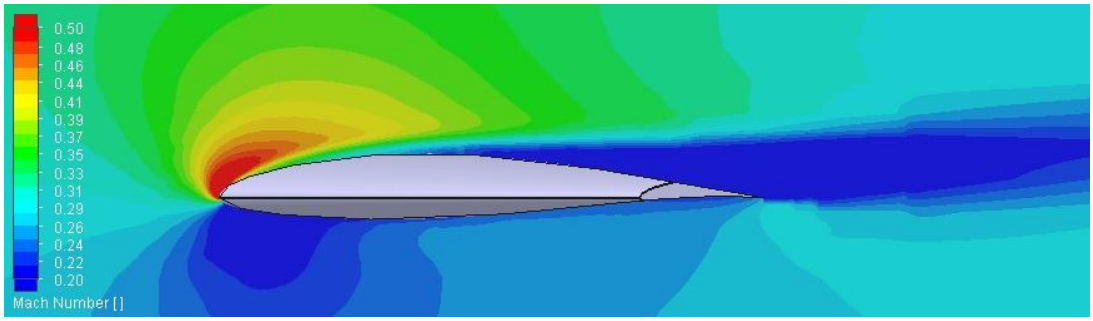

Mid wing Configuration

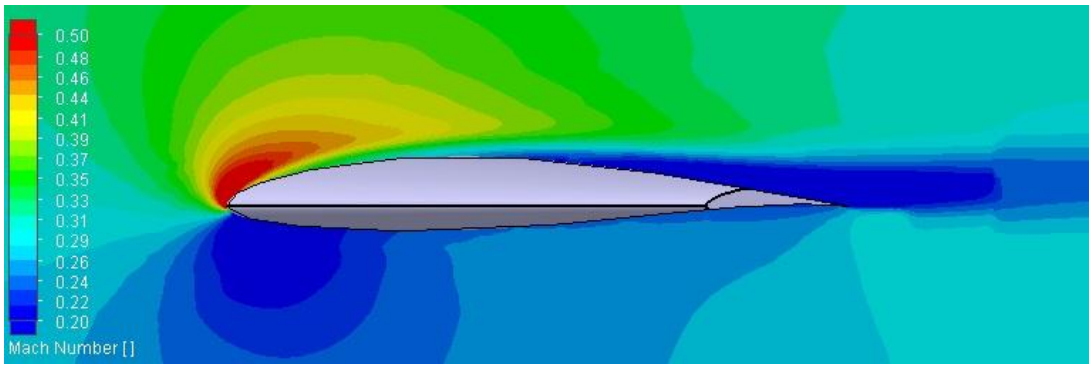

Low wing Configuration

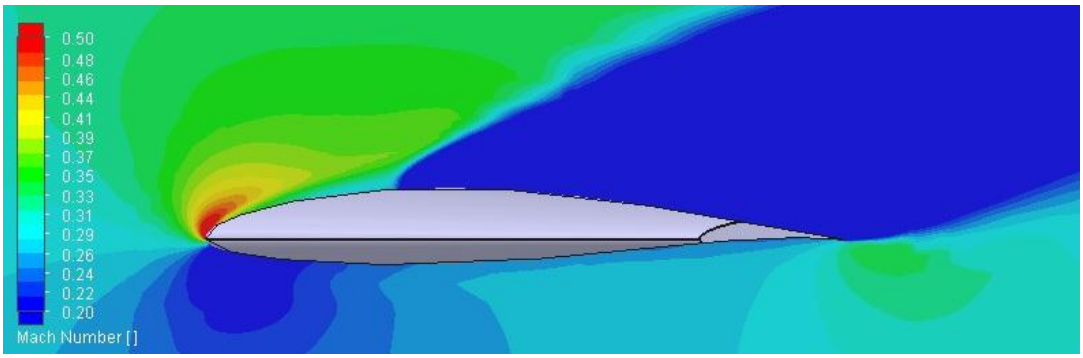

Figure 4.37 Mach Number Contours 0.417m from centerline for High Wing, Mid wing and Low wing Configurations at $\alpha=14^0$

Unlike figure 4.38 and 4.39, at $\alpha=14^0$, mach number contour of the low wing is different than other configurations, stall phenomena starts at low wing configuration. 0.13m cut plots showed that, low wing configuration is more prone to flow

separation. Figure 4.40 confirms that, low wing stall resistance is less than other configurations.

4.7.1.3 Wing Comparison Pressure Coefficient Results From 0.417m from Centerline

CP distribution curves were plotted from wing aerodynamic center spanwise direction which is located 0.417m spanwise direction from centerline.

$\alpha=2^0$

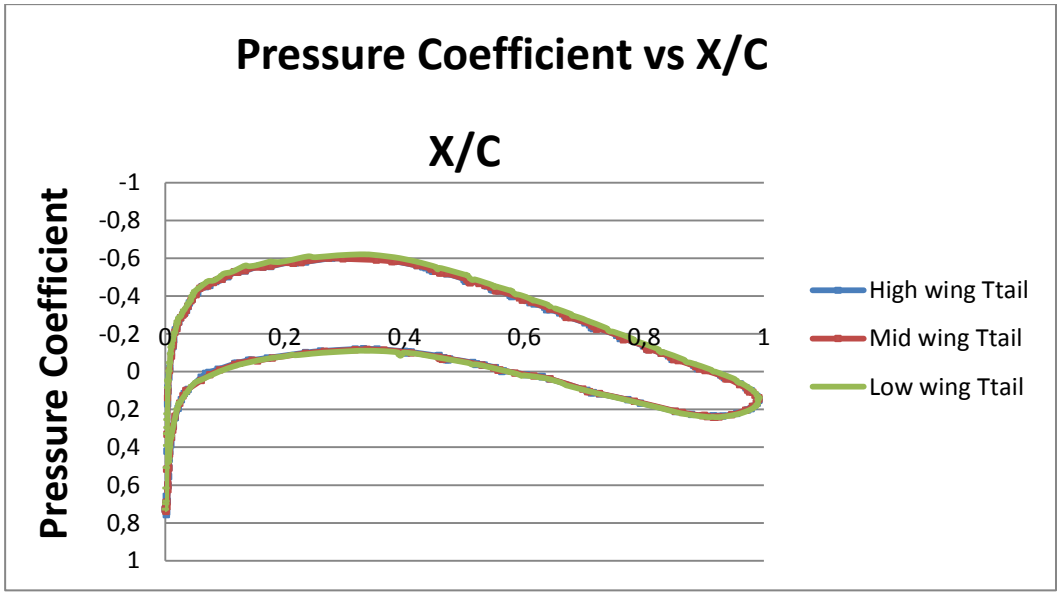

Figure 4.38 Pressure Coefficient distribution 0.417m from centerline for High wing, Mid wing and Low wing at $\alpha=2^0$.

$\alpha=6^0$

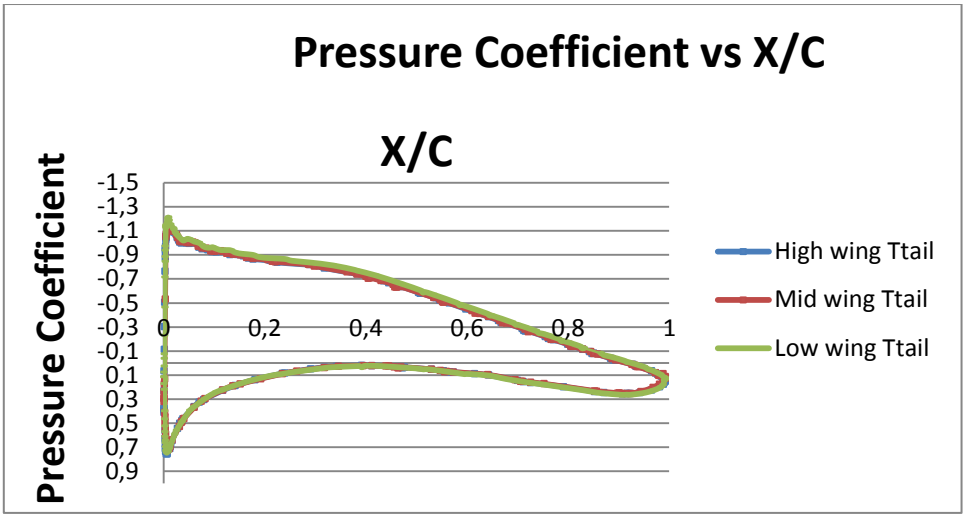

Figure 4.39 Pressure Coefficient distribution 0.417m from centerline for Highwing, Midwing and Lowwing at $\alpha=6^0$.

At 0.417m spanwise location, the CP distributions are exactly same for different wing combinations for $\alpha=2^0$ and $\alpha=6^0$. It can be concluded that, fuselage interference is not present or it is negligibly small in this spanwise direction at low angles of attack.

$\alpha=14^0$

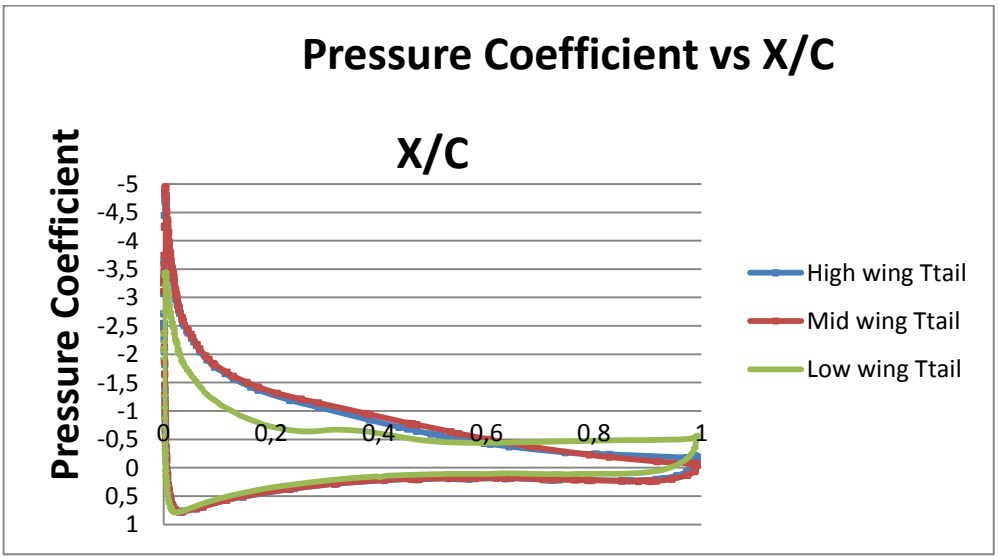

Figure 4.40 Pressure Coefficient distribution 0.417m from centerline for High wing, Mid wing and Low wing at $\alpha=14^0$.

At $\alpha=14^0$however, CP distribution of low wing is shifted. Which means that the low wing configuration experiences an earlier flow separation. The reason could be the fuselage interference effect on the upper surface of the airfoil of the low wing. In previous section, it was shown that the fuselage effect forces the flow to separate at the trailing edge at 0.13m cut plot. This situation leads to enter to stall earlier than other configurations.

4.7.1.4 Lift, Drag and Moment Coefficients for Wing Selection

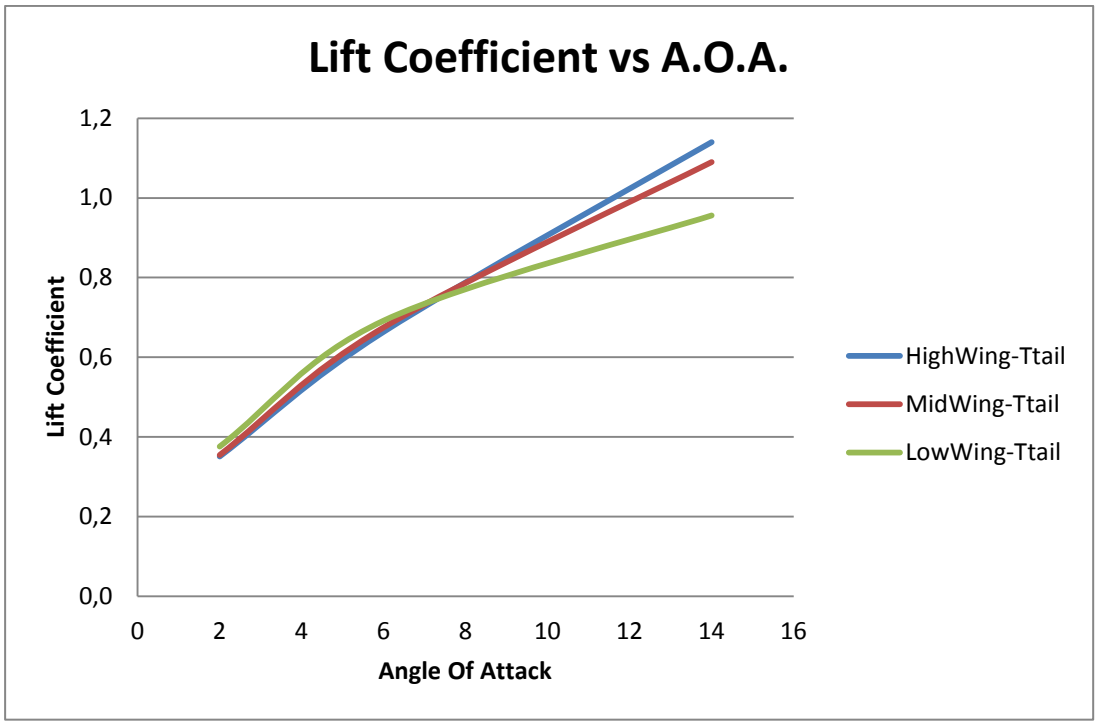

Figure 4.41 Lift Coefficient versus Angle of attack of High wing, Mid wing and Low wing

Low wing lift coefficient values are higher than other configurations for $\alpha=2^0$ and $\alpha=6^0$. However, the lift efficiency quickly drops and the maximum lift coefficient of low wing becomes the lowest one. The reason could be early flow separation. At $\alpha=2^0$ and $\alpha=6^0$, the pressure drop at trailing edge contributes ekstra lift to the aircraft.

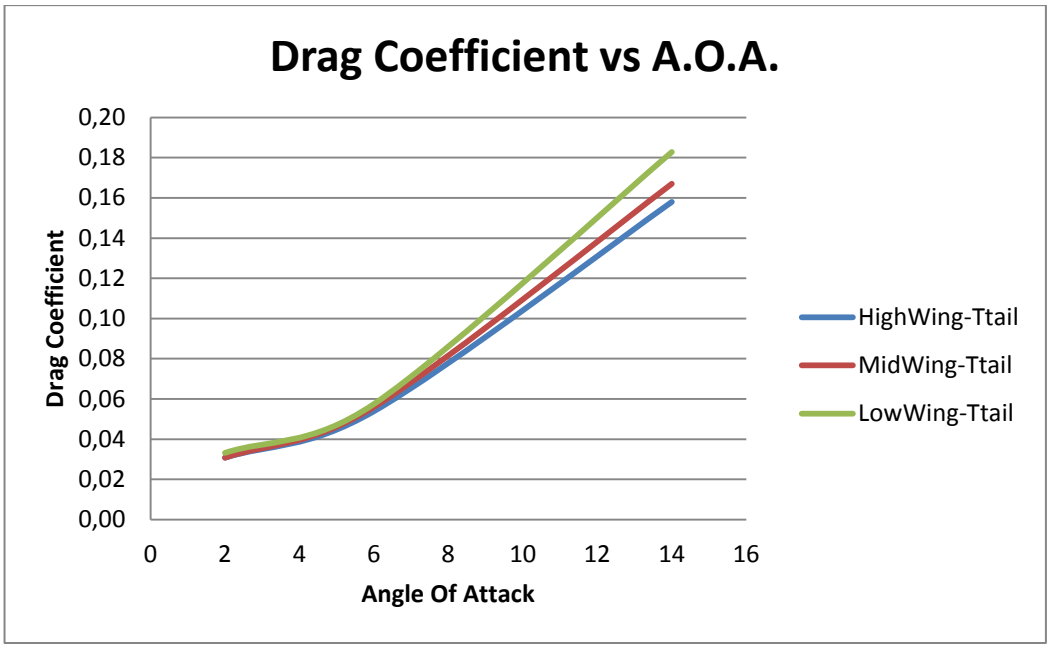

Figure 4.42 Drag Coefficient versus Angle of attack of High wing,Mid wing and Low wing

As expected, mid wing configuration yields lowest drag for low angles of attack because of low fuselage interference. However, at higher angles of attack, high wing configuration is more advantageous. It generates the lowest drag at high angles of attack. The fuselage interference has a positive effect on high wing configuration for high α values.

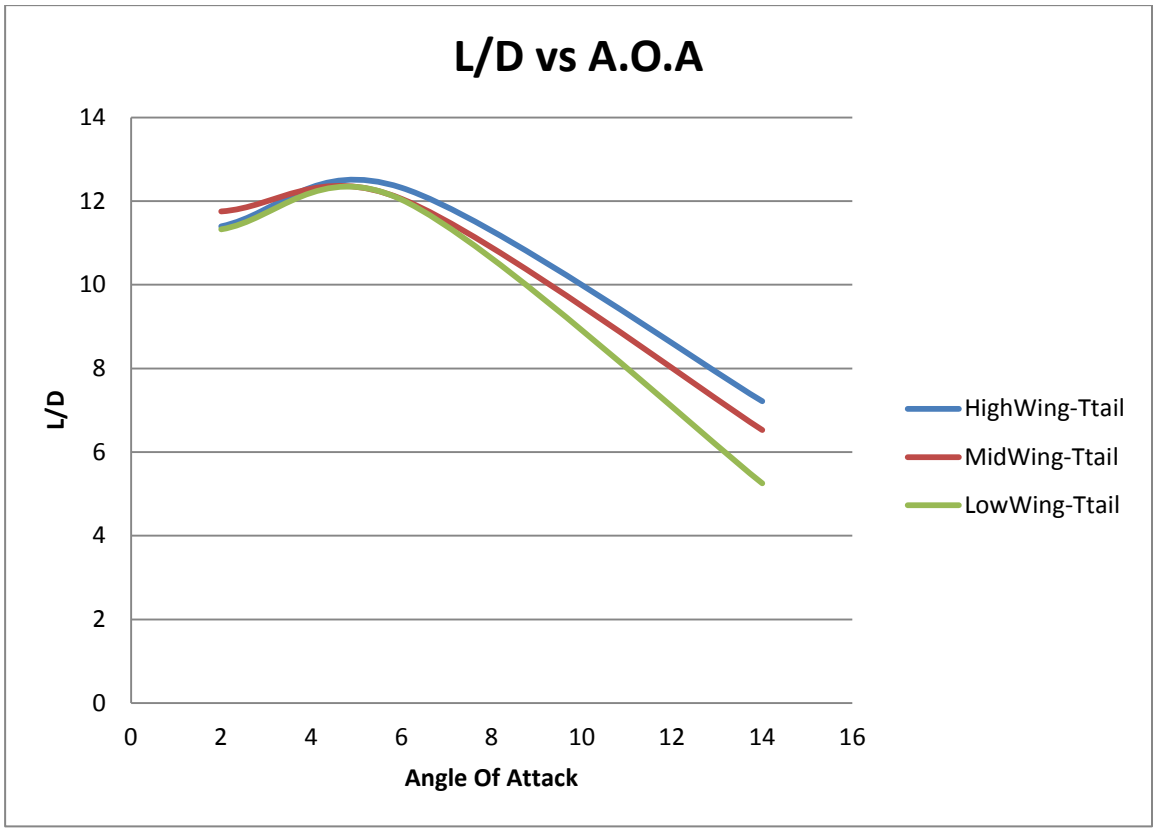

Figure 4.43 L/D versus Angle of attack of High wing, Mid wing and Low wing

L/D graph shows that, Mid wing aircraft has advantage on High wing for low values of α, whereas, High wing aircraft has advantage on Mid wing for high values of α.

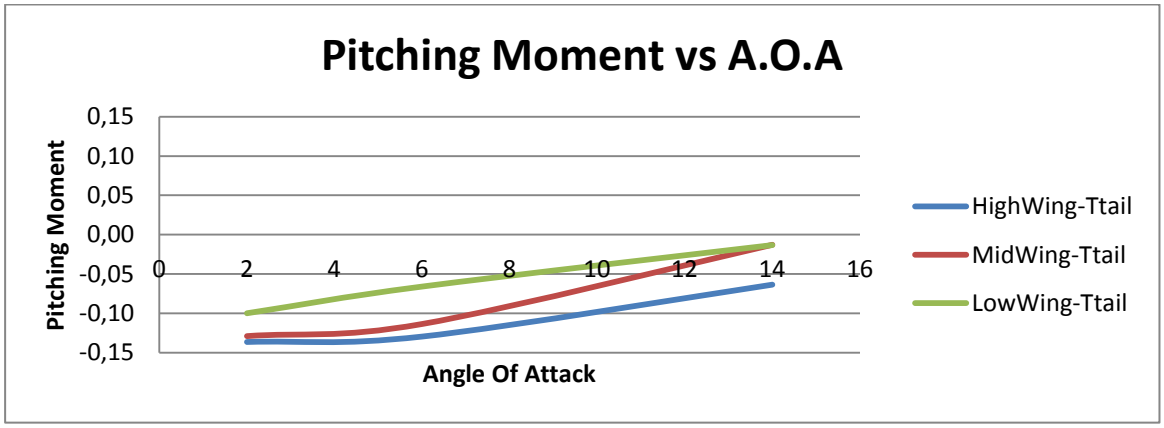

Figure 4.44 Pitching Moment Coefficient versus Angle of attack of High wing, Mid wing and Low wing

From aircraft parameters, Aircraft is calculated as stable. However, the pitching moment curve shows that aircraft is unstable. Figure 4.47 show that High wing configuration has most negative C_M value.

CFD analysis claim that fuselage effect negatively effects the low wing and forces the flow to separate and makes the low wing prone to the stall and reduces its lift efficiency. It makes low wing worst wing vertical position aircraft among all configurations. High wing and mid wing shows similar pattern. High wing has more advantage for high angles of attack.

CFD analysis revealed that for low angles of attack, mid wing configuration has lowest drag and highest L/D values. Whereas for higher angles of attack, High wing configuration yields lowest drag coefficient, highest maximum lift coefficient(C_{Lmax}) with 1.14 and gave highest L/D values. Unlike theory presented in Chapter 3, High wing configuration model yielded the lowest drag at higher angles of attack compared to other configurations. Therefore, High wing was selected for wing configuration.

4.7.2 Tail Comparison Results

After selecting high-wing configuration, Highwing configuration was kept constant and tail configurations were altered.

In this section stall angle 16 Degrees of A.O.A. results are added, because wing wake should be seen at stall condition. Pressure and mach number contours during $\alpha=14^0$ and $\alpha=16^0$. were shown in figures. $\alpha=2^0$and $\alpha=6^0$ were also analyzed however, wing wake is insignificant in these degrees.

The lift, drag, L/D and pitching moment values were also obtained during CFD analysis. Note that, the contour cut plots were obtained from the M.A.C of the horizontal tail which is located from 0.231m from centerline of the aircraft.

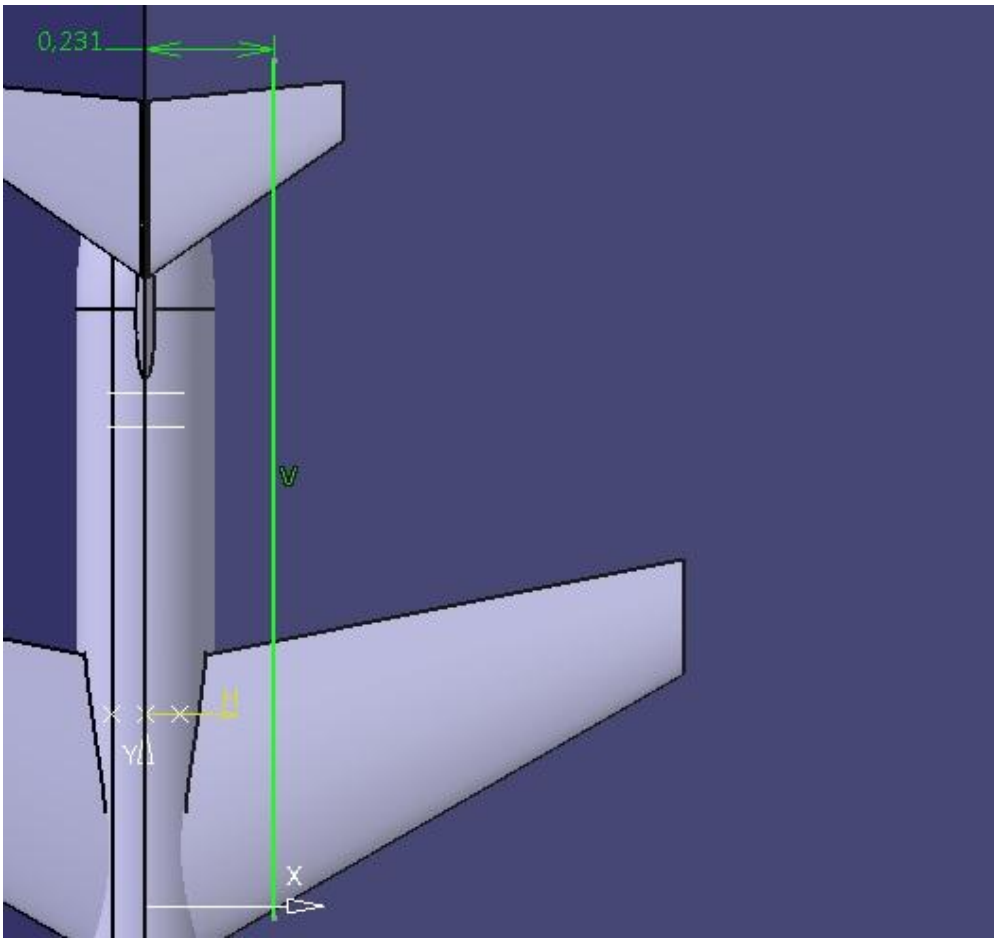

Figure 4.45 Vertical Plane Cut Plot 0.231m spanwise direction from centerline

4.7.2.1 Pressure Contours from 0.231m Spanwise Direction

$\alpha=14^0$

T Ttail Configuration

Cruciform Tail Configuration

Conventional Tail Configuration

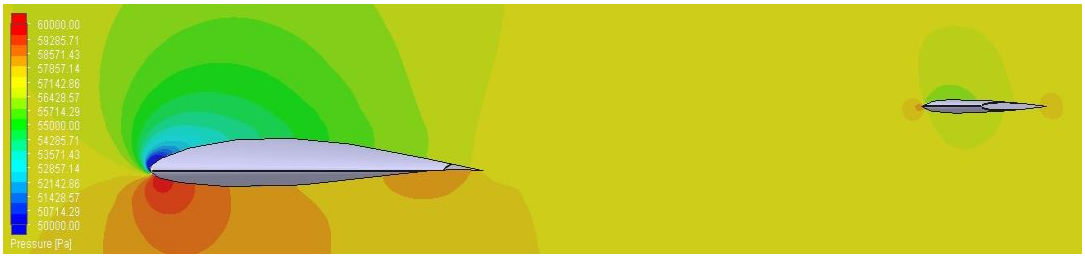

Figure 4.46 Pressure Contour Cut plots 0.231m from centerline of T-tail,Cruciform tail and Conventional Tail at $\alpha=14^0$

$\alpha=16^0$

T-tail Configuration

Cruciform Tail Configuration

Conventional Tail Configuration

Figure 4.47 Pressure Contour Cut plots 0.231m from centerline of T-tail,Cruciform tail and Conventional Tail at $\alpha=16^0$

Figure 4.49 and 4.50 shows that the pressure difference between upper and lower surface of the wing is the same, but the T-tail has a larger pressure difference contour. Therefore, symmetric airfoil of the T-tail generates more lift since, it is out of the wake. Mach number contours should also be plotted to confirm that T-tail is out of the wing wake.

4.7.2.2 Mach Number Contours from 0.231m Spanwise Direction

$\alpha=14^0$

T-tail Configuration

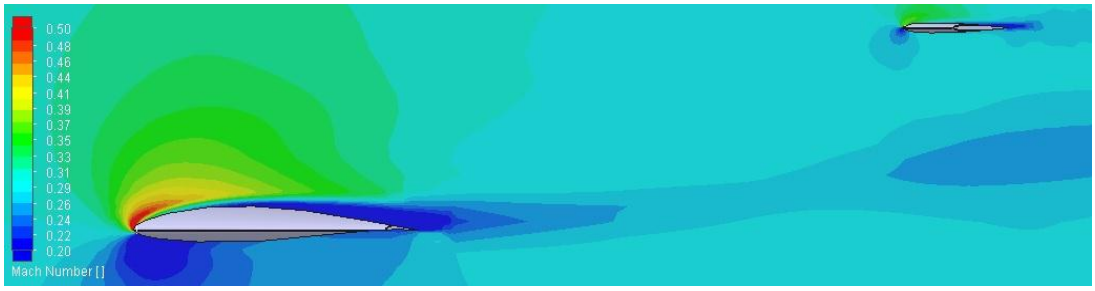

Cruciform Tail Configuration

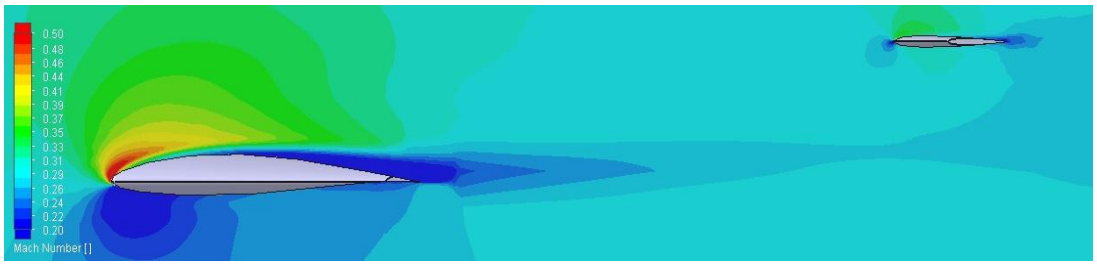

Conventional Tail Configuration

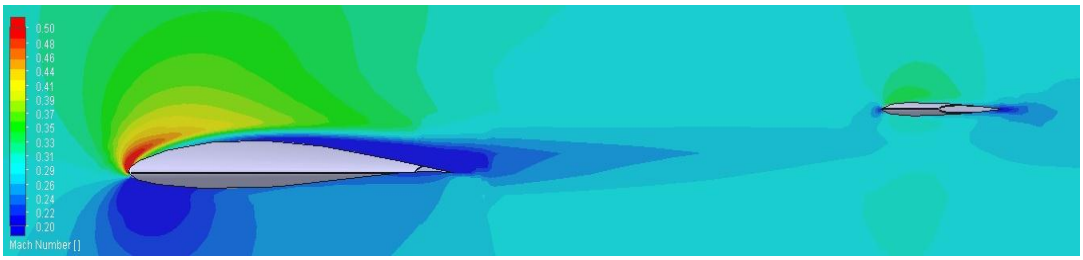

Figure 4.48 Mach Number Contour Cut plots 0.231m from centerline of T-tail,Cruciform tail and Conventional Tail at $\alpha=14^0$

$\alpha=16^0$

T -Tail Configuration

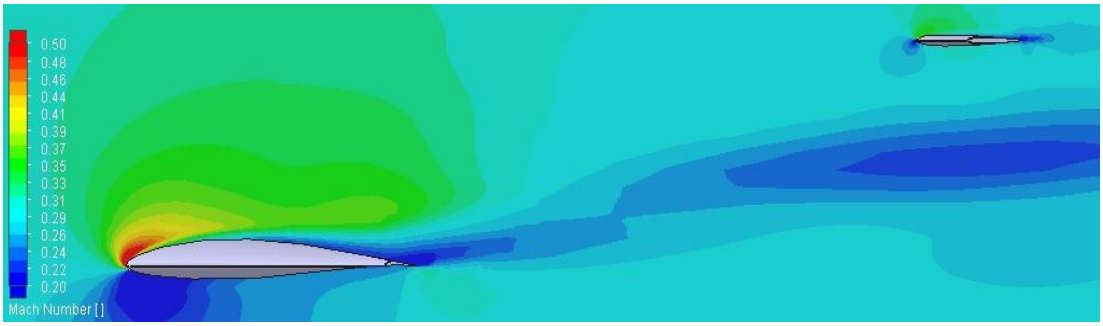

Cruciform Tail Configuration

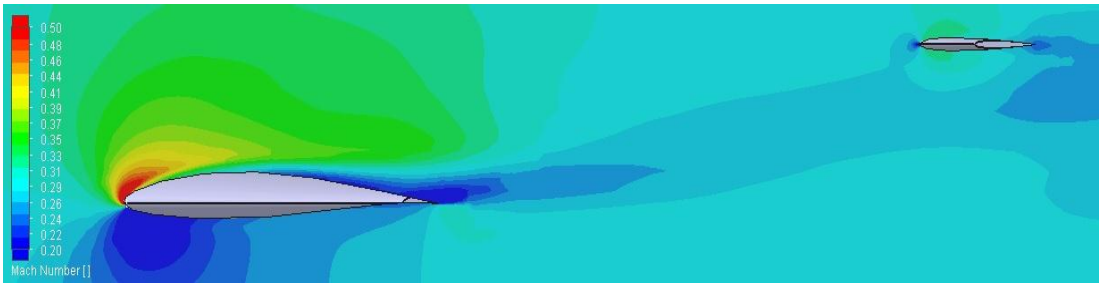

Conventional Tail Configuration

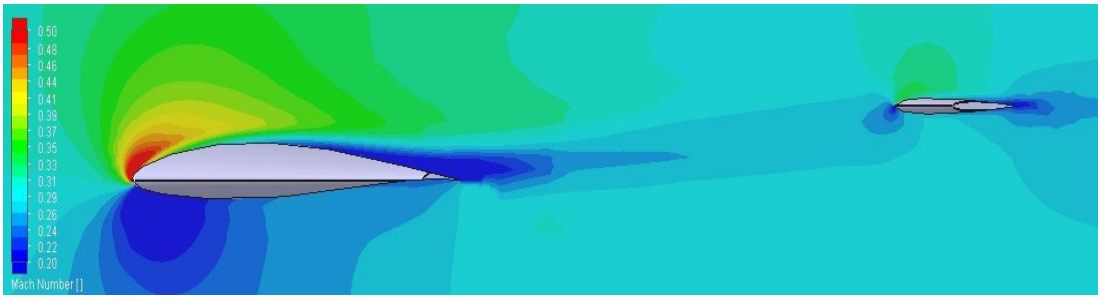

Figure 4.49 Mach Number Contour Cut plots 0.231m from centerline of T-tail,Cruciform tail and Conventional Tail at $\alpha=16^0$

Mach number 0.417m plots and 0.231m plots imply that stall phenomena starts from wing tips and it was not reached to 0.231m spanwise direction. Therefore, stall wakes were not seen clearly in tail analyses cut plots. The T-tail mach number cut plots show a small wing wake and only T-tail is clearly out of this wing wake.

To sum up, mach number contour plots confirm that the 0.231 m section of the horizontal T-tail is out of the wake.

0.231m cut plots can confirm that High wing is the best alternative, but it is not sufficient to show that complete horizontal tail is out of the wake. Therefore, Stall phenomena should be investigated in a greater detail. The stall phenomena of the T-tail will be specially investigated in a different section.

4.7.2.3 Wing CP Distribution For Tail Configuration Difference

$\alpha=2^0$

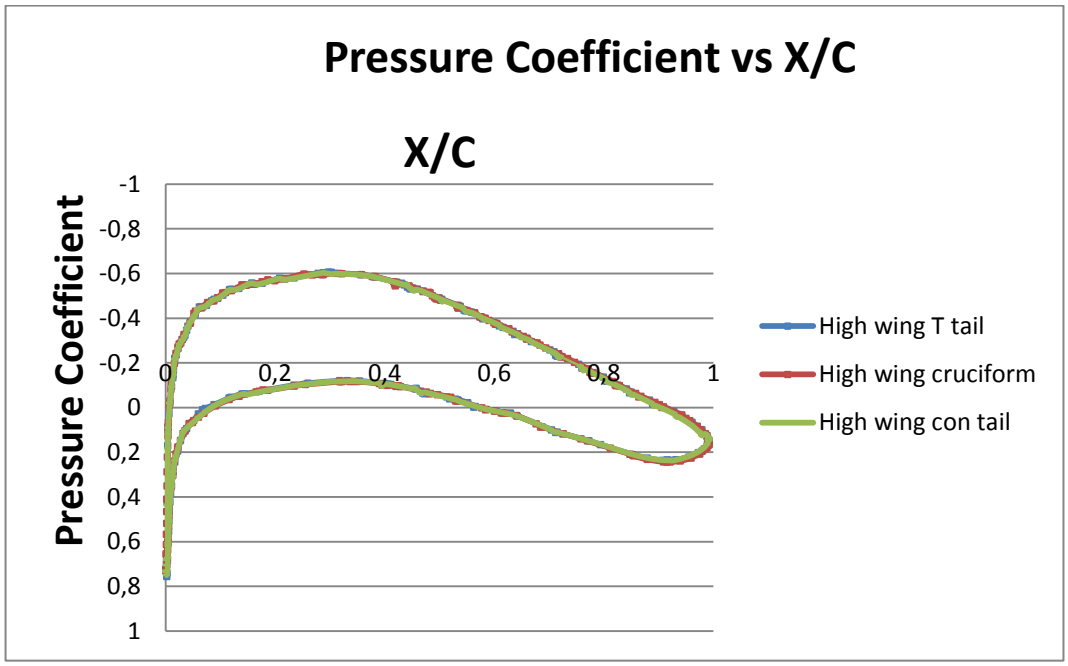

Figure 4.50 Pressure Coefficient distribution 0.231m from centerline for Ttail, CruciformTail and Conventional Tail at 2^0 A.O.A.

α=6^0

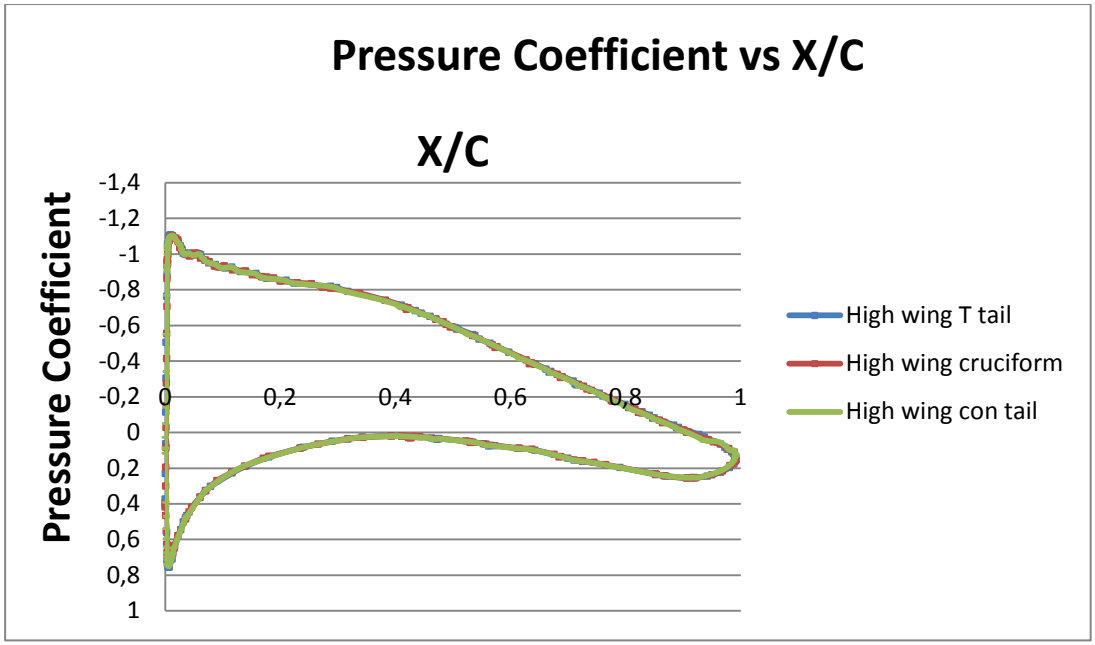

Figure 4.51 Pressure Coefficient distribution 0.231m from centerline for Ttail, CruciformTail and Conventional Tail at α=6^0.

α=14^0

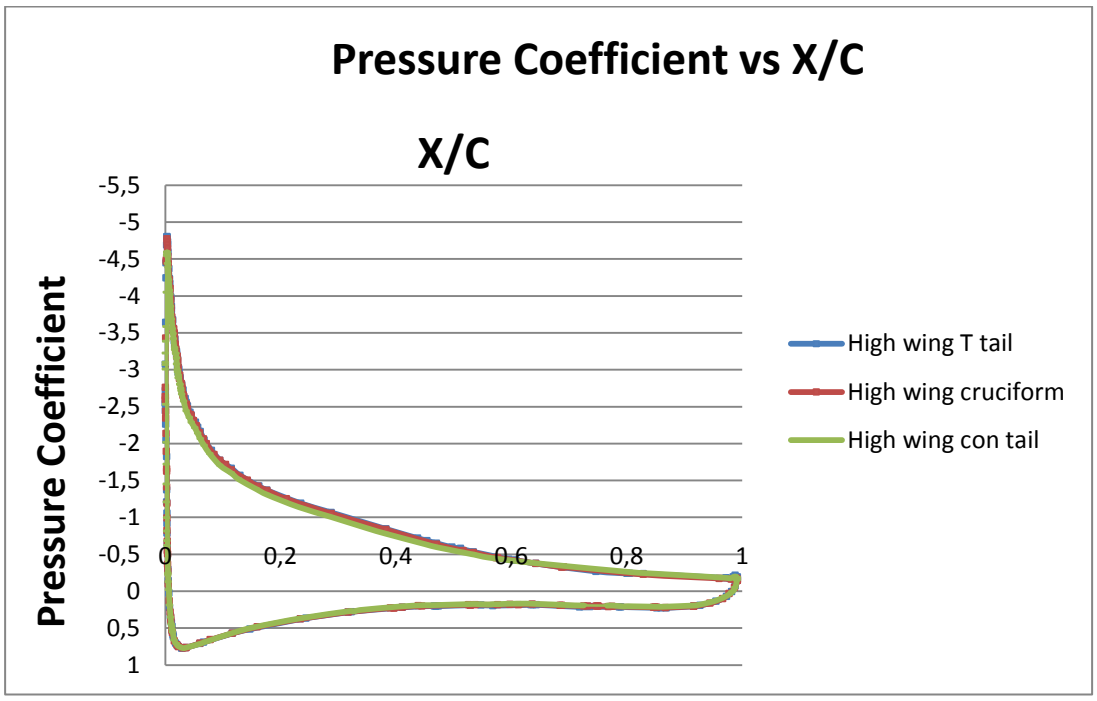

Figure 4.52 Pressure Coefficient distribution 0.231m from centerline for Ttail, CruciformTail and Conventional Tail at α=14^0

The CP graphs of $\alpha=2^0$, $\alpha=6^0$and $\alpha=14^0$ are very similar to each other, the reason is the produced lift coefficient by the wing is same since wing positions are the same.

4.7.2.4 Lift, Drag and Moment Coefficients for Tail Selection

CL, CD, L/D , CM vs A.O.A graphs are given below.

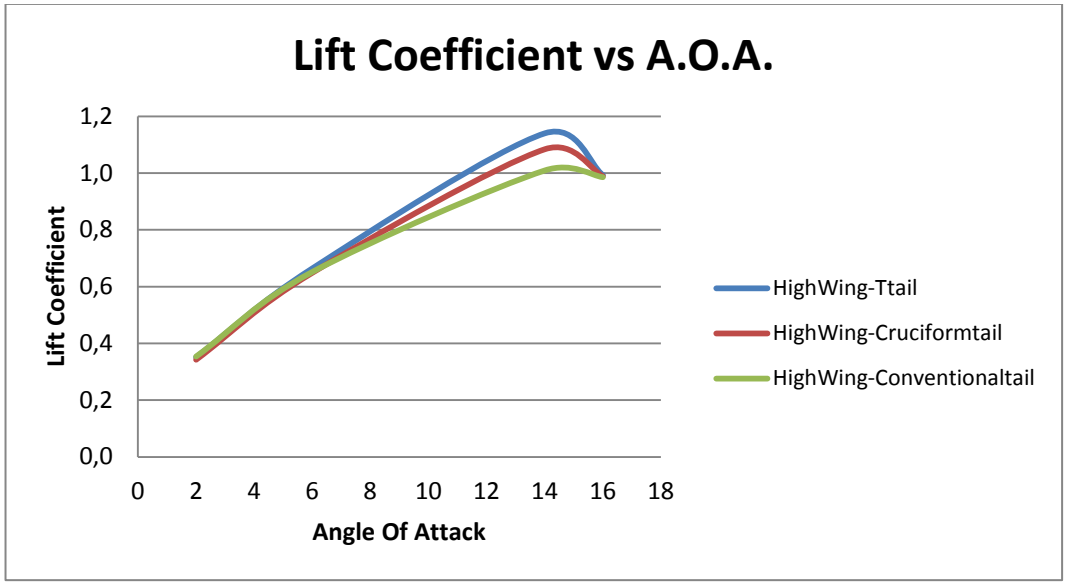

Figure 4.53 Lift Coefficient versus Angle Of Attack of T-tail, Cruciform tail and Conventional tail combinations of Highwing Configuration

This lift coefficient graph is crucially important to understand the tail effect on total lift. The wing pressure coefficient distributions are the same at $\alpha=14^0$. Tail is made of a symmetric airfoil which does not produce lift at $\alpha=0^0$. When α increases, Tail starts to produce lift and it contributes to the total lift. Since T-tail is out of the wake, it contributes more to the lift than cruciform and conventional tail. This explains why the maximum lift coefficient of T-tail is highest.

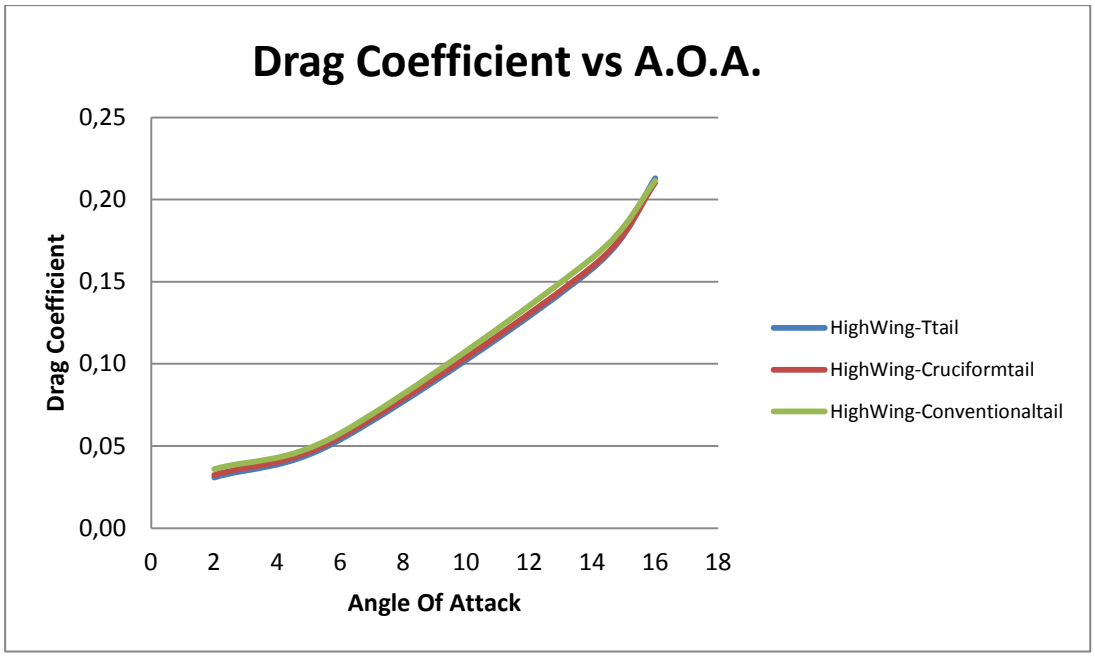

Figure 4.54 Drag Coefficient versus Angle Of Attack of T-tail, Cruciform tail and Conventional tail combinations of High wing Configuration

According to the figure 4.57, tail configurations do not change too much drag. However, T tail yields the least drag and Conventional tail configuration yields highest drag coefficient for all angles of attack. This shows the fuselage horizontal tail interference effect. As horizontal tail closes to fuselage, interference effect increases and as a result, drag coefficient increases.

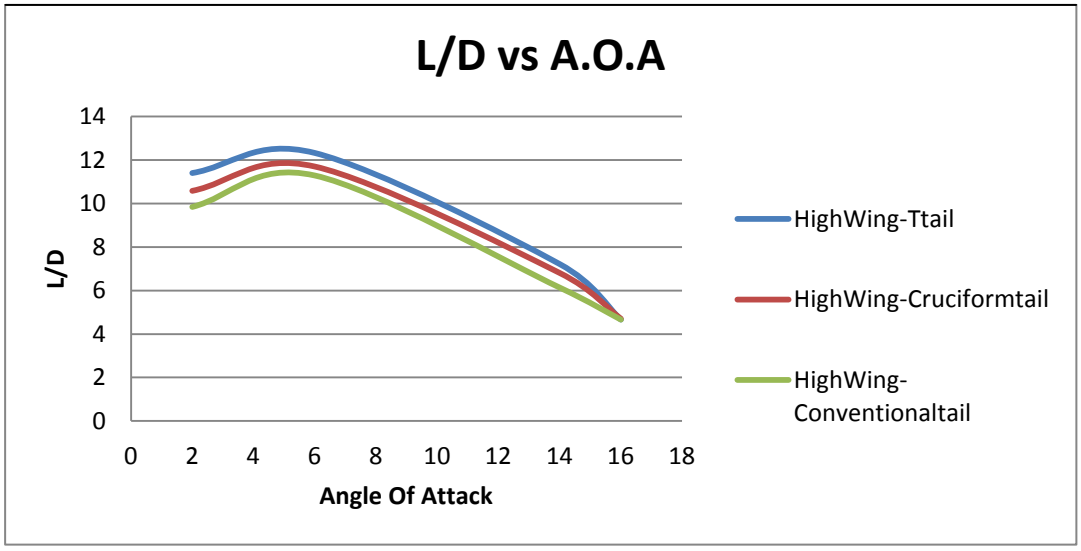

Figure 4.55 L/D versus Angle Of Attack of T-tail, Cruciform tail and Conventional tail combinations of High wing Configuration

Drag coefficients are very close to each other. T tail drag value is lower than other tail configurations. Drag is not significantly effected from tail position. As a result, the L/D values are most efficient at T-tail configuration.

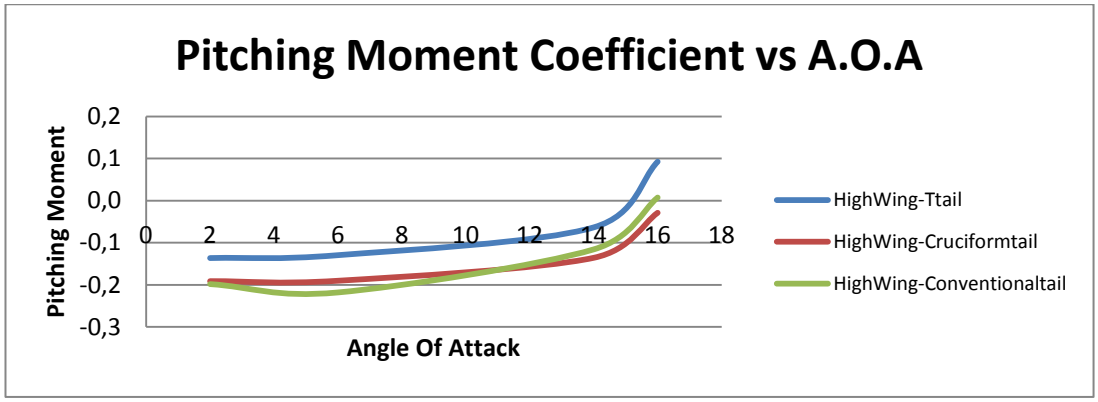

Figure 4.56 Pitching Moment Coefficient versus Angle Of Attack of T tail, Cruciform tail and Conventional tail combinations of Highwing Configuration

Pitching moment values are very similar and more negative for cruciform and conventional tail. The pitching moment(CM) values are closest to 0 at T-tail configuration and it goes to positive(+) values at high α values.

To sum up, different vertical wing and tail positions have been compared in CFD analyses. High wing and T tail combination has been selected since it has highest lift coefficient values, lowest drag coefficient values for high angles of attack. Unlike low wing, fuselage interference with high wing did not generate high drag coefficient as expected in theory. Moreover, it has increased the generated lift as expected since it has higher exposed wing upper surface more than other configurations. The T tail have positive effect on aircraft. With T tail, the aircraft has been optimized for lowest fuselage horizontal tail interference drag and highest lift coefficient for high angles of attack.

4.8 High Wing-T tail Configuration Deep Stall Analysis

Three different tail configurations had been discussed in previous section and T-tail seems to be wing wake free. Since, deep stall is very important phenomena, the stall angle $\alpha=16^0$ should be discussed in a higher detail to proove that deep stall will not occur.

4.8.1 Vertical Plane Cut Plots

Vertical plane velocity cut plots was made for four different spanwise directions, 0, 0.15m, 0.231m and 0.333m respectively. Cut plot spanwise directions are shown in next figure.

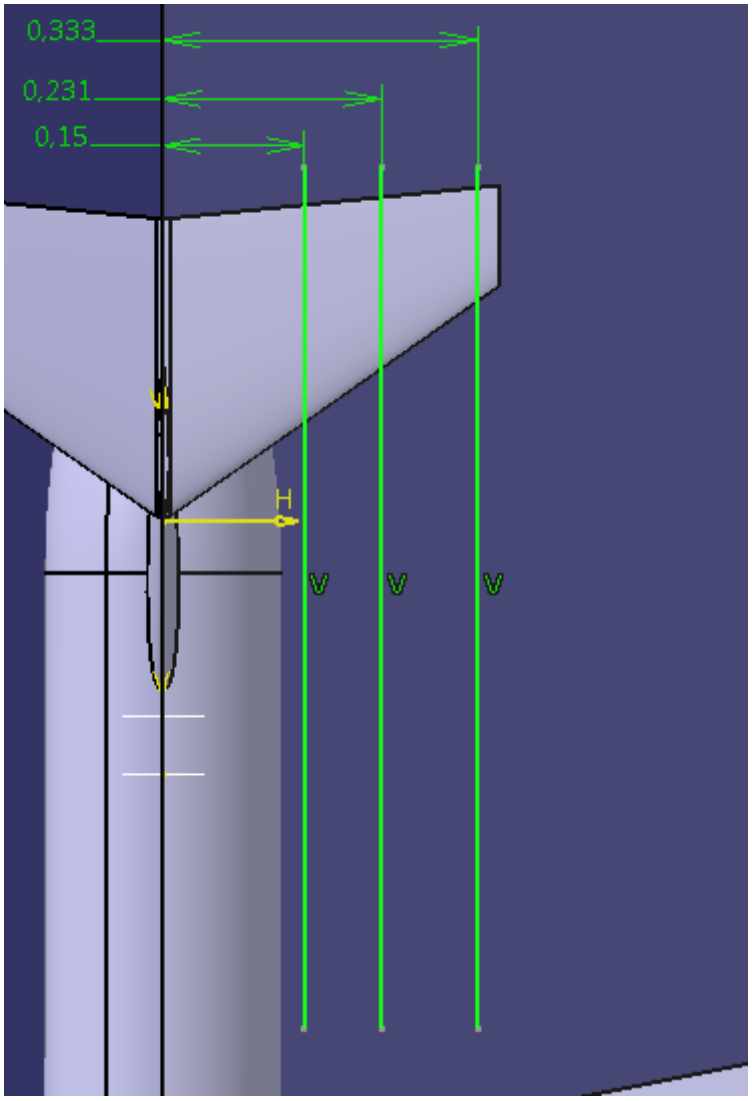

Figure 4.57 Deep Stall Analysis Vertical Plane Cut Plot Locations

0m from Centerline

0.15m from Centerline

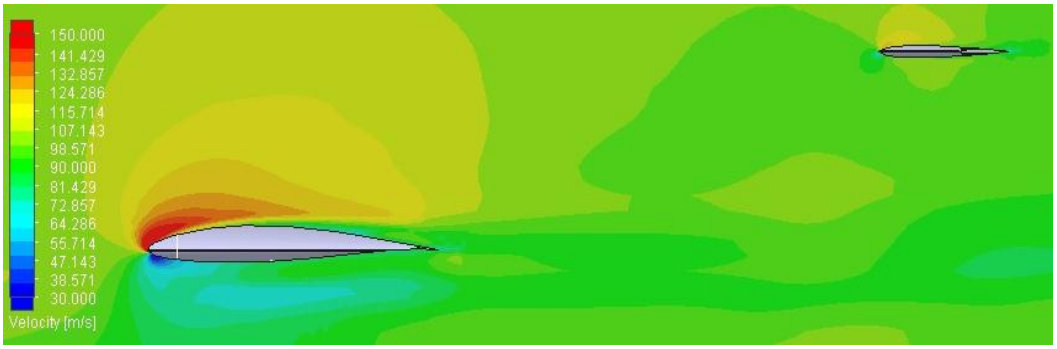

0.231m from Centerline

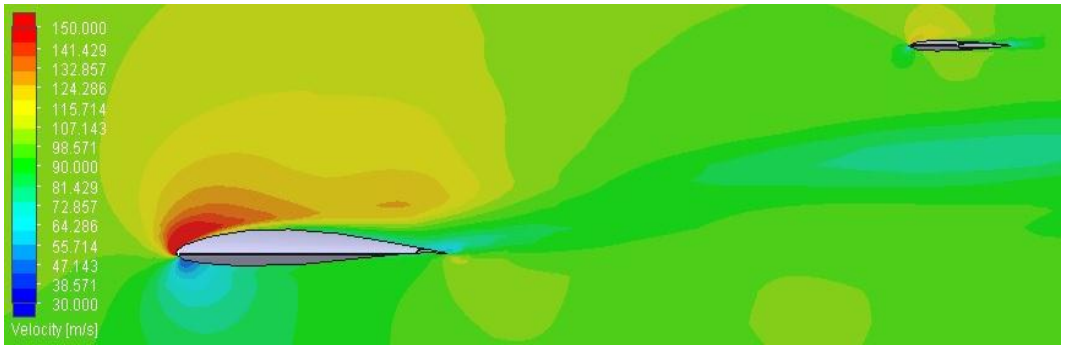

0.333m from Centerline

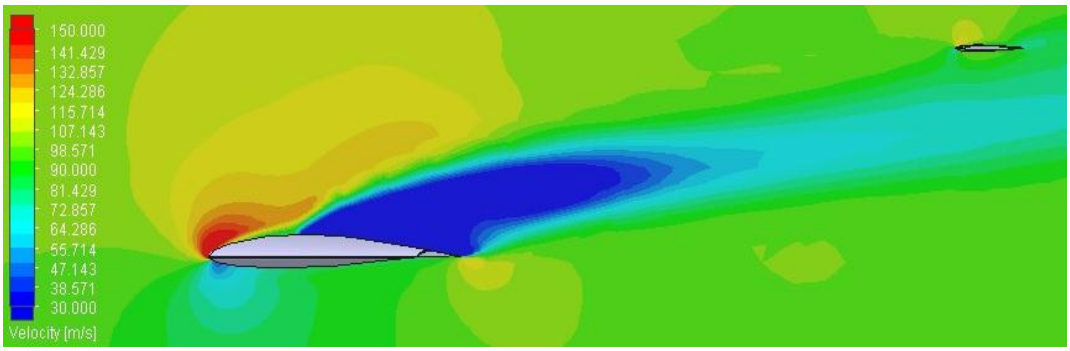

Figure 4.58 HighWing-Ttail Configuration Deep Stall Analysis Vertical Plane Velocity Cut Plots at $\alpha=16^0$

Vertical cut plot figure yields that Vertical tail is not effected from wing wake at 16 degrees A.O.A. Horizontal tail tip is slightly effected from High-wing configuration stall. Effected area is insignificantly small.

4.8.2 Horizontal Plane Cut Plots

After Vertical cut plots, horizontal cut plots were also drawn for deep stall analysis. In this section, vertical tail was divided into 3 cut plot sections, cut plots are shown in the next figure.

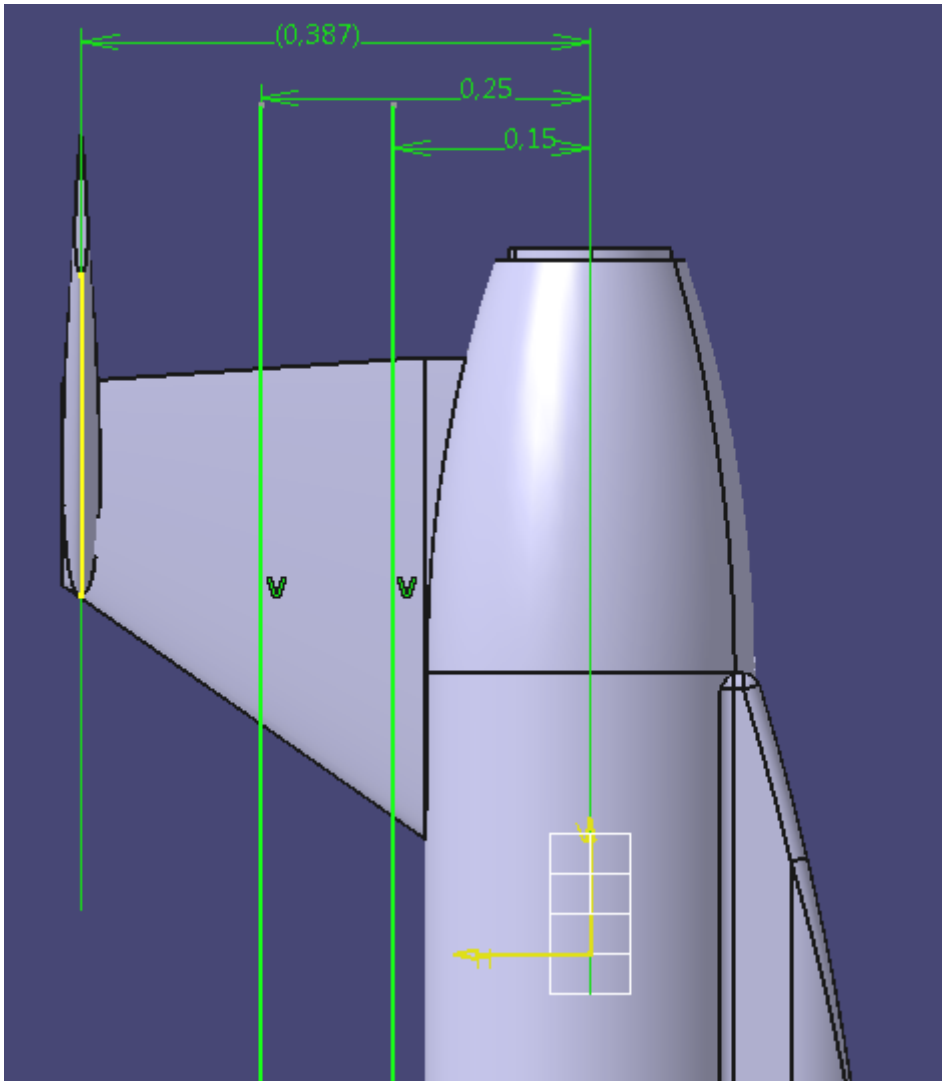

Figure 4.59 Deep Stall Analysis Horizontal Plane Cut Plots

0.15m from Centerline

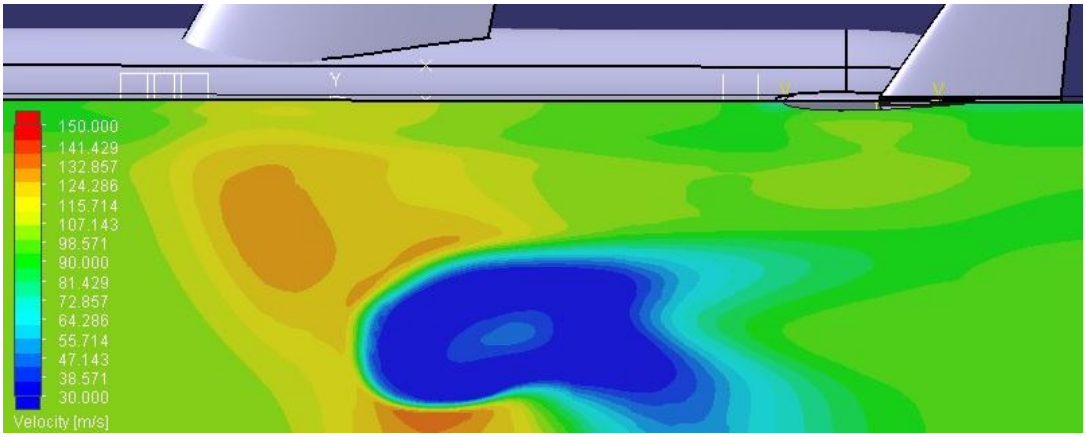

0.25m from Centerline

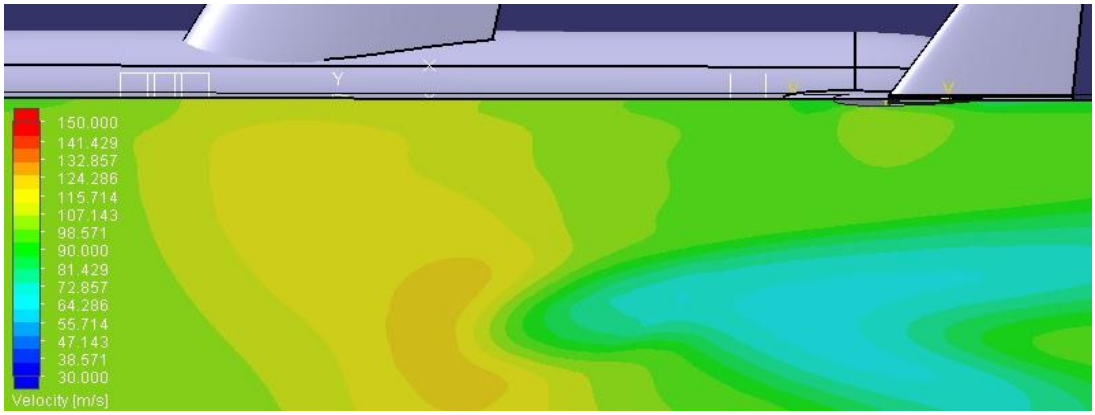

0.387m from Centerline

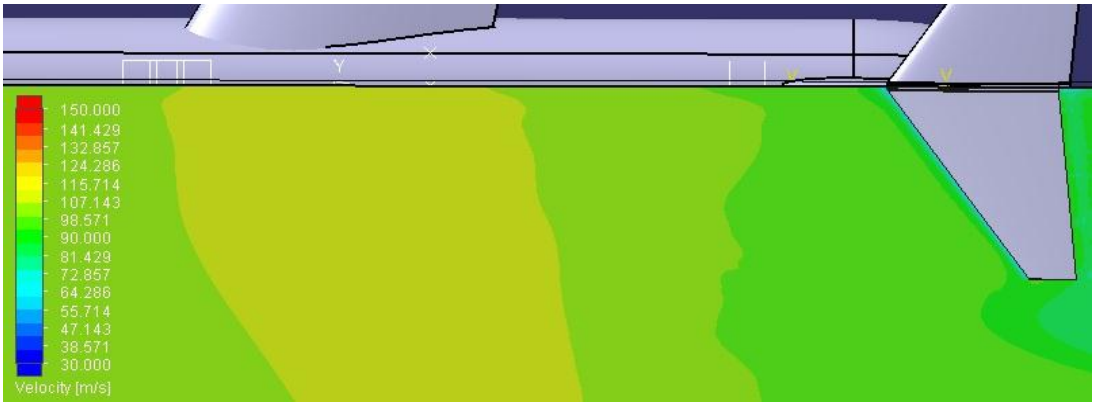

Figure 4.60 HighWing-Ttail Configuration Deep Stall Analysis Horizontal Plane Velocity Cut Plots at $\alpha=16^0$

Horizontal plane cut plots show that flow separation pass under horizontal tail. 0.387m velocity cut plot concludes that stall does not effect horizontal T- tail.

4.8.3 Flow Trajectories

In order to see occurance of the stall phenomena completely, 3D flow trajectories were plotted. 200 pipe lines were used to show the flow trajectories through wing.

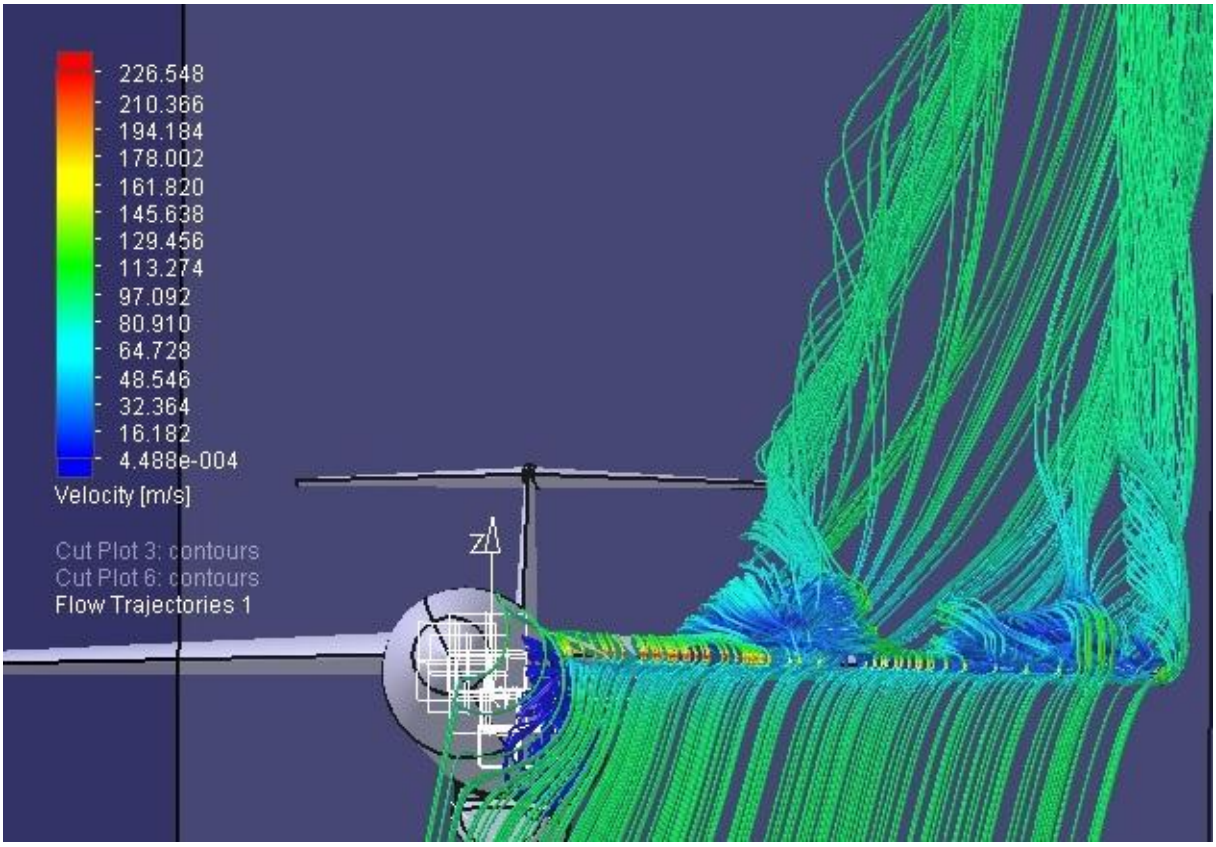

Figure 4.61 3-D Flow Trajectories at $\alpha=16^0$ of T- tail

3D Flow trajectories finally confirms that the T-tail configuration horizontal tail tips are insignificantly effected by stall wing wake.

4.9 Cruise speed Investigation

Since Highwing-Ttail combination has been selected, selected aircraft has been tested for different mach numbers for $\alpha=0^0$, 2^0 and 6^0 at cruise altitude. Drag polar curve with CFD results has been plotted to choose the best cruise mach number.

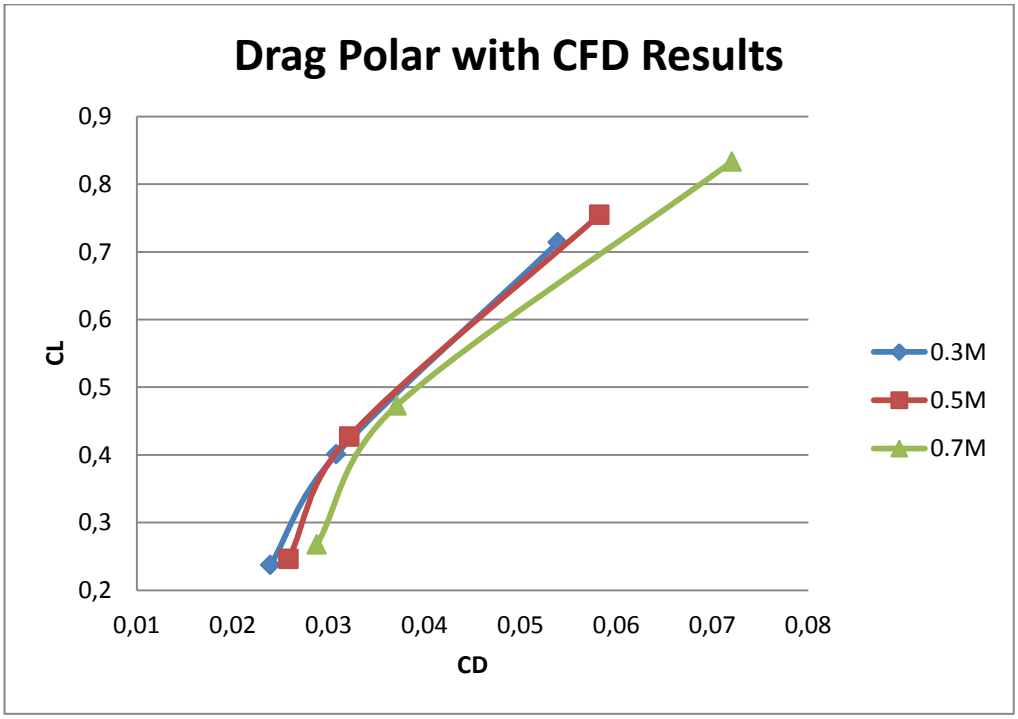

Figure 4.62 Drag Polar Curve with CFD Values for Different Mach Numbers

Drag polar shows that during cruise CL value, 0.3M and 0.5M shows very similar pattern.

After plotting drag polar curve, $CL^{(1/2)}/CD$ curve has been plotted to get the best cruise speed curve.

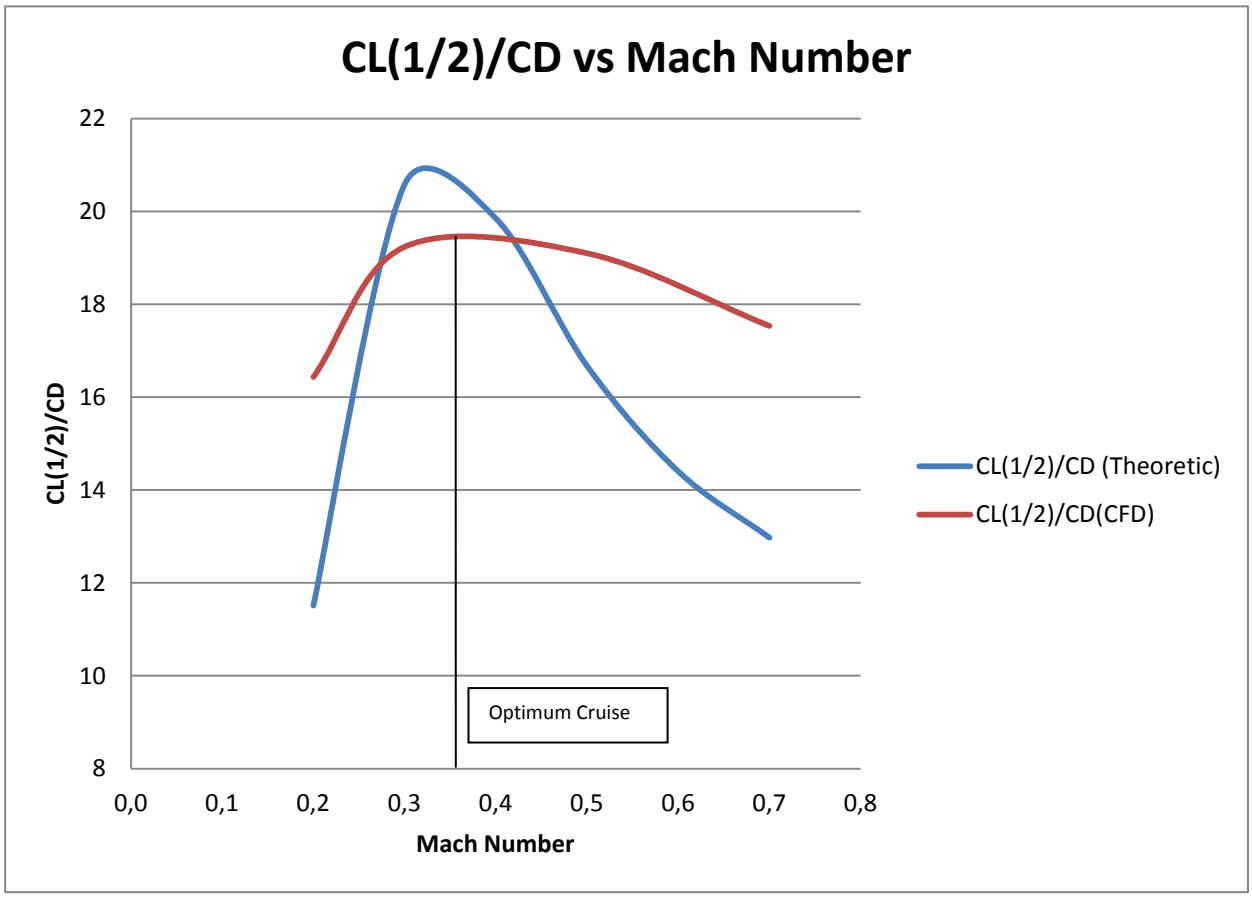

Figure 4.63 CL(1/2)/CD vs Mach Number Curve with Theoretic and CFD values

According to theoretic drag polar and $CL^{(1/2)}/CD$ curve, 0.32 M was the best cruise velocity. However, CFD curve is more smooth and CFD values shows that the optimum cruise velocity is approximately 0.37 M.

4.10 Maximum Speed Investigation

Designed decoy UAV is supposed to operate at 0.7 M velocity. 0.7 M is a transonic critical mach number for aircrafts. When operating at critical mach number, there is a danger of the exceeding flow velocity at the upper surface of the airfoil above 1 Mach. When shock wave occurs, shockwave interacts with the boundary layer and flow separation over wing occurs. When shock wave occurs, drag force generated by the aircraft increases rapidly because new component called wave drag is added to the total drag.

0, 2 and 6 degrees of angle of attack values were analyzed for 0.7 M flow, at 6 degrees angle of attack, FloEFD supersonic flow warning occured.

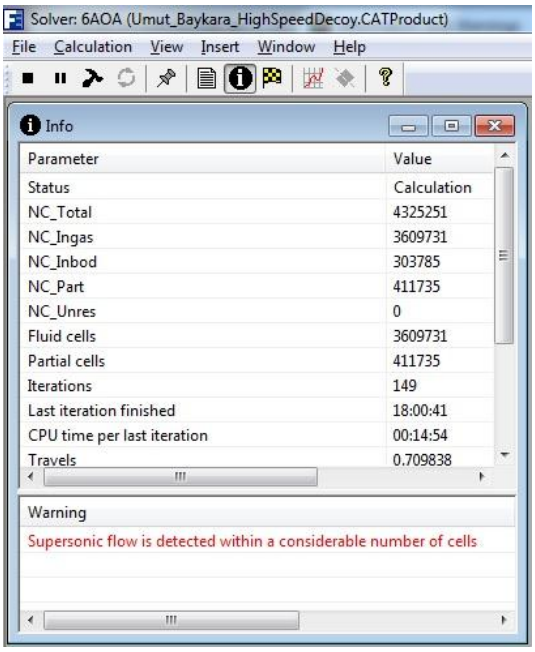

Figure 4.64 FloEFD supersonic flow warning at 6 degrees A.O.A

4.10.1 Drag Coefficient

CFD analyses are also made for 0.5M, 0.7M and 0.9M for 0 degrees angle of attack. From CFD results, drag divergence curve is plotted. Drag divergence curve is given below.

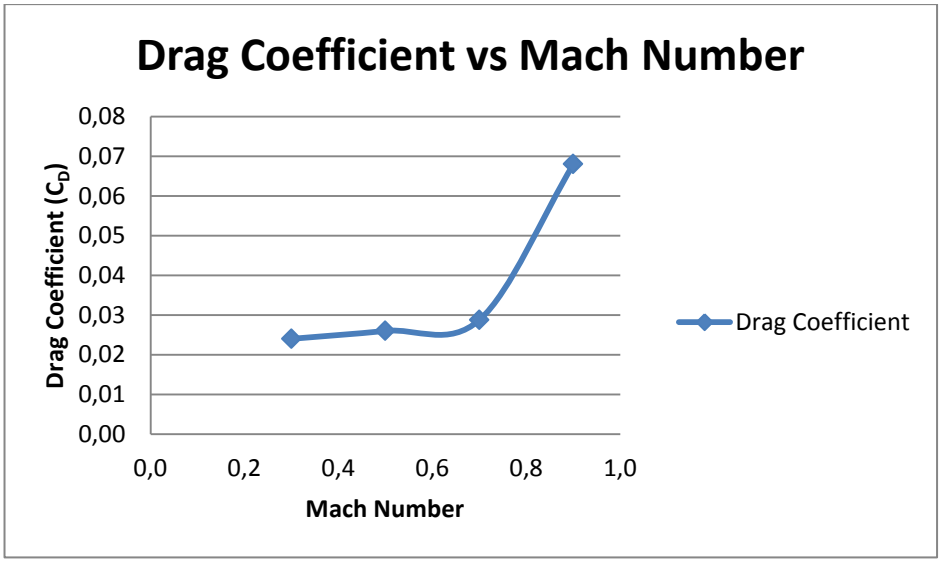

Figure 4.65 Drag Divergence Curve from CFD

Table 4.3 Drag Coefficient values for 0.3M and 0.7M values

	0.3 M	0.7 M	Difference
$\alpha=0^0$	0.02393	0.02877	20.22%
$\alpha=2^0$	0.0308	0.0371	20.5%
$\alpha=6^0$	0.05392	0.07207	33.66%

Drag coefficient is furtherly increases when angle of attack increases. The reason is shockwave occurance on the wing. Supersonic bubbles sizes will be shown in next section. Aircraft maximum speed is directly related to the thrust requirement and thrust requirement is directly related to the drag coefficient produced by the aircraft.

$$T_R = q * S * C_D \tag{2.70}$$

The Required thrust and Available thrust curves were plotted from CFD values.

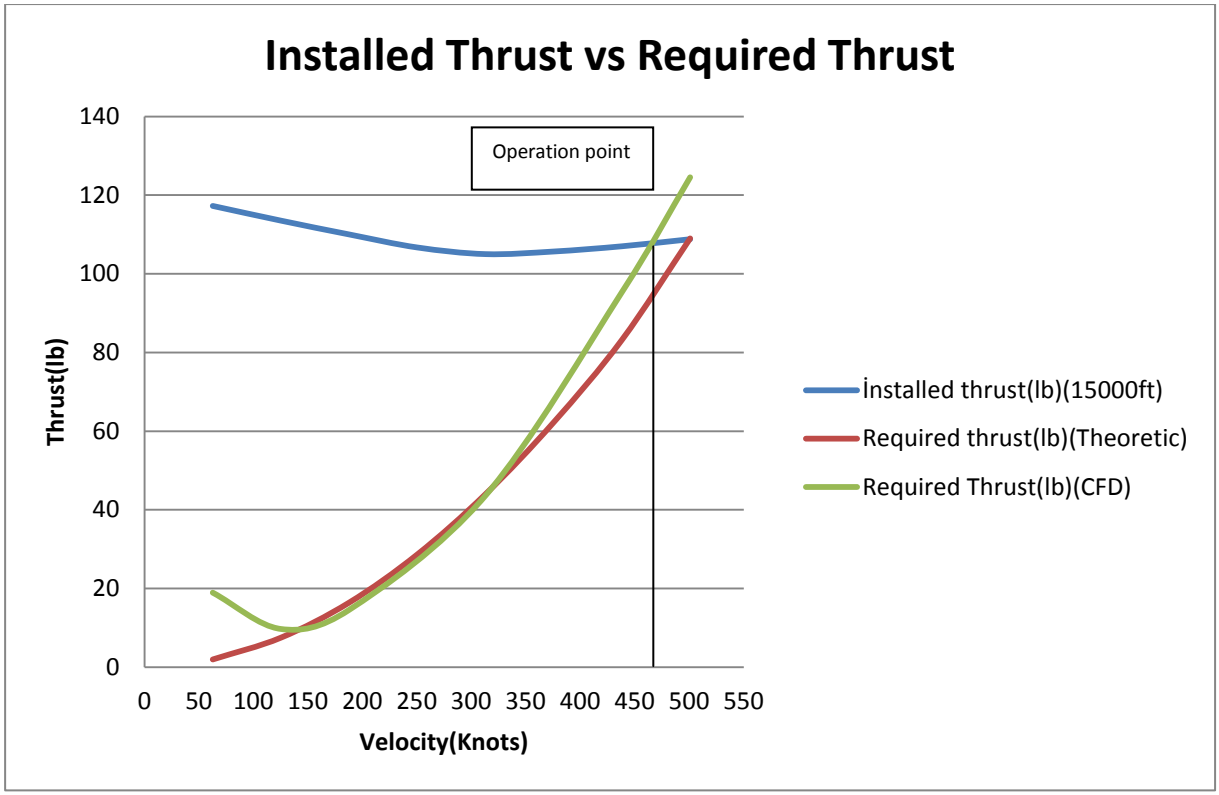

Figure 4.66 The required Thrust and Available Thrust Curve at 15000 ft altitude with CFD values

Parasitic drag and drag due to lift theoreticly decreases as Mach number increases. However, CFD analysis implies that drag further increases and the intersection becomes at lowered point. If the designed high speed decoy flies at 0 degrees angle of attack, CFD analysis confirms that maximum speed exceeds 450 Knots and therefore designed drone satisfies the maximum speed requirement.

4.10.2 Mach Number

Cut plots from tail spanwise direction(0.231m), wing M.A.C spanwise direction (0.417m) and 0.8m has been taken for mach number cut plots for 0.7 M speed.

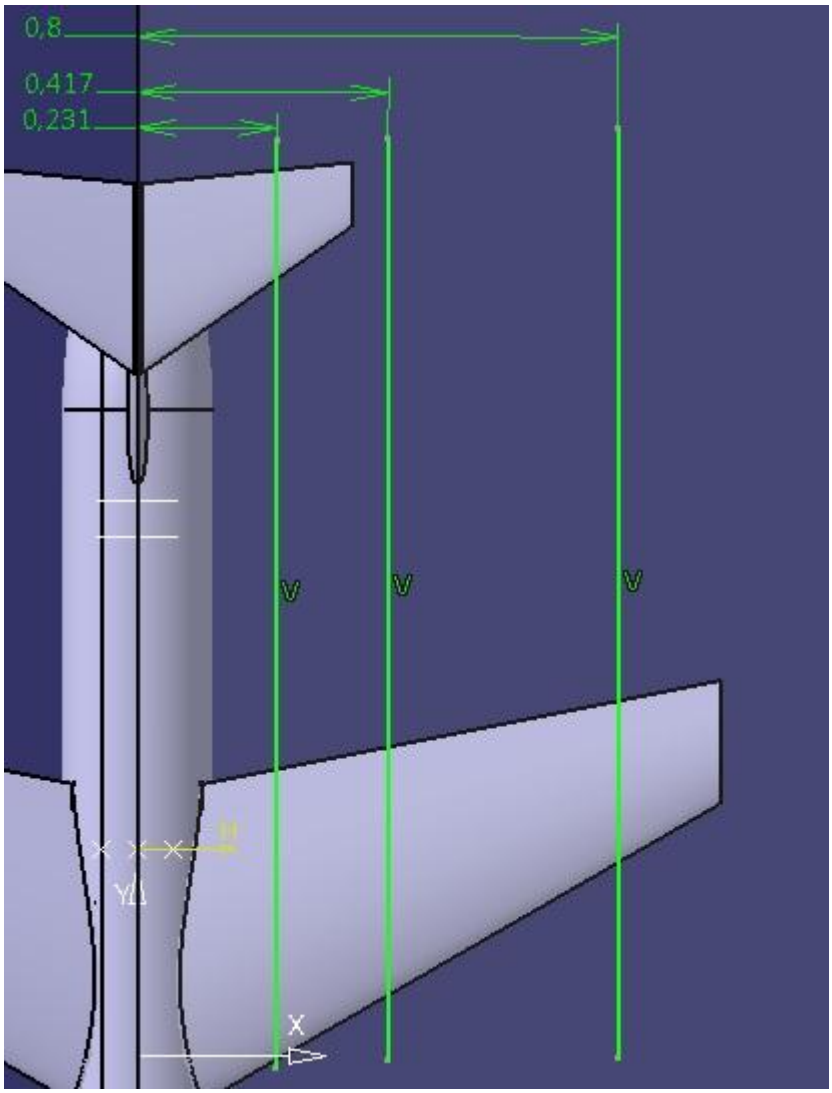

Figure 4.67 Mach Number Horizontal Plane Cut Plot locations

$\alpha=0^0$

0.231 m spanwise direction:

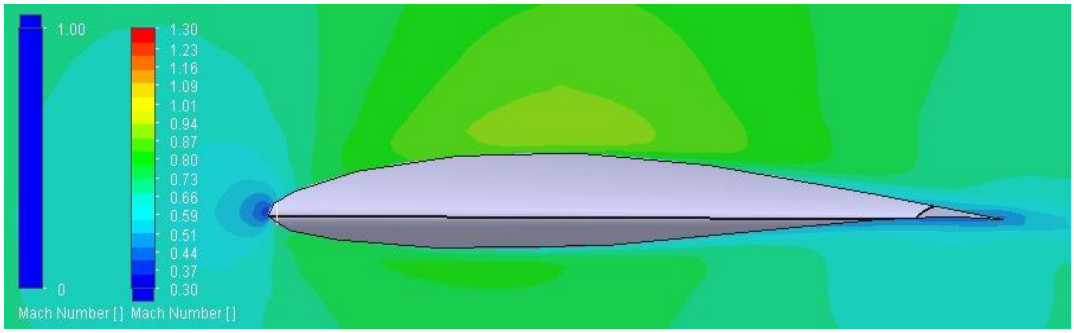

0.417 m spanwise direction:

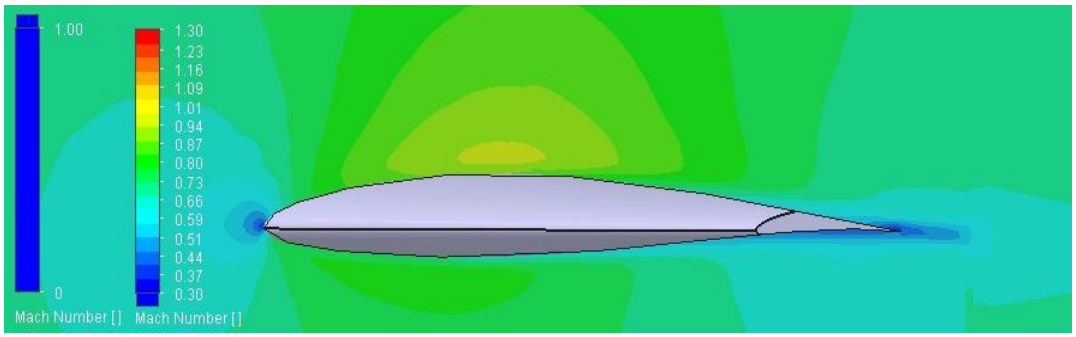

0.8 m spanwise direction:

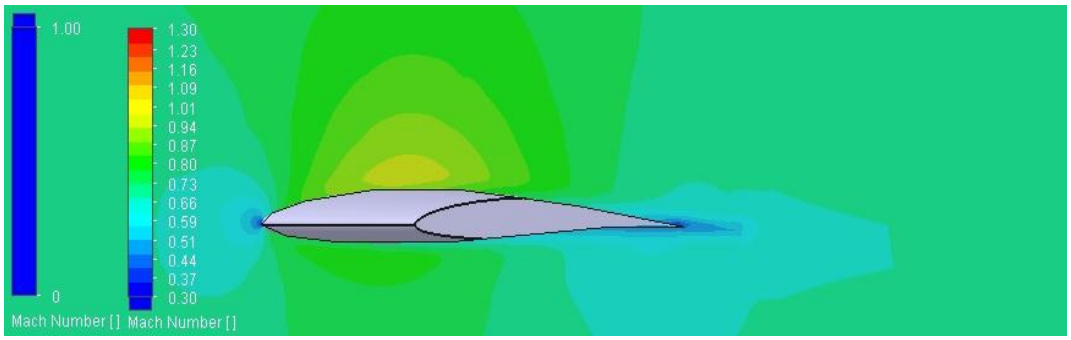

Figure 4.68 Maximum Speed Investigation Vertical Plane Mach Number Cut Plots at $\alpha=0^0$

CFD results show that At $\alpha=0^0$, the mach number did not exceed 1 at the upper surface of the airfoil. It remained between 0.94 and 0.96. Aircraft can operate at this α without facing shock wave during flight at 0.7M.

$\alpha=2^0$

0.231 m spanwise direction:

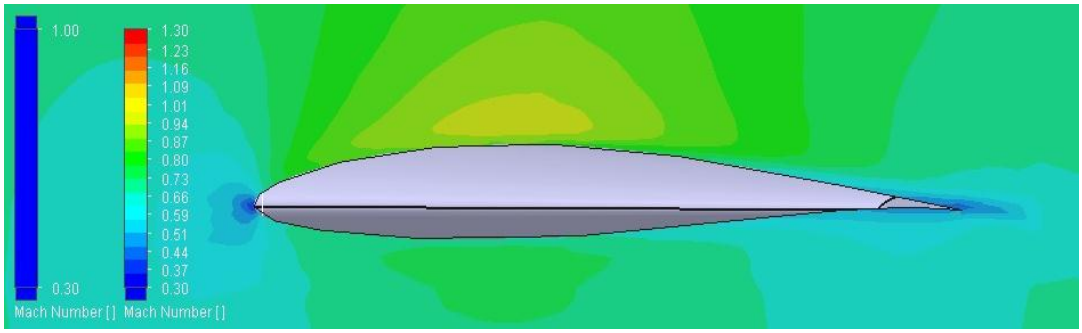

0.417 m spanwise direction:

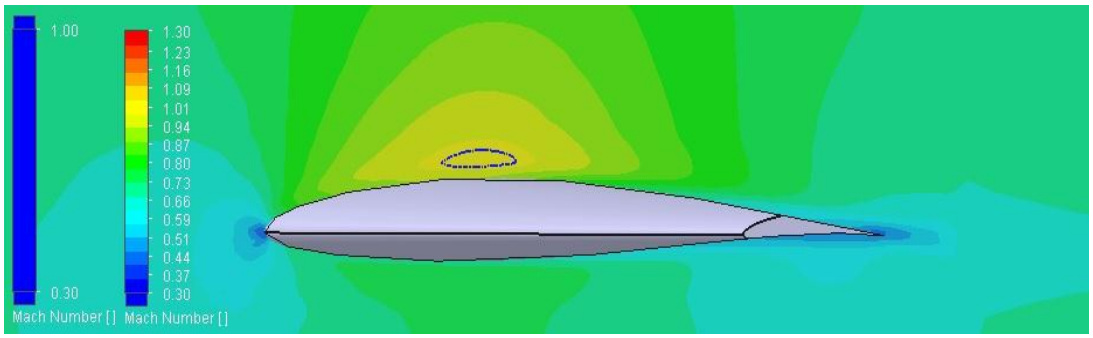

0.8 m spanwise direction:

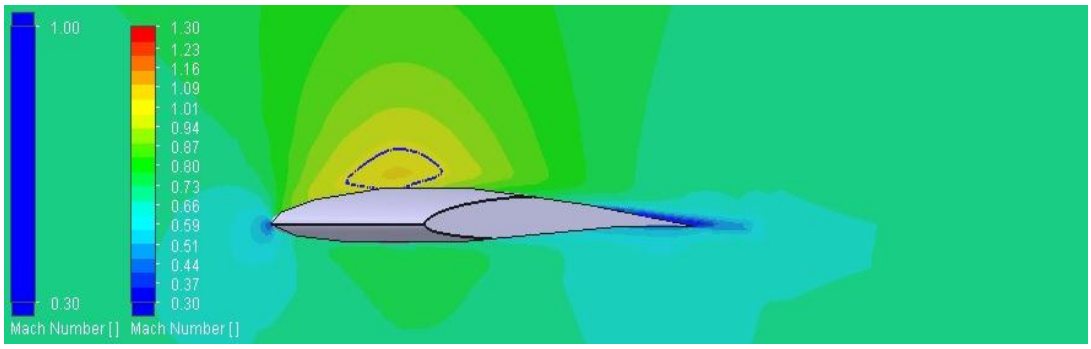

Figure 4.69 Maximum Speed Investigation Vertical Plane Mach Number Cut Plots at $\alpha=2^0$

At 2 a.o.a , mach number exceeded 1 at the upper surface of the airfoil and the supersonic bubble dimensions has been increased slightly to the wing tip. Blue isoline show the area above mach 1. Maximum mach numbers from up to down cut plots are 0.96, 1.01 and 1.05 respectively.

$\alpha=6^0$

0.231 m spanwise direction:

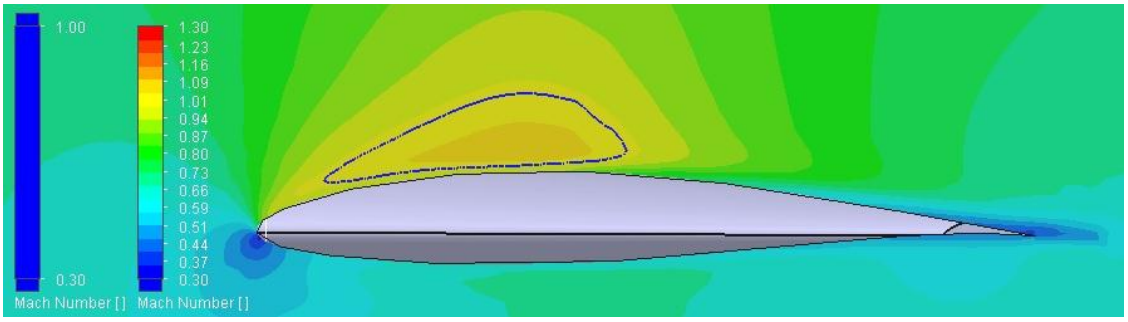

0.417 m spanwise direction:

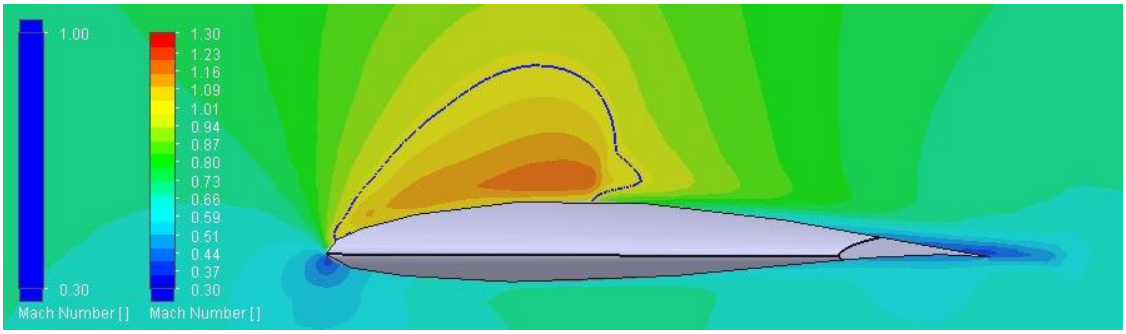

0.8 m spanwise direction:

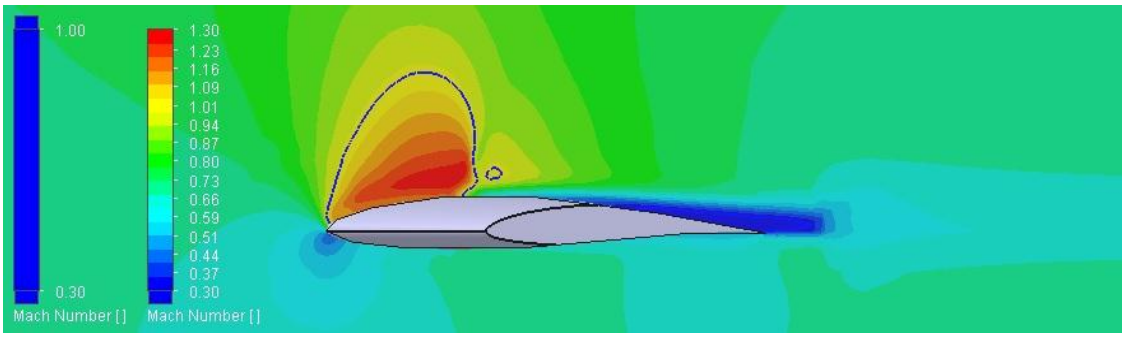

Figure 4.70 Maximum Speed Investigation Vertical Plane Mach Number Cut Plots at $\alpha=6^0$

At $\alpha=6^0$, supersonic bubbles can be clearly observed around the airfoil at all cut plots.. Maximum mach numbers from up to down cut plots are 1.07, 1.18 and 1.3 respectively. There is a small amount of flow separation because of boundary layer shock interaction.

4.10.3 CP plots and Shock Strength

At 2 and 6 degrees angle of attack, supersonic flow bubbles can be seen on the wing upper surface. In this section, pressure coefficient values are plotted. Pressure coefficient drop ratios on CP plots determines the shock strength.

First, CP vs X/C curves are plotted from 0.417m from centerline and second CP vs X/C curves are plotted from 0.8m from centerline.

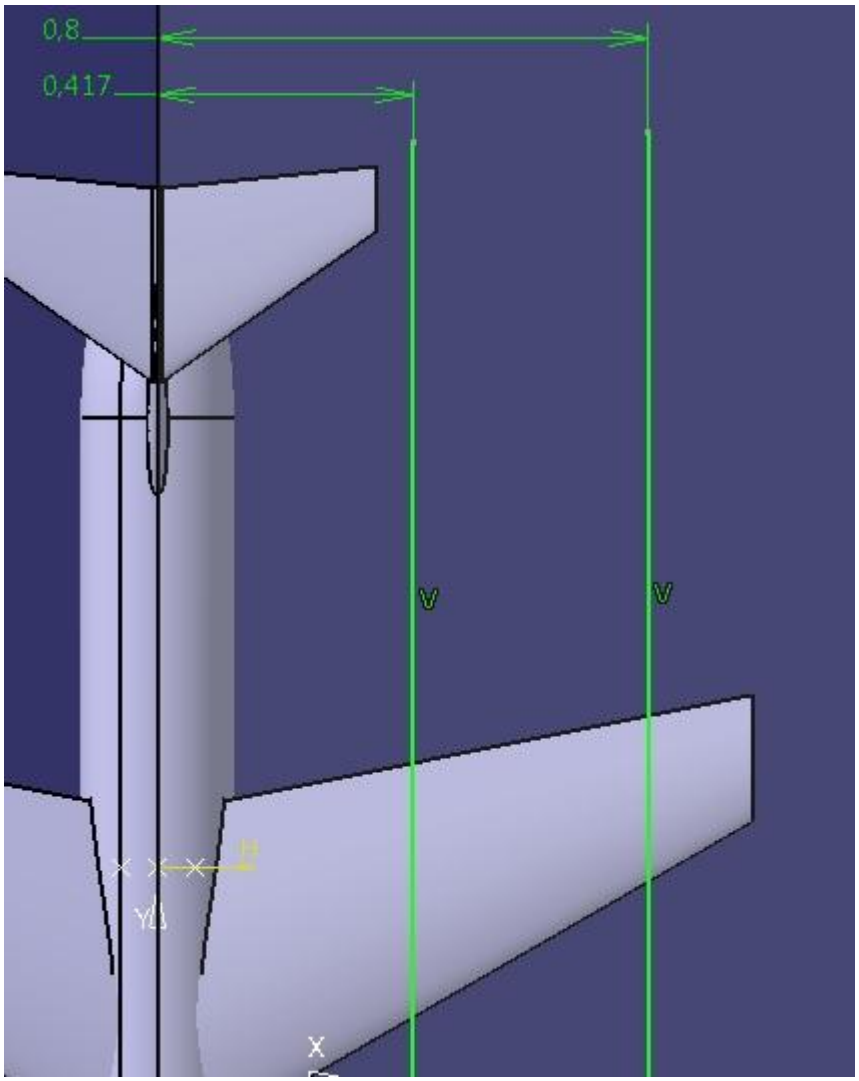

Figure 4.71 0.7 M analysis CP plots spanwise directions

$\alpha=2^0$

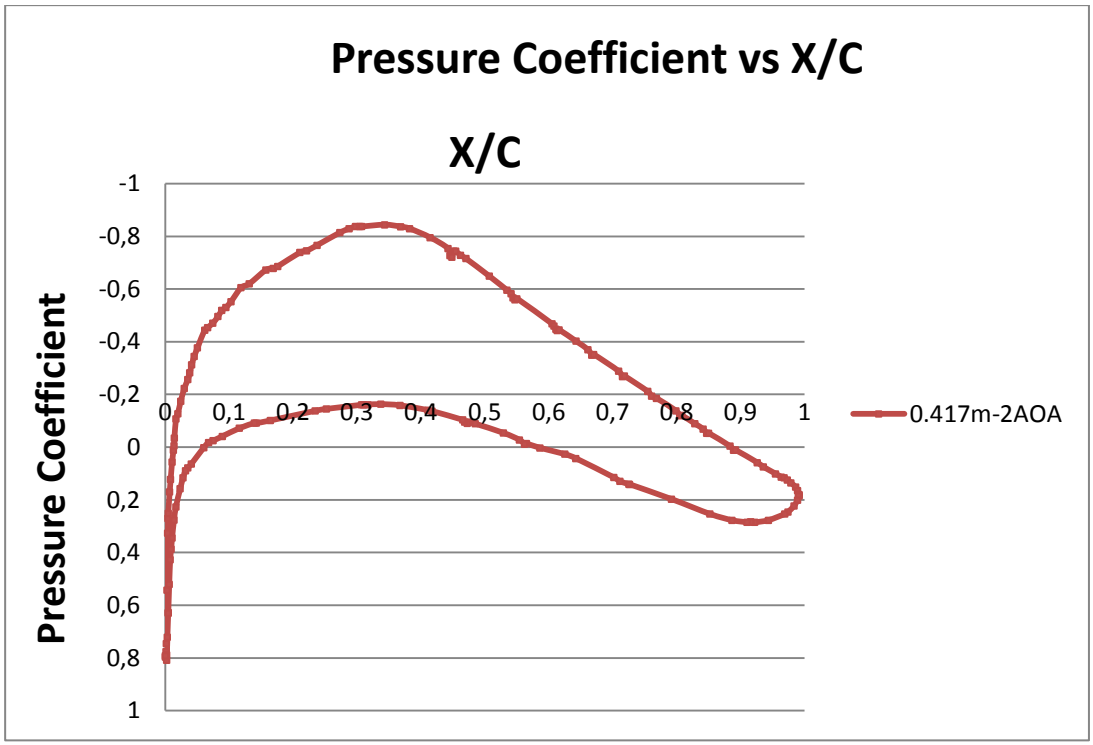

Figure 4.72 Pressure Coefficient vs X/C at 0.7 M at $\alpha=2^0$for 0.417m spanwise direction

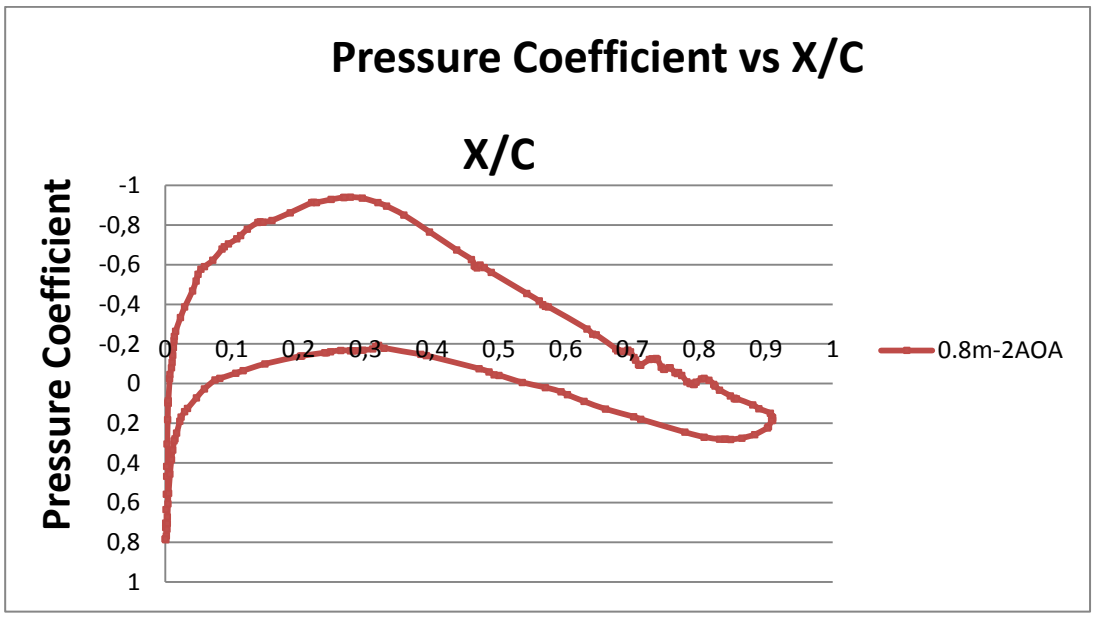

Figure 4.73 Pressure Coefficient vs X/C at 0.7 M at $\alpha=2^0$ for 0.8m spanwise direction

From 2 degrees A.O.A CP distribution curves, the pressure drop at the upper surface of the airfoil seems to be unclear. This means that supersonic bubble is negligible.

Maximum mach number at 0.417m cut plot was 1.01 and the maximum mach number at 0.8m cut plot was 1.05. 2 A.O.A CP plots show that, there is no observed shock wave in 2 degrees angle of attack.

6 AOA

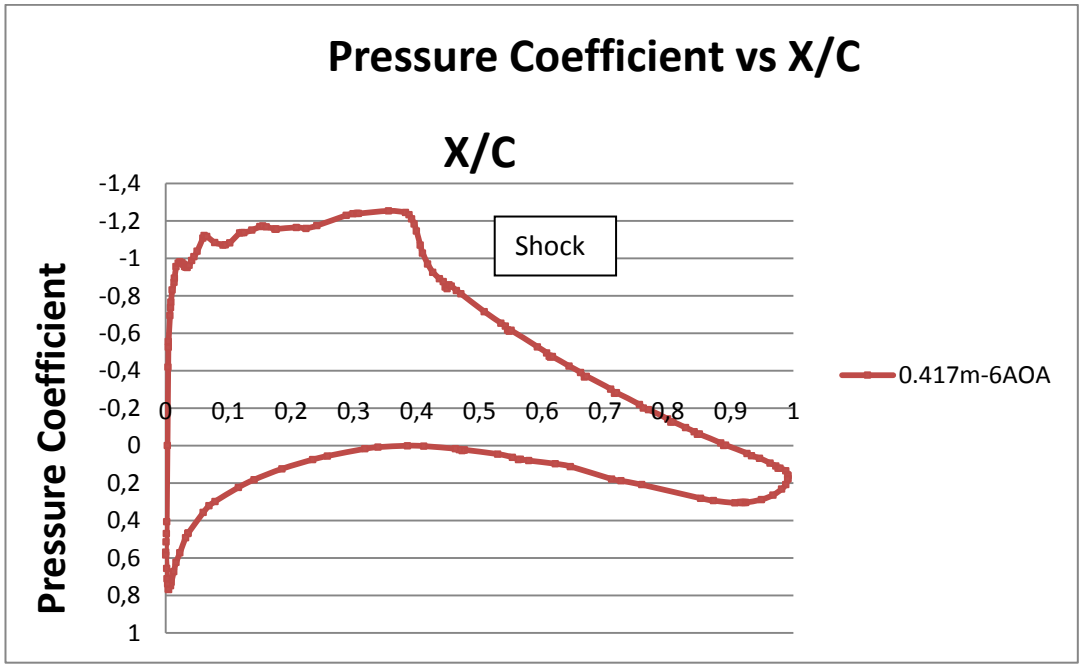

Figure 4.74 Pressure Coefficient vs X/C at 0.7 M at $\alpha=6^0$ for 0.417m spanwise direction

6 Degrees A.O.A analysis show that there is an observable pressure difference on the upper surface of the airfoil. The pressure drop at 0.417m is weak.

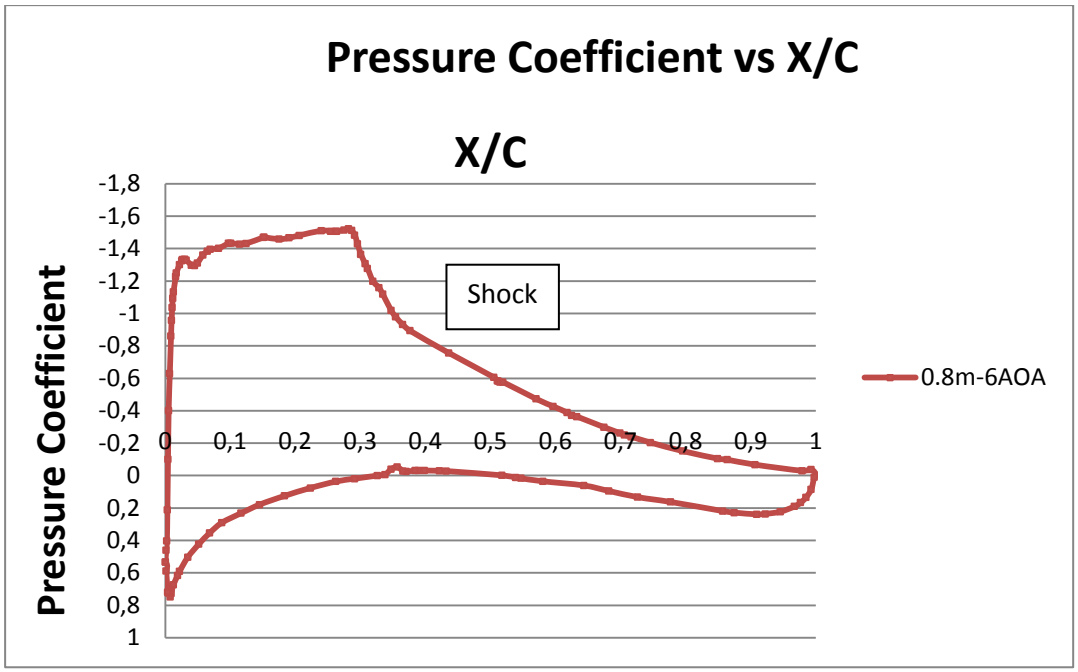

Figure 4.75 Pressure Coefficient vs X/C at 0.7 M at $\alpha=6^0$ for 0.8m spanwise direction

The pressure drop at 0.8m CP plot is little bit stronger than 0.417m CP plot. In fact, this shock is not strong enough to give structural damage the airplane. Therefore, aircraft can fly at 6 $\alpha=6^0$ for a short amount of time.

4.11 Corner Velocity Investigation

Corner velocity point is the maneuver point of the aircraft. At this point, maximum lift coefficient and the limit load factor are simultaneously at their maximum value in the flight envelope. Therefore, the aircraft can achieve minimum turn radius and maximum turn rate at corner velocity [4].

This aircraft was simulated in CFD environment at the angle of attack where it gives its maximum lift coefficient.

Table 4.4 CL_{max} Value Comparison at Corner Velocity Point

	Theoretic	CFD Result
CL_{max}	1.0935	1.056

Corner velocity update should be made for the new CL_{max} value.

$$V_{combat} = \sqrt{\frac{2 * 9}{(1.496 * 10^{-3}) * 1.056} * 18.365} = 458.75 \frac{ft}{s}$$

4.12 Discussion of Results

From CFD results, aircraft wing and tail vertical position has been optimized and it has been seen that, aircraft can satisfy its maximum speed requirement and It will not face deep stall situation since, wing wake will stay below the horizontal T- tail. Now, aerodynamic values coming from CFD analysis and theoretic values will be compared. The comparison table is given in the next table.

Table 4.5 Comparison between Theoretic values and CFD Results of selected High Speed Decoy UAV

Parameter:	Conceptual Design (Theoretic)	HighWing-T tail (CFD)
$C_{L\ Design(theoretic)}$ $C_{L\ Cruise(CFD)}$	0.236	0.187
$C_{D\ cruise}$	0.024	0.0239
$C_{L\ Max(corner\ velocity)}$	1.0935	1.056
$L/D_{\ cruise}$	9.86	7.84
$L/D_{\ max}$	12.72	12.61

The CFD values are not much different from theoretical values. However, lift coefficient values are below the expectations. Thus, the aircraft new lower L/D values should be discussed.

Table 4.6 L/D values and Mission weight fraction comparison of selected decoy UAV

Parameter:	Conceptual Design (Theoretic)	HighWing-T tail (CFD)
L/D_{cruise}	9.86	7.84
L/D_{max}	12.72	12.61
Cruise Mission Weight Fraction	0.935	0.92
Loiter Mission Weight Fraction	0.858	0.857

Cruise and loiter mission weight fractions cost an approximate 1 minute combat time reduction of the mission profile. Now, the decoy aircraft aerodynamic and performance parameters should be compared to show that it is a competitive aircraft. Unfortunately, this aircraft type is a military aircraft so, it is impossible to find aerodynamic and performance output values.

Table 4.7Aerodynamic Parameters Comparison with a Previously Created Decoy UAV

Parameter:	Designed DECOY UAV	DECOY UAV Designed by Ender Özyetiş
L/D_{cruise}	7.84	4.82
C_{D0}	0.0196	0.0086
$C_{L\alpha\ wing}$(1/rad)	4.213	2.21
$C_{Lmax\ (corner\ velocity)}$	1.056	0.95

Table 4.8 Performance Parameter comparison with a Created Decoy UAV

Parameter:	Designed DECOY UAV	DECOY UAV Designed by Ender Özyetiş
Maximum load Factor	9	9.12
Rate Of Climb(ft/s)	188	160
Maximum Velocity(ft/s)	758	564.3

From the aerodynamic and performance values from tables given above, designed high speed decoy is a competitor UAV and it can be manufactured.

CHAPTER 5

CONCLUSIONS

In this study, a high speed decoy UAV has been designed. The requirements had been chosen according to the past high speed Decoy UAV design experiences. For this design, 231 m/s of maximum speed, 1 hour endurance of time and 100 km of range have been aimed. The geometric specifications of this decoy UAV are given as: Payload of 10 kg, maximum take off weight of 85.3 kg, wing span of 1.94 m, wing taper ratio of 0.36 and wing leading edge sweep angle of 30 degrees. The specifications of the UAV is based on previous successful decoy UAV designs and iterative aircraft design calculations. Inlet shape and required jet engine has been selected and selected jet engine has been modeled and integrated to fuselage body in Catia-v5 CAD software.

For baseline design, Mid-wing and T-tail configuration has been selected to achieve lowest drag due to wing-tail interference. Mid-wing configuration is more streamlined compared to high and low wing. Moreover, Mid-wing contains the advantages of both low and high wing. In order to discuss the theoretic knowledge and to find the optimum vertical wing and tail position, different configurations have been designed and configuration matrix was set up. Some configurations have been tested in CAD embedded CFD software FloEFD. Aerodynamic performance tests have been made in 15000 ft cruise condition for 2, 6, 14 and 16 degrees of angle of attack. Mesh dependence test have been implemented to achieve the best efficiency between mesh number and computational time. Intensity-length turbulence model has been selected and automatic convergence criteria has been set for FloEFD. CFD analysis show that, High wing-T tail configuration yields interference. However, interference does not reduce the aircraft performance. It gives lowest drag coefficient and highest lift coefficient values for high angles of attack. Therefore, High wing-T tail configuration was selected. After optimum configuration was

selected, the aircraft was tested for deep stall condition. Both Horizontal and vertical velocity cut plots were used. Aircraft has been passed from deep stall analysis test.

Finally, decoy UAV has been tested in FloEFD during maximum velocity, corner velocity and cruise velocity. CFD results shows that aircraft will be able to fly at the required maximum velocity without strong shock occurance. Optimum cruise velocity has been found as 0.38 M from drag polar curves. Then, Optimum corner velocity is found from CFD result $C_{L\,max}$.

To sum up, design is an iterative process which requires great effort. During design process, prototypes should be created and tested in wind tunnel to understand the aerodynamic performance. Wind tunnel testing is considered indispensible for getting the most accurate aerodynamic performance. However, creating prototype of every configurations and testing all of them in a wind tunnel is too much time consuming and expensive for a designer. Therefore, high tech CFD softwares are very helpful to reduce the prototype number. In our study, Catia-v5 embedded FloEFD software was used to successfully optimize the aircraft and test the aircraft performance during different operations such as cruise, manuever and maximum speed.

In the future, FloEFD can be used to furtherly optimize the wing sweep angle, aspect ratio, air inlet location and inlet shape. After these steps, this aircraft is going to be an optimized manufacturable prototype.

CHAPTER 6

FUTURE WORK

High speed decoy UAV configuration highwing-Ttail which gives the best aerodynamic performance has been chosen. However, further optimization can be made for the selected decoy UAV. In this chapter, the future work ideas for the selected configuration were discussed.

The future work steps are given as follows:

6.1 CFD Optimization

6.1.1 Wing Sweep Angle Optimization

Leading edge wing sweep angle ($\Lambda_{LE\ wing}$) was chosen as 30^0 considering the critical mach number. In fact, wing sweep angle can easily be optimized by FloEFD CFD tool. In order to make the optimization, different models of leading edge sweep angle should be modelled in Catia-v5 CAD software, then the FloEFD temptate property helps to copy the project to all models. Finally, the models should be re tested at maximum flight speed 450 knots for different A.O.A values. The efficiency of the wing sweep can easily be observed and compared.

6.1.2 Aspect Ratio Optimization

Aspect ratio has been chosen as 5 considering the average values of the high speed decoy models in literature. Aspect ratio can be tuned by setting the wing area constant. Since the AR of the wing is given as;

$$AR_{wing} = \frac{b^2}{S_{wing}} \tag{2.16}$$

By altering wing span, different AR models can be created and mounted to fuselage using Catia-v5 CAD software. Then, the models can be tested in cruise condition for different A.O.A values in FloEFD easily by following the steps in 5.1.

6.1.3 Inlet Location and Inlet Shape Optimization

For high speed decoy model, inlet had been mounted under the fuselage such as the shape of F-16 fighter aircrafts. The elliptic inlet shape has been chosen and blank has been left between fuselage and inlet to prevent the boundry layer.

Inlet shape can be optimized by designing different shaped inlets and these different inlet shapes can be mounted to fuselage differently. For example, 2 inlets can be mounted to sides of aircraft fuselage such as F-4 aircraft inlets. These inlet concepts can easily be modelled in Catia-v5 CAD system and tested in FloEFD software for different α values.

6.2 More Detailed Design and Stability

In this study, although some parts of the high speed decoy(Engine, Fuel tank, payload) has been designed, whole parts of the aircraft were not designed in detail. Therefore, before producing the prototype, the inner part of the decoy UAV should be designed in a high detail. Since the detailed design will have a different C.G point, the stability calculations should be made again. New neutral point location should be found and the static margin should be calculated.

6.3 Structural Analysis

Since High Speed Decoy UAV is a highly manuverable aircraft, it should endure to high loads. Our aircraft is expected to endure to 9g load during manuever. During manuever condition, aircraft pressure forces should be used as a boundry condition to perform the structural analysis. High load is also applied during catapult launch. Decoy UAV is expected to endure to pneumatic catapult launch loads.

During maximum speed flight, aircraft is exposed to shock waves on its wing. From CFD results, shock location and C.P. distribution curves are given. Now, structural analysis should be performed to test the endurance of the wing structure to these shock waves.

REFERENCES

[1] Gundlach, J. (2012), "*Designing Unmanned Aircraft Systems: A Comprehensive Approach*. Aurora Flight Sciences Manassas, Virginia

[2] Roskam, J., Tau Edward, L., Airplane *Aerodynamics and Performance*," DarCorporation, 1997.

[3] Özyetiş, E. (2013), "*Yüksek Hızlı Hedef Uçağı Tasarımı ve Üretimi,*" VII th National Aerospace Engineering Council, TMMOB Makine Mühendisleri Odası, Eskişehir,TURKEY.

[4] Anderson, John D. (1999), "*Aircraft Performance and Design*, Mc-Graw-Hill. University of Maryland

[5] Raymer, D.P. (2012), *Aircraft Design: A Conceptual Approach*(5th ed.), Washington: American Institute of Aeronautics and Astronautics.

[6] Dept. of Defense, Unmanned Systems Roadmap 2007-2032, Office of the Secretary of Defense, Washington, D.C., 10 Dec. 2007.

[7] Marovic, B. (2015), *JSAE Benchmark of Automative Aerodynamic Test Measurements,* Mentor Graphics, S.W. Boekman Road, Wilsonwille, Oregon 97070-7777 ,USA

[8] Sadraey M., Mohammad H. (2013). *Aircraft Design:A Systems Engineering Approach,* Daniel Webster College, New Hampshire, USA.

[9] Composite Engineering, Inc., "*Firejet Technical Data & BQM-167A Techical Data*," , LLC, Online whitepaper, www.kratosusd.com, Sacramento, USA. [retrieved 14 December 2014].

[10] Meggitt Defence Systems Ltd, "*Banshee twinjet Specifications*," https://meggitttargetsystems.com/static/media/files/Banshee_Twin_Jet_2015.pdf The Boulevard, Orbital Park ,Ashford Kent, TN24 0GA, UK. [retrieved 16 April 2016].

[11] Etkin B., Reid L. D. (1996), *Dynamics of Flight, Stability and Control*, (3rd ed.),Wiley.

[12] Butler, M. C., Montanez, R., *"How to Select and Qualify a Parachute Recovery System for Your UAV,"* Butler Parachutes, LLC, Online whitepaper.

[13] AMT Nederlands B.V.(2012), *Description of the AMT Nederlands Nike Gasturbine,* www.amtjets.com, Spaarpot 34 NL-5667 KX Geldrop, Holland, NEDERLANDS. [Retrieved 15 February 2015]

[14] Meggitt Defence Systems Ltd, "*Pneumatic air vehicle launcher*," https://meggitttargetsystems.com, The Boulevard, Orbital Park ,Ashford Kent, TN24 0GA, UK. [retrieved 17 April 2016].

[15] Mentor Graphics Corporation, "*FloEFD Best Practice guide-How To Simulate External Aerodynamics*," 8005 S.W. Boekman Road, Wilsonwille, Oregon 97070-7777,USA

[16] Mentor Graphics Corporation, "*FloEFD Aerospace Validation and Test-Cases*," 8005 S.W. Boekman Road, Wilsonwille, Oregon 97070-7777,USA

[17] Mentor Graphics Corporation, "*NASA Common Research Model Aerodynamics*,", 8005 S.W. Boekman Road, Wilsonwille, Oregon 97070-7777,USA.

[18] Turkish Aerospace Industries, www.tai.com.tr, "*Aerial Targets Specification Table*," Fethiye Mahallesi, Havacılık Bulvarı No:17 Kazan Ankara TURKEY. [retrieved 02 September 2015].

[19] Mayurakshi Equipments P ltd, www.mayurakshi.net, F.F.-26 B Som Datt Plaza,Plot No:10, The Mall Kanpur-208 001 INDIA. [retrieved 03 September 2015].

[20] Photo Sonics International Ltd, Retrieved from http://www.photo-sonics.co.uk/products/optical-tracking-systems/portable-tracking-systems/miss-distance-indicator-mdi,5 Thame Park Business Centre Wenman Road THAME Oxfordshire UK. [retrieved 03 September 2015].

[21] Meggitt Defence Systems Ltd, Retrieved from https://meggitttargetsystems.com/static/media/files/AMDI_2015.pdf, The Boulevard, Orbital Park ,Ashford Kent, TN24 0GA, UK. [retrieved 16 April 2016].

[22] Dr. A. Sobachkin, Dr. G. Dumnov, "*Numerical Basis of CAD-Embedded CFD*," 8005 S.W. Boekman Road, Wilsonwille, Oregon 97070-7777,USA.

[23] Mentor Graphics Corporation, "*Enhanced Turbulence Modeling in FloEFD*," 8005 8005 S.W. Boekman Road, Wilsonwille, Oregon 97070-7777,USA.

[24] BSK Defence S.A. ,"*Yperion Specifications Table*" Retrieved from http://www.redstar.gr/Foto_red/Eng/HAF/BSK_defense/Yperion.html, Sykolia N.Kydonias Chania Greece P.C. 73100 [retrieved 07 March 2016]

[25] BSK Defence S.A. ,"*Nemisis Specifications Table*" Retrieved from http://www.redstar.gr/Foto_red/Eng/HAF/BSK_defense/Nemisis.html, Sykolia N.Kydonias Chania Greece P.C. 73100 [retrieved 07 March 2016].

[26] Özgen S., Güngör O., İnekçi M., Büyüksural T., Erdem U., Gürler M, Karagöz F., Aydın E., Yaşa Z. ,"*Von Karman Institute UAV Design Competition*" Project Report, Middle East Technical University.

[27] XFOİL, https://en.wikipedia.org/wiki/XFOIL [retrieved 07 March 2016]

[28] Sadraey M.,VDM Verlag Dr. Müller, (2009), "*Aircraft Performance Analysis",* Daniel Webster College, New Hampshire, USA.

APPENDICES

DESIGN CALCULATIONS

A1 Initial Calculations

Speed of sound at 15000 ft is 626 Knots. Therefore, the maximum mach number when cruising at the maximum speed of 450 knots becomes;

$$M_{max} = \frac{V_{max}}{a} = \frac{450\ knots}{626\ knots} \cong 0.7\ M$$

The dynamic pressure value at stall condition at sea level is given as;

$$q_{stall} = \frac{1}{2}(2.377 * 10^{-3} slugs/ft^3)(140.32 ft/s)^2 = 23.4012\ lb/ft^2$$

The dynamic pressure value at cruise condition at 15000 ft is given as;

$$q_{cruise} = \frac{1}{2}(1.496 * 10^{-3} slugs/ft^3)(323.232 ft/s)^2 = 78.15 lb/ft^2$$

The dynamic pressure value at combat condition at 15000 ft is given as;

$$q_{combat} = \frac{1}{2}(1.496 * 10^{-3} slugs/ft^3)(452 ft/s)^2 = 152.82\ lb/ft^2$$

The dynamic pressure value at loiter condition at 15000 ft is given as;

$$q_{loiter} = \frac{1}{2}(1.496 * 10^{-3} slugs/ft^3)(237.2 ft/s)^2 = 42.1\ lb/ft^2$$

Table A1 Nike Jet Engine SFC Table During Mission Profiles

	Nike Engine SFC (1/h)
Cruise	**2.36**
Loiter(15000ft)	**2.325**
Combat	**2.237**

C_{D0} value is initially estimated from Ref[5] by assuming S_{wet}/S_{ref}, 4 and

$$C_{D0} = C_{fe}(\frac{S_{wet}}{S_{ref}})$$

$$C_{D0} = 0.0035(4) = 0.014$$

Then, after iterations in Appendix A9, this value became approximately to 0.0195.

AR is chosen 5 from historical trends. The oswald efficiency factor for 30^0 swept wing is calculated as,

$$e = 4.61(1 - 0.045(5)^{0.68})(\cos 30)^{0.15} - 3.1 = 0.8051$$

To calculate the drag due to lift, K is calculated from,

$$K = \frac{1}{\pi * AR * e} = \frac{1}{3.1416 * 5 * 0.8051} = 0.07907$$

A2 T/W and W/S Calculation

A2.1 T/W

A2.1.1 Initial T/W Calculation

Initially, T/W is estimated using,

$$(\frac{T}{W})_{take\ off} = 0.648(0.72)^{0.594} = 0.53312$$

At combat condition at 15000 ft and combat speed is initially assumed as 267 knots, assuming that typical (Wcombat/Wo) is 0.8.

$$\left(\frac{T}{W}\right)_{combat} = \left(\frac{T}{W}\right)_{take\ off}\left(\frac{1}{0.8}\right)\left(\frac{500N}{784N}\right) = 0.425$$

A2.1.2 Max speed constraint

After initial weight analysis , T/W is calculated for a refined weight analysis , T/W sea level constraint for max speed is checked

$$\left(\frac{T}{W}\right) = \rho_0 {V_{max}}^2 C_{D_0} \frac{1}{2(\frac{W}{S})} + \frac{2K}{\rho\sigma {V_{max}}^2}(\frac{W}{S})$$

$$\left(\frac{T}{W}\right) = (2.377 * 10^{-3} slugs/ft^3) * (759.51\ ft/s)^2 * (0.0196)\frac{1}{2 * (23.209 lb/ft^2)} + \frac{2 * 0.07907}{1.496 * 10^{-3} slugs/ft^3 * 0.629 * (759.51\ ft/s)^2}(23.209 lb/ft^2)$$

$$\left(\frac{T}{W}\right)_{takeoff} = 0.582$$

A2.1.3 Sustained Turn Rate constraint

$$\left(\frac{T}{W}\right)_{combat} = \frac{qC_{D0}}{(\frac{W}{S})} + \left(\frac{W}{S}\right)\frac{n^2}{q\pi Ae} = \frac{152.819 lb/ft^2 * 0.0195}{18.514 lb/ft^2} + 18.514 lb/ft^2 * \frac{6^2}{152.819 lb/ft^2 * 3.1416 * 5 * 0.805} = 0.506$$

$$\left(\frac{T}{W}\right)_{takeoff} = 0.506 * 0.8 * \frac{784}{500} = 0.635(chosen)$$

Choose the highest T/W option

A2.2 W/S

A2.2.1 Maximum Cruise Constraint

For maximum cruise,

$$(\frac{W}{S})_{cruise} = 78.247 lb/ft^2 \sqrt{\frac{3.14 * 5 * 0.8051 * 0.0195}{3}} = 22.433\ lb/ft^2$$

$$(\frac{W}{S})_{take\ off} = \frac{22.433 lb/ft^2}{0.9666} = 23.209\ lb/ft^2 (Chosen)$$

A2.2.2 Maneuver constraint

C_{Lmax} at corner velocity is 1.0935 from aerodynamics calculations. For 9g instantaneous turn rate at corner velocity at 15000 ft,

$$(\frac{W}{S})_{combat} = \frac{152.819 lb/ft^2 * 1.0935}{9} = 18.514\ lb/ft^2$$

the take off wing loading is approximately calculated as,

$$(\frac{W}{S})_{take\ off} = \frac{18.514 lb/ft^2}{0.8} = 23.209\ lb/ft^2$$

A2.2.3 Catapult constraint

Choosing V_{end} 87 knots[10] , Velocity coming from engine thrust 6.5 knots[5] and CLmax as 1.093, Catapult launcher constraint is given as;

$$(\frac{W}{S})_{takeoff} = \frac{1}{2}\rho(V_{end} + V_{thrust})^2(\frac{C_{L_{max}}}{1.21})$$

$$(\frac{W}{S})_{takeoff} = \frac{1}{2}(2.377 * 10^{-3} slugs/ft^3)(146.839\ ft/s + 10.970 ft/s)^2(\frac{1.0935}{1.21})$$

$$(\frac{W}{S})_{takeoff} = 26.748\ lb/ft^2$$

By choosing smallest wing loading, the take off wing loading is choosen as 23.209 lb/ft^2

A3 Refined weight analysis

Total weight of UAV is calculated from,

$$W_0 = W_{payload} + W_{fuel} + W_{empty}$$

Calculations were altered during iterations and every iterations cannot be shown. Refined weight analysis is made for 0.0196 parasitic drag coefficient.

From mission profile, all weight segment calculations are made.

1- For take off phase,

$$\frac{W_1}{W_0} = 0.99$$

2- Climb phase to 15000 ft altitude to 0.309 Mach,

$$\frac{W_2}{W_1} = 1.0065 - 0.0325(0.309)$$

$$\frac{W_2}{W_1} = 0.9965$$

3- 100 km range (328083ft) Cruise phase,

$$(\frac{W}{S})_{cruise} = \left(\frac{W}{S}\right)_{takeoff} (0.99) * (0.9965) = 22.89 lb/ft^2$$

$$V_{cruise} = \sqrt{\frac{2 * 22.89 lb/ft^2}{1.496 * 10^{-3} slugs/ft^3} \sqrt{\frac{3}{0.0196 * 3.14 * 5 * 0.8051}}} = 326\ \frac{ft}{s}$$
$$= 193.14\ Knots$$

$$(\frac{L}{D})_{cruise}$$
$$= \frac{1}{\frac{(79.7 lb/ft^2)(0.0196)}{22.890 lb/ft^2} + (22.89 lb/ft^2)(\frac{1}{79.7 lb/ft^2 * 3.14 * 5 * 0.8051})}$$
$$= 11.013$$

The L/D cruise value has been updated to 9,86 from aerodynamics section during iterations.

$$\frac{W_3}{W_2} = e^{-(\frac{(328083 ft) * (2.36/3600)}{(326.5)(9.86)})} = 0.935$$

4- Loiter phase for 50 min at 15000 ft altitude,

$$(\frac{W}{S})_{loiter} = (23.209 lb/ft^2)(0.99)(0.9965)(0.935) = 21.12\ lb/ft^2$$

For best loiter performance, the loiter velocity is given as,

$$V_{loiter} = \sqrt{\frac{2 * (21.193 lb/ft^2)}{1.496 * 10^{-3} slugs/ft^3} \sqrt{\frac{1}{0.0196 * 3.14 * 5 * 0.8051}}} = 240 \left(\frac{ft}{s}\right)$$
$$= 141.3\ Knots$$

The (L/D)loiter is calculated from,

$$\left(\frac{L}{D}\right)_{loiter} = \frac{1}{\frac{43.07lb/ft^2 * 0.01955}{21.12lb/ft^2} + \frac{21.12lb/ft^2}{43.07lb/ft^2 * 3.1416 * 5 * 0.8051}} = 12.717$$

Loiter mission weight fraction is given as;

$$\frac{W_4}{W_3} = e^{-\left(\frac{(50*60)\left(\frac{2.325}{3600}\right)}{13.055}\right)} = 0.857$$

5- Combat phase during operating at corner velocity at 15000 ft altitude for 10 mins is divided into 2 parts, every part consists of 5 mins

$$\frac{W_{4,1}}{W_4} = 1 - \left((6.214 * 10^{-4}) * 0.506 * (5 * 60\ s)\right) = 0.905$$

$$\frac{W_{4,2}}{W_{4,1}} = 1 - \left((6.214 * 10^{-4}) * \frac{0.506}{0.905} * (5 * 60\ s)\right) = 0.895$$

Total combat weight fraction is the multiplication of the two segments,

$$\frac{W_5}{W_4} = 0.905 * 0.895 = 0.811$$

Total mission weight fraction,

$$\frac{W_5}{W_0} = \frac{W_1}{W_0} * \frac{W_2}{W_1} * \frac{W_3}{W_2} * \frac{W_4}{W_3} * \frac{W_5}{W_4}$$

$$\frac{W_5}{W_0} = (0.99)(0.9965)(0.935)(0.857)(0.811) = 0.642$$

The fuel fraction,

$$\frac{W_f}{W_0} = 1.06\left(1 - \frac{W_8}{W_0}\right) = 1.06(1 - 0.642) = 0.38$$

$$W_0 = \frac{22\ lb + 4.4lb}{1 - 0.38 - 0.48} = 187.97\ lb = 85.26kg$$

$$W_f = 0.38 * 188 = 71.345\ lb$$

A4 Wing Parameters Calculation

W_0 = 188 lbs

From wing loading Formula, the wing reference area becomes,

$$S_{wing} = \frac{W}{(\frac{W}{S})_{takeoff}} = \frac{188\ (lb)}{23.209(\frac{lb}{ft^2})} = 8.10ft^2$$

From given AR, the wing span becomes,

$$AR = \frac{b^2}{S_{wing}}$$

$$b = \sqrt{AR * S_{wing}} = \sqrt{5 * 8.1(ft^2)} = 6.364\ ft$$

From wing area, the root chord and tip chord becomes,

$$S = \frac{(C_r + C_t) * b}{2}$$

$$(C_t + C_r) = \frac{2 * S}{b} = \frac{2 * 8.115(ft^2)}{6.37\ ft} = 2.55\ ft$$

Taper ratio,

$$\lambda = 0.36 = \frac{C_t}{C_r}$$

C_r = 1.87 ft
C_t = 0.674 ft

Mean aerodynamic chord(MAC) and the position of the MAC in spanwise direction;

$$\overline{C_{Wing}} = \frac{2}{3} * 1.87 * \frac{1 + 0.36 + 0.36^2}{1 + 0.36} = 1.368\ ft$$

$$\bar{y} = \left(\frac{6.37ft}{6}\right)\frac{1 + 2(0.36)}{1 + 0.36} = 1.341\ ft$$

A5 Fuselage Parameters Calculation

İnitial fuselage length,

$$l_{fuselage}(initial) = aW_0^c = 0.93 * (188)^{0.39} = 7.176\ ft$$

26% length difference factor is added which comes from previous designs,

$$l_{fuselage} = 7.176\ ft + 7.176ft * 0.26 = 9.0425\ ft$$

From chosen slenderness value(f), the fuselage diameter(d),

$$f = 11 = \frac{l_{fuselage}}{d} = \frac{9.0425\ ft}{d}$$

$$d_{fus} = 0.822\ ft = 0.25\ m$$

Engine diameter should be smaller than fuselage diameter. The Nike engine diameter is 20.1 cm, which is smaller than fuselage diameter.

Fuel space in fuselage is calculated by assuming that jet-A1 is used,

$$V_f = \frac{W_f}{\rho_f} = \frac{71.345(lb)}{6.71\left(\frac{lb}{gal}\right)} = 10.632\text{gal} = 0.04026\ \text{m}^3$$

A6 Tail Parameters Calculation

L_{HT} and L_{VT} are found from fighter plane assumption[8],

$$L_{HT} = 0.3 l_{fuselage} = 2.712\ ft$$

$$L_{VT} = 0.3 l_{fuselage} = 2.712\ ft$$

Horizontal and vertical tail volume coefficients were fighter plane assumptions[5],

A6.1 Horizontal tail

The horizontal surface area;

$$S_{HT} = \frac{c_{HT} \bar{C}_W S_W}{L_{HT}} = \frac{0.4 * 1.368ft * 8.1\ ft^2}{2.712\ ft} = 1.634\ ft^2$$

Horizontal tail AR can be estimated from wing AR as follows[8].

$$AR_{HT} = \frac{2}{3} AR_{wing} = \frac{2}{3} * 5 = 3.333$$

Horizontal tail AR;

$$AR_{HT} = \frac{{l_{HT}}^2}{S_{HT}} = 3.333 = \frac{{l_{HT}}^2}{1.637 ft^2}$$

Horizontal tail span $l_{HT} = 2.336\ ft$

From wing area, the root chord and tip chord becomes,

$$S_{HT} = \frac{(C_{r\,HT} + C_{t\,HT}) * l_{HT}}{2} = \frac{(C_{r\,HT} + C_{t\,HT}) * 2.336ft}{2}$$

$$(C_{t\,HT} + C_{r\,HT}) = \frac{2 * S_{HT}}{l_{HT}} = \frac{2 * 1.637(ft^2)}{2.336\ ft} = 1.4\ ft$$

$$\lambda_{HT} = \frac{C_{t\,HT}}{C_{r\,HT}} = \frac{1}{3}$$

$C_{r\,HT}$ = 1.051 ft
$C_{t\,HT}$ = 0.350 ft

Horizontal tail Mean Aerodynamic Chord;

$$\overline{C_{HT}} = \left(\frac{2}{3}\right) c_{rHT} \frac{1 + \lambda_{HT} + {\lambda_{HT}}^2}{1 + \lambda_{HT}} = \left(\frac{2}{3}\right) * (1.051\ ft) * \frac{1 + \frac{1}{3} + (\frac{1}{3})^2}{1 + \frac{1}{3}} = 0.759ft$$

A6.2 Vertical Tail

Vertical tail surface area;

$$S_{VT} = \frac{c_{VT} b_W S_W}{L_{VT}} = \frac{0.07 * 6.3741ft * 8.115ft^2}{2.712\ ft} = 1.334\ ft^2$$

Vertical tail AR,

$$AR_{VT} = \frac{{l_{VT}}^2}{S_{VT}} = 1.3 = \frac{{l_{VT}}^2}{1.334}$$

Vertical tail span $l_{VT} = 1.317\ ft$

From wing area, the root chord and tip chord becomes,

$$S_{VT} = \frac{(C_{r\,VT} + C_{t\,VT}) * l_{VT}}{2} = \frac{(C_{r\,VT} + C_{t\,VT}) * 1.317\ ft}{2}$$

$$(C_{t\,VT} + C_{r\,VT}) = \frac{2 * S_{VT}}{l_{VT}} = \frac{2 * 1.32402(ft^2)}{1.312\ ft} = 2.026\ ft$$

$$\lambda_{HT} = \frac{C_{t\,VT}}{C_{r\,VT}} = \frac{1}{3}$$

$C_{r\,VT}$ = 1.52 ft
$C_{t\,VT}$ = 0.5064 ft

$$\overline{C_{VT}} = \left(\frac{2}{3}\right) c_{r\,VT} \frac{1 + \lambda_{HT} + {\lambda_{HT}}^2}{1 + \lambda_{HT}} = \left(\frac{2}{3}\right) * (1.52\ ft) * \frac{1 + \frac{1}{3} + (\frac{1}{3})^2}{1 + \frac{1}{3}} = 1.0973\ ft$$

A7 Control Surfaces

A7.1 Aileron

$$\frac{C_{aileron}}{C_{wing}} = 0.25 = \frac{C_{aileron}}{1.368\ ft}$$

$C_{aileron}$ = 0.342 ft

$$\frac{b_{aileron}}{b_{wing}} = 0.38 = \frac{b_{aileron}}{6.37\ ft}$$

$b_{aileron}$ = 2.42 ft

A7.2 Elevator and Rudder

There will be no elevators but moving horizontal tail in aerial target.

For rudders,

$$\frac{C_{rudder}}{\bar{C}_{VT}} = 0.25 = \frac{C_{rudder}}{1.0973}$$

C_{rudder} = 0.27433

A8 Recovery System Calculations

The Wrecovery is calculated by the formula;

$$W_{recovery} = 0.62 * W_0 = 0.62 * 188lb = 116.56\ lb$$

By selecting the Rate of Decent 29 ft/s, from table given in Ref[12] canopy loading is selected as 1 lb/ft^2. The Drag area ($C_D S_{parachute}$) value becomes,

$$C_D S_{parachute} = \frac{W_{recovery}}{CL} = \frac{117lb}{1\ lb/ft^2} = 116.56 ft^2$$

Assuming the drag efficiency (C_{eff}) 50 ft^2/lb, the parachute weight is calculated from[12];

$$W_P = \frac{C_D S_{parachute}}{C_{eff}} = \frac{116.56\ ft^2}{50\ ft^2/lb} = 2.3312\ lb$$

By selecting the pack density 25 lb/ft^3, the volume required for the parachute is calculated as[12];

$$V_{parachute} = \frac{2.34\ lb}{25\ lb/ft^3} = 0.09215\ ft^3$$

Finally, assuming that $C_{Dparachute}$ is 1.1, the parachute diameter is calculated from[12];

$$D_{parachute} = \sqrt{\frac{8W_{recovery}}{\pi\rho {V_T}^2 C_{D_{parachute}}}}$$

$$= \sqrt{\frac{8 * 116.56}{3.1416 * (22.25 * 10^{-4} slugs/ft^3) * (29 ft/s)^2 * 1.1}}$$

$$D_{parachute} = 12.060\ ft$$

A9. Aerodynamic Calculations

A9.1 Airfoil Selection

A9.1.1 Reynolds Number

The approximate reynolds number at cruise, combat, loiter and maximum speed condition at 15000 ft is given as;

$$Re_{cruise} = \frac{\rho_{alt} V_{cruise} \bar{c}}{\mu} = \frac{14.96*10^{-4}\left(\frac{slugs}{ft^3}\right)*323.685\left(\frac{ft}{s}\right)*1.368(ft)}{3.43*10^{-7}\left(\frac{lb.s}{ft^2}\right)} = 2{,}000{,}000$$

$$Re_{combat} = \frac{\rho_{alt} V_{combat} \bar{c}}{\mu} = \frac{14.96*10^{-4}\left(\frac{slugs}{ft^3}\right)*452\left(\frac{ft}{s}\right)*1.368(ft)}{3.43*10^{-7}\left(\frac{lb.s}{ft^2}\right)} = 2{,}700{,}000$$

$$Re_{loiter} = \frac{\rho_{alt} V_{loiter} \bar{c}}{\mu} = \frac{14.96*10^{-4}\left(\frac{slugs}{ft^3}\right)*241.462\left(\frac{ft}{s}\right)*1.368(ft)}{3.43*10^{-7}\left(\frac{lb.s}{ft^2}\right)} = 1{,}500{,}000$$

$$Re_{max} = \frac{\rho_{alt}\, V_{loiter}\, \bar{c}}{\mu} = \frac{14.96*10^{-4}\left(\frac{slugs}{ft^3}\right)*759.514\left(\frac{ft}{s}\right)*1.368(ft)}{3.43*10^{-7}\left(\frac{lb.s}{ft^2}\right)} = 4{,}500{,}000$$

At stall condition, RE is given as;

$$Re_{stall} = \frac{\rho_{sl}\, V_{stall}\, \bar{c}}{\mu} = \frac{23.77*10^{-4}\left(\frac{slugs}{ft^3}\right)*133.634\left(\frac{ft}{s}\right)*1.368(ft)}{3.737*10^{-7}\left(\frac{lb.s}{ft^2}\right)} = 1{,}162{,}000$$

The operating RE is between 1.2-4.5 million.

A9.1.2 Mach Number

The mach number at cruise and maximum mach number,

$$M_{cruise} = \frac{v}{a} = \frac{191.78knots}{626knots} \cong 0.3$$

$$M_{max} = \frac{v}{a} = \frac{450knots}{626knots} \cong 0.7$$

A9.1.3 Ideal(Design) Airfoil Lift Coefficient

$$C_{L\,ideal} = \frac{1}{q_{(cruise)}}\left(\frac{W}{S}\right)_{average} = \frac{1}{79.75\,\frac{lb}{ft^2}}\left(\frac{\frac{14.704lb}{ft^2} + \frac{23.209lb}{ft^2}}{2}\right) = 0.242$$

Airfoil ideal lift coefficient becomes,

$$C_{l_{ideal}} = \frac{C_{L_{ideal}}}{0.9cos\Lambda_{0.25c}} = \frac{0.242}{0.9 * 0.9} = 0.3$$

Where, $cos\Lambda_{0.25c} = \cos(25{,}8) = 0.9$

A9.1.4 Maximum Airfoil Lift Coefficient

To calculate the stall speed, the wing loading at take off condition is selected, which is 23.209lb/ft^2

$$C_{Lmax} = 1.0935 = \frac{1}{q_{(stall)}}\left(\frac{W}{S}\right)_{takeoff} = \frac{1}{q_{(stall)}}\left(23.209\,\frac{lb}{ft^2}\right)$$

$$q_{(stall)} = 21.224\ lb/ft^2$$

The dynamic pressure value at stall condition at sea level is given as;

$$q_{stall} = \frac{1}{2}(2.377 * 10^{-3} slugs/ft^3)(V_{stall})^2 = 21.224\ lb/ft^2$$

Stall velocity(V_{stall}) becomes 40.63 m/s, which is 133.634 ft/s (79 KTS). This stall velocity value is very consistent with the launch speed of the Twinjet Banshee aircraft which is 87 knots[10].

$$C_{l_{max}} = \frac{C_{L_{max}}}{0.9 cos\Lambda_{0.25c}} = \frac{0.95}{0.9 * 0.9} = 1.173$$

t/c ratio of the airfoil is selected 12% by considering the maximum mach number.

İnitially 0.95 CLmax has been selected, then during iterations, 1.35 Clmax airfoil has been found and

$$C_{L_{max}} = 1.35 * 0.9 * 0.9 = 1.0935$$

6 different airfoils were compared and the airfoil NACA63-412 has been selected.

For Horizontal and Vertical Tail, NACA 0009 Smoothed symmetric A/F has been selected.

A9.2 Lift Curve Slope

A9.2.1 Wing Lift Curve Slope

S_{ref} = 8.115 ft^2

$S_{wing\ in\ fus}$ = 1,476 ft^2

$$S_{wing\ exposed} = S_{wing} - S_{wing\ in\ fus}$$

$$S_{wing\ exposed} = 8.115ft^2 - 1.476ft^2 = 6.638\ ft^2$$

$$C_{L_{\alpha\,Wing}} = \frac{2\,\pi\,(AR_{wing})}{2 + \sqrt{4 + \frac{(AR)^2\,\beta^2}{\eta^2}\left(1 + \frac{tan^2(\Lambda_{c/2})}{\beta^2}\right)}}\left(\frac{S_{exposed}}{S_{ref}}\right)F$$

$\beta = \sqrt{1 - M^2} = \sqrt{1 - (0.31)^2} = 0.95074$

$F = 1.07\,(1 + \frac{D_{fuselage}}{l_{fuselage}})^2 = 1.07\left(1 + \left(\frac{1}{11}\right)^2\right) = 1.2734$

$C_{l\alpha}$ = 0.12 deg^{-1} = 6.8755 rad^{-1}

$\eta = 0.95$

$$C_{L_{\alpha wing}} = \frac{2 * \pi * 5}{2 + \sqrt{4 + \frac{(5)^2 * 0.95074^2}{(0{,}95)^2}\left(1 + \frac{tan^2(21.26)}{(0.95074)^2}\right)}}\left(\frac{6.638}{8.09}\right)1.2734$$
$$= 0.077\ deg^{-1}$$

A9.2.2 Horizontal Tail Lift Curve Slope

$$For\ T - tail, \qquad S_{HT\ exposed} = S_{ref\ HT} = 1.637ft^2$$

$$C_{L_{\alpha\,HT}} = \frac{2\,\pi\,(AR_{HT})}{2 + \sqrt{4 + \frac{(AR_{HT})^2\,\beta^2}{\eta^2}\left(1 + \frac{tan^2(\Lambda_{c/2HT})}{\beta^2}\right)}}\left(\frac{S_{exposed\ HT}}{S_{refHT}}\right)F$$

$\beta\ and\ F\ are\ same\ with\ previous\ calculation$

$C_{l\alpha} = 0.1\ deg^{-1} = 5.73\ rad^{-1}$

$$\eta(HT) = \frac{C_{l_\alpha}}{\frac{2\pi}{\beta}} = 0.867$$

$$C_{L_{\alpha\,HT}} = \frac{2 * \pi * 3.333}{2 + \sqrt{4 + \frac{(3.333)^2 * 0.95074^2}{(0.867)^2}\left(1 + \frac{tan^2(21.812)}{(0.95074)^2}\right)}}\left(\frac{1.637}{1.637}\right) 1.2734$$
$$= 0.02812\ deg^{-1}$$

A9.2.3 Downwash Factor

$\frac{\partial \varepsilon}{\partial \alpha}$ arises due to wing trailing vortex contributions to the downwash of the tail. This will be computed using Appendix B.5 in Ref[11].

$$\frac{\partial \varepsilon}{\partial \alpha} = 4.44[K_A * K_\lambda * K_H * \left(Cos\Lambda_{\frac{c}{4}}\right)^{0.5}]^{1.19}$$

Where, K_A, K_λ and K_H are Aspect ratio factor, taper ratio factor and horizontal tail location factor respectively

$$K_A = \frac{1}{A} - \frac{1}{1+A^{1.7}} = \frac{1}{5} - \frac{1}{1+5^{1.7}} = 0.139$$

$$K_\lambda = \frac{10-3\lambda}{7} = \frac{10-3*0.36}{7} = 1.274$$

$$K_H = \frac{1-\frac{h_{HT}}{b}}{(\frac{2*L_{HT}}{b})^{\frac{1}{3}}} = \frac{1-\frac{1.3158ft}{6.364ft}}{(\frac{2*3.71ft}{6.364ft})^{\frac{1}{3}}} = 0.837$$

$$\frac{\partial \varepsilon}{\partial \alpha} = 4.44[0.139 * 1.274 * 0.837 * (Cos25.8)^{0.5}]^{1.19} = 0.3806$$

A9.3 Drag Coefficient

A9.3.1 Parasite Drag Coefficient

Parasite drag is initially assumed at start. However, the actual parasite drag should be found from the total wetted area of the aircraft.

Wing wetted area;

$$S_{wetted\ Wing} = S_{\exp wing}\left(1.977 + 0.52 * \left(\frac{t}{c}\right)\right)$$
$$= 6.638\ ft^2 * (1.977 + 0.52 * 0.12) = 13.539\ ft^2$$

Fuselage wetted area;

From Catia-CAD software, fuselage wetted area is calculated as;

$$S_{wetted\ Fuselage} = 21.38\ ft^2$$

Horizontal tail wetted area;

$$S_{HT} = S_{\exp HT} = 1.637\ ft^2$$

$$S_{wetted\ HT} = S_{exposed\ HT}\left(1.977 + 0.52\left(\frac{t}{c}\right)_{HT}\right)$$
$$= 1.637 ft^2 * (1.977 + 0.52 * 0.09) = 3.313\ ft^2$$

Vertical tail exposed area;

$$S_{\exp VT} = S_{ref\ VT} - S_{VT\ in\ Fuselage} = 1.333 ft^2 - 0.549 ft^2 = 0.774\ ft^2$$

Vertical tail wetted area;

$$S_{\text{wetted}\,VT} = 0.774 ft^2 * (1.977 + 0.52 * 0.09) = 1.5665\ ft^2$$

Approximate total wetted area:

$$S_{tot\ wetted} = S_{wetted\ Wing} + S_{wetted\ Fuselage} + S_{wetted\ HT} + S_{\text{wetted}\,VT}$$

$$S_{tot\ wetted} = 13.539 ft^2 + 21.38 ft^2 + 3.313 ft^2 + 1.5665 ft^2 = 39.8\ ft^2$$

Component build-up method for parasitic drag estimation;

$$C_{D_0} = \frac{\sum(C_{f_c} FF_c Q_c S_{wet_c}}{S_{ref}} + C_{D\,misc} + C_{D\,L\&P}$$

The interference factor Q is assumed 1 for all the components of the high speed aerial target.

From the calculated Reynolds number of the components of the Wing, fuselage, HT and VT,
flat plate skin friction coefficient formula is given as[5];

$$C_f = \frac{0.455}{(log_{10}R)^{2.58}(1+0.144M^2)^{0.65}}$$

$$C_{f\,fuselage} = \frac{0.455}{(log_{10}13000000)^{2.58}(1+0.144(0{,}31)^2)^{0.65}} = 0{,}00286$$

Similarly, the C_f values of wing, HT and VT are found as 0.00392, 0.00436 and 0.00408

Form factor (FF) for wing, tail, strut and pylon is found from following formula[5];

$$FF_{Wing} = \left[1 + \frac{0.6}{\left(\frac{x}{c}\right)_m}\left(\frac{t}{c}\right) + 100\left(\frac{t}{c}\right)^4\right][1.34M^{0.18}(cos\Lambda_m)^{0.28}]$$

$$FF_{Wing} = \left[1 + \frac{0.6}{0.4} * 0.12 + 100(0.12)^4\right][1.34(0.31)^{0.18}(cos23.11)^{0.28}] = 1.273$$

Similarly, for horizontal and vertical tail,

$$FF_{HT} = \left[1 + \frac{0.6}{0.309}0.09 + 100(0.09)^4\right][1.34(0.31)^{0.18}(cos27.327)^{0.28}] = 1.24$$

$$FF_{VT} = \left[1 + \frac{0.6}{0.309}(0.09) + 100(0.09)^4\right][1.34(0.31)^{0.18}(cos24.822)^{0.28}] = 1.248$$

Form factor(FF) for fuselage and smooth canopy;

$$FF_{Fuselage} = (1 + \frac{60}{f^3} + \frac{f}{400}) = 1 + \frac{60}{11^3} + \frac{11}{400} = 1.072$$

Using the FF, C_f , Q, S_{wet} of individual components, and the reference area, the sum of the drag is found by

$$C_{D_0} = \frac{\sum(C_{f_c}FF_cQ_cS_{wet_c})}{S_{ref}} = 0.0196$$

A9.3.2 Total Drag Coefficient

Total Drag is calculated from parasitic drag coefficient and lift coefficient,

$$C_D = C_{D0} + K{C_L}^2$$

$$C_D = 0.0196 + 0.079 * 0.242^2 = 0.024$$

This is the drag coefficient when cruise velocity is 0.31 M. K value was calculated from Oswald span efficiency method. Better approximation was made from the leading edge suction method. Total drag values can be chosen from drag polar curve.

A10. Stability Calculations

A10.1 Wing Factor, Horizontal Tail Factor and Downwash Factor

Wing and horizontal tail factors are pitching moment derivative of wing and horizontal tail. Which are given as,

$$C_{L_{\alpha wing}} = 0.077\ deg^{-1}$$

$$C_{L_{\alpha HT}} = 0.02812\ deg^{-1}$$

Downwash factor was also calculated in aerodynamics calculations,

$$\frac{\partial \varepsilon}{\partial \alpha} = 0.3806$$

A10.2 Fuselage Factor

Fuselage factor is calculated as;

$$C_{m_{\alpha fus}} = \frac{K_{fus} * {W_f}^2 * L_f}{\bar{c} * S_w} = \frac{0.055(deg^{-1}) * 1.1(ft)^2 * 9.032ft}{1.366ft * 8.1(ft)^2} = 0.0543\ deg^{-1}$$
$$= 3.11\ rad^{-1}$$

A10.3 Neutral Point and Static Margin Calculations

$$\bar{X}_{np} = \frac{C_{L_\alpha}\bar{X}_{acw} - C_{m_{\alpha fus}} + \eta_h \frac{S_h}{S_w} C_{L_{\alpha h}} \frac{\partial \alpha_h}{\partial \alpha} \bar{X}_{ach}}{C_{L_\alpha} + \eta_h \frac{S_h}{S_w} C_{L_{\alpha h}} \frac{\partial \alpha_h}{\partial \alpha}}$$

$$\bar{X}_{np} = \frac{4.213(rad^{-1}) * 3.75 - 3.11(rad^{-1}) + 0.867 * \frac{1.634(ft^2)}{8.1(ft^2)} * 1.611(rad^{-1}) * 11.48 * (1 - 0.3806)}{4.213(rad^{-1}) + 0.867 * \frac{1.634(ft^2)}{8.1(ft^2)} * 1.611(rad^{-1}) * (1 - 0.3806)}$$

$$\bar{X}_{np} = 3.35$$

$$X_{np} = \bar{X}_{np} * \bar{C} = 3.35 * 1.366ft = 4.6082\ ft$$

From Catia-v5 drawing it is given that,

$$X_{cg} = 4.475\ ft$$

$$\bar{X}_{cg} = \frac{4.475(ft)}{1.366(ft)} = 3.2741$$

Finally static margin becomes at 0.3M velocity,

$$SM = \bar{X}_{np} - \bar{X}_{cg} = 3.35 - 3.2741 = +0.0756 = 7.56\%\ stable$$

A11 Performance Calculations

A11.1 Thrust Required and Available Thrust

$$D = T = \frac{1}{2}\rho V^2 S C_D$$

where $C_D = C_{D0} + K{C_L}^2 = 0.024$ at cruise condition.

$$T_R = q * S * C_D$$

The available thrust curve and required thrust intersection curves give the theoretical maximum speed.

These two curves intersect at 520 Knots, therefore the theoretical maximum speed becomes 520 Knots at sea level.

A11.2 Rate Of Climb

$$ROC_{max} = \sqrt{\frac{\left(\frac{W}{S}\right)Z}{3\rho_\infty C_{D_0}}}\left(\frac{T}{W}\right)^{\left(\frac{3}{2}\right)}\left[1 - \frac{Z}{6} - \frac{3}{2\left(\frac{T}{W}\right)^2\left(\frac{L}{D}\right)_{max}^{\ 2}Z}\right]$$

Where,

$$\left(\frac{L}{D}\right)_{max} = \sqrt{\frac{1}{4 * C_{D_0} * K}} = \sqrt{\frac{1}{4 * 0.01955 * 0.07907}} = 12.717$$

$$Z = 1 + \sqrt{1 + \frac{3}{\left(\frac{L}{D}\right)_{max}^{\ 2}\left(\frac{T}{W}\right)^2}} = 1 + \sqrt{1 + \frac{3}{(12.717)^2 * (0.635)^2}} = 2.025$$

$$ROC_{max} = \sqrt{\frac{(23.209) * (2.025)}{3 * (2.377 * 10^{-3}) * 0.01955}}(0.635)^{\left(\frac{3}{2}\right)}\left[1 - \frac{2.025}{6} - \frac{3}{2(0.602)^2 * (12.717)^2 * 2.025}\right]$$

$$ROC_{max} = 188.85\ ft/s$$

A11.3 Maximum Load Factor

Maximum load factor for a given (T/W), (W/S)

$$n_{max} = \sqrt{\left[\frac{\frac{1}{2}\rho V^2}{K\left(\frac{W}{S}\right)}\left[\left(\frac{T}{W}\right)_{max} - \frac{1}{2}\rho V^2\frac{C_{D_0}}{\left(\frac{W}{S}\right)}\right]\right]}$$

At combat condition, T/W is 0.506 and W/S is 18.365 lb/ft^2

$$n_{max} = \sqrt{\left[\frac{(152.819\ lb/ft^2)}{0.07907 * (18.365\frac{lb}{ft^2})}\left[0.506 - (152.819\frac{lb}{ft^2})\frac{0.01955}{(18.365\frac{lb}{ft^2})}\right]\right]} = 6$$

This is the load factor value for sustained turn rate. The requirement load factor for the sustained turn rate satisfied.

However maximum load factor for the instantaneous turn rate is 9 and it is constrained by max lift coefficient.

A11.4 Minimum Turn Radius

Minimum Turn Radius at combat condition;

$$R_{min} = \frac{{V_{combat}}^2}{g * \sqrt{n^2 - 1}} = \frac{(450 ft/s)^2}{32.174\ ft/s^2 * \sqrt{(6)^2 - 1}} = 1063\ ft$$

A11.5 Maximum Sustained Turn Rate

Maximum turn rate at combat condition is given as[4];

$$\omega_{max} = \frac{g * \sqrt{n^2 - 1}}{V_{combat}} = \frac{(32.174\ \frac{ft}{s^2}) * \sqrt{(6)^2 - 1}}{450\ ft/s}$$

$$\omega_{max} = 0.422\ \text{rad/s} = 24.187\text{deg/s}$$

A11.6 Pull up and Pull down Instantaneous Turn Manuevers

The load factor becomes 9 for instantaneous turn rate.

For pull up manuever,

Turn radius is given as[4];

$$R = \frac{{V_{combat}}^2}{g(n-1)} = \frac{(450\ ft/s)^2}{(32.174\ \frac{ft}{s^2}) * (9-1)} = 786\ ft$$

Instantaneous turn rate;

$$\omega = \frac{g(n-1)}{V_{combat}} = \frac{(32.174\ \frac{ft}{s^2}) * (9-1)}{450\ ft/s} = 0.572\ rad/s\ = 29.1257\ deg/s$$

For pull down manuever,

Turn radius is given as;

$$R = \frac{{V_{combat}}^2}{g(n+1)} = \frac{(450\ ft/s)^2}{(32.174\ ft/s^2) * (9+1)} = 629\ ft$$

Instantaneous turn rate;

$$\omega = \frac{32.174 ft/s^2 * (9+1)}{450\ ft/s} = 0.715\ rad/s = 36.407\ deg/s$$

A11.7 Corner velocity

$$V_{corner} = \sqrt{\frac{2n_{max}}{\rho * C_{L_{max}}} * (\frac{W}{S})_{combat}}$$

$$= \sqrt{\frac{2 * 9}{(1.496 * 10^{-3}\ slugs/ft^3) * 1.093} * 18.365\ \frac{lb}{ft^2}} = 450 \frac{ft}{s}$$

$$= 266.6\ Knots$$

The combat maneuver speed has been calculated as 266.6 Knots.

A11.8 V-n Diagram

To calculate the flight envelope, limiting load factors were calculated as follows,

n_{limit} = 9 g (positive limit load factor)
n_{ult} = 9*1.5 = 13.5 (ultimate load factor)
$n_{neg\ limit}$ = -2 g (chosen negative limit load factor)
$n_{neg\ ult}$ = -2 *1.5 = -3.5 (negative ultimate load factor)

There are limits of V-n diagram. Ref.[28] yields that $V_{Dive} \geq 1.55*V_{cruise}$ for an maneuverable aircraft. Optimum cruise is 0.38M that is 410 ft/s. Thus, V_{Dive} should be at least 635.5 ft/s.

Aircraft maximum speed is 0.7 M , that corresponds to 760 ft/s. It is appropriate to choose V_{Dive} as 1.2 times of the maximum speed.

$V_{Dive} = 1.2*V_{max}$
$V_{Dive} = 912$ ft/s

There is a given structural limit of the dive velocity dynamic pressure $q_{Dive} = 1800$ lb/ft^2,

$q_{Dive} = 1/2 * \rho*(V_{Dive})^2$

$q_{Dive} = 1/2 * (1.496*10^{-3}$ slugs/ft$^3)*(912$ ft/s$)^2 = 622.15$ lb/ft$^2 < 1800$ lb/ft^2

It is appropriate to choose the dive velocity as 912 ft/s

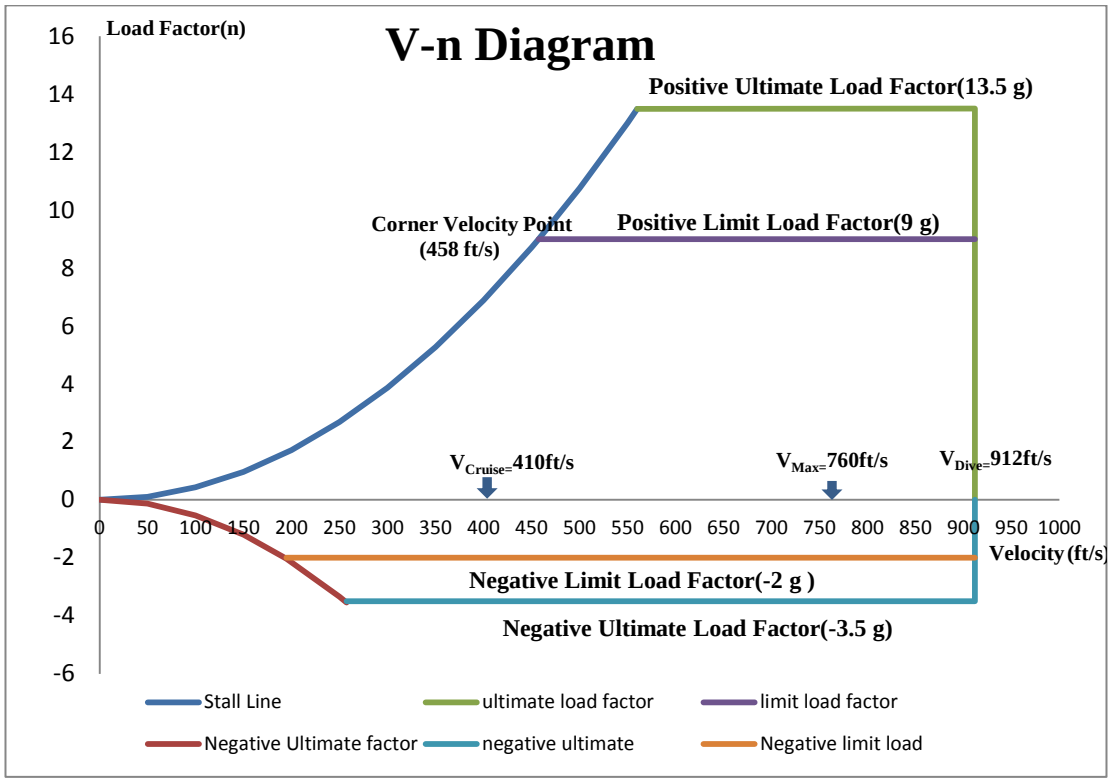

Figure A2 V-n Diagram of High Speed Decoy UAV